

CAPSULE-PIPELINE FLOW -- A THEORETICAL STUDY

A THEORETICAL STUDY  
OF  
INCOMPRESSIBLE FLOW IN A PIPE  
CONTAINING  
A VERY LONG, FREE-FLOWING, ECCENTRIC, CYLINDRICAL CORE

by  
Vijay K. Garg, B. Tech.

A Thesis  
Submitted to the Faculty of Graduate Studies  
in Partial Fulfilment of the Requirements  
for the Degree  
Master of Engineering

McMaster University

August 1969

MASTER OF ENGINEERING (1969)

McMASTER UNIVERSITY

(Mechanical Engineering)

Hamilton, Ontario

TITLE: A Theoretical Study of Incompressible Flow in a  
Pipe Containing a very Long, Free-Flowing,  
Eccentric, Cylindrical Core.

AUTHOR: Vijay K. Garg, B. Tech. (Mech. Eng.)  
I.I.T. Delhi, India

SUPERVISOR: Professor G. F. Round

NUMBER OF PAGES: xi 128

SCOPE AND CONTENTS:

Theoretical predictions of the behaviour of various parameters governing the free flow of a single, very long, denser-than-liquid carrier, cylindrical capsule in a horizontal pipeline are reported in this dissertation. The study was carried out for average flow velocities of approximately 1 to 10 ft/sec in pipes of diameters 4, 6, 12 and 24 in. with diameter ratios varying from 0.9 to 0.99. While two liquid carriers -- water and an oil ( $\mu = 10$  cP and sp. gr. = 0.85) were used, the eccentricity of the capsule-pipe system was fixed at 0.999. The theoretical solution was found to be in good agreement with the experimental results.

## ACKNOWLEDGMENTS

The author takes this opportunity to express his deep gratitudes and sincere thanks to Professor G. F. Round of McMaster University for his able guidance and keen interest throughout the investigation.

Financial assistance received through the Department of University Affairs and the National Research Council under grant no. A5183 is also gratefully acknowledged.

## TABLE OF CONTENTS

|  | <u>Page</u> |
|--|-------------|
| List of Figures                          | vi          |
| Nomenclature                             | viii        |
| <u>Chapter</u>                           |             |
| 1. Introduction                          | 1           |
| 2. Literature Survey                     | 4           |
| 3. Theoretical Analysis                  | 12          |
| 3.1 End Effects                          | 12          |
| 3.2 Force Balance                        | 14          |
| 3.3 Assumptions                          | 17          |
| 3.4 Nature of Flow in the Annulus        | 19          |
| 3.5 Velocity Profiles                    | 22          |
| 3.5.1 Laminar Flow                       | 22          |
| 3.5.2 Turbulent Pressure Flow            | 27          |
| 3.5.3 Turbulent Couette Flow             | 29          |
| 4. Numerical Technique                   | 39          |
| 4.1 Clearance                            | 39          |
| 4.2 Division of Annulus                  | 42          |
| 4.3 Calculation of Geometrical Constants | 44          |
| 5. Results and Discussion                | 47          |
| 5.1 f-Re Plot (Fig. 5.1)                 | 48          |
| 5.1.1 Effect of $d/D$ on $f$             | 49          |

|       |  |    |
|-------|--|----|
| 5.1.2 | f-Re in Comparison to $f_f - Re_f$                               | 49 |
| 5.1.3 | Critical Reynolds Number   | 51 |
| 5.2   | $R_p - R_v$ Plot (Fig. 5.2)                                      | 53 |
| 5.2.1 | Effect of $d/D$ and $V_{av}$ on $R_v$                            | 56 |
| 5.3   | $R_p - V_{av}$ Plots (Fig. 5.3, 5.4)                             | 58 |
| 5.3.1 | Effect of $d/D$ on $R_p$   | 58 |
| 5.3.2 | Effect of $V_{av}$ on $R_p$                                      | 59 |
| 5.3.3 | Effect of $D$ on $R_p$   | 59 |
| 5.3.4 | Effect of Fluid Characteristics on $R_p$                         | 61 |
| 5.4   | Energy Requirements vs. $V_{av}$ (Fig. 5.5, 5.6)                 | 62 |
| 5.4.1 | Effect of $V_{av}$ on the Energy Requirements                    | 63 |
| 5.4.2 | Effect of $d/D$ on the Energy Requirements                       | 63 |
| 5.4.3 | Effect of $D$ and Fluid Properties on the<br>Energy Requirements | 64 |
| 5.5   | Solution of a Problem in General                                 | 64 |
| 5.6   | Velocity Distribution (Figs. 5.7, 5.8)                           | 66 |
| 5.7   | Comparison with Experiment (Figs. 5.9, 5.10)                     | 68 |
| 5.7.1 | Laminar Flow in the Annulus                                      | 70 |
| 5.7.2 | Turbulent Flow in the Annulus                                    | 72 |
| 6.    | Conclusions  | 84 |

### Appendices

|                   |   |     |
|-------------------|---|-----|
| AI                | Geometry of the Eccentric Annulus                   | 87  |
| AII               | Laminar Velocity Profile in a Concentric<br>Annulus | 96  |
| AIII              | Computer Solution                                   | 101 |
| <u>References</u> |   | 124 |

## LIST OF FIGURES

| <u>Number</u> | <u>Title</u>                                   | <u>Page</u> |
|---------------|--|-------------|
| 2.1           | Velocity Profile in Turbulent Couette Flow     | 10          |
| 3.1           | Forces Acting on a Capsule in a Pipe           | 13          |
| 3.2           | End Effects due to the Capsule                 | 13          |
| 3.3           | Shear Stress on a fixed Capsule                | 16          |
| 3.4           | Shear Stress on a Moving Capsule               | 16          |
| 3.5           | Thrust and Drag Forces on a Capsule            | 16          |
| 3.6           | Nature of Flow in the Annulus                  | 20          |
| 3.7           | Part of the Annulus                            | 20          |
| 3.8           | Locally Concentric Elements of the Annulus     | 24          |
| 3.9           | Velocity Profiles in Turbulent Couette Flow    | 31          |
| 3.10          | Velocity Profiles in Turbulent Couette Flow    | 31          |
| 3.11          | Various Regimes for Velocity Profile           |             |
|               | Calculation in Turbulent Couette Flow          | 33          |
| 3.12          | Actual and Predicted Velocity Profiles in      |             |
|               | Turbulent Couette Flow                         | 36          |
| 4.1           | Division of Annulus                            | 41          |
| 4.2           | Determination of $\xi$ Values of Elemental     |             |
|               | Sections                                       | 43          |
| 5.1           | Darcy-Weisbach Friction Factor                 | 74          |
| 5.2           | $R_p - R_v$ Plot                               | 75          |
| 5.3           | Variation of Pressure Ratio with Average       |             |
|               | Velocity, Pipe Diameter and Diameter Ratio for |             |
|               | Water as the Liquid Carrier                    | 76          |

|        |   |     |
|--------|---|-----|
| 5.4    | Variation of Pressure Ratio with Average Velocity, Pipe Diameter and Diameter Ratio for an Oil as the Liquid Carrier  | 77  |
| 5.5    | Variation of Energy Required with Average Velocity, Pipe Diameter and Diameter Ratio for Water as the Liquid Carrier  | 78  |
| 5.6    | Variation of Energy Required with Average Velocity, Pipe Diameter and Diameter Ratio for an Oil as the Liquid Carrier   | 79  |
| 5.7    | Velocity Distribution in the Smallest and Widest Gaps for Water Flowing at Average Velocities of 2,4,6,8 and 10 ft/sec in Pipes of Diameters 4,6,12,24 in. having a Freely Flowing Capsule of Diameter Ratio 0.9  | 80  |
| 5.8    | Velocity Distribution in the Smallest and Widest Gaps for Water Flowing at Average Velocities of 2,4,6,8 and 10 ft/sec in Pipes of Diameters 4,6,12,24 in. having a Freely Flowing Capsule of Diameter Ratio 0.99 | 81  |
| 5.9    | Comparison with Experimental Data in Fig. 8 of Part 9 (14)  | 82  |
| 5.10   | Comparison with Experimental Data in Fig. 12 of Part 9 (14)   | 83  |
| AI-1   | Complex Z Plane   | 88  |
| AI-2   | Polar Co-ordinates of a Point in the Annulus  | 91  |
| AI-3   | Arc Length Determination  | 94  |
| AII-1  | The Concentric Annulus  | 97  |
| AIII-1 | Linear Approximations to the True Value   | 109 |

NOMENCLATURE\*

| <u>Symbol</u>     | <u>Description</u>   |
|-------------------|--|
| <u>Upper Case</u> |  |
| A                 | Area   |
| $C_f$             | Skin friction coefficient as defined for turbulent Couette flow              |
| D                 | Pipe diameter  |
| $D_h$             | Hydraulic diameter of the annulus or a section                               |
| F                 | Contact frictional force per unit area                                       |
| L                 | Chord length of an arc   |
| $L_c$             | Length of the capsule  |
| P                 | Static Pressure  |
| Q                 | Volumetric flow rate   |
| $Q_c$             | Volumetric flow rate due to capsule alone<br>( $= \frac{1}{4} \pi d^2 V_c$ ) |
| R                 | Radius of either pipe or capsule   |
| Re                | Reynolds number  |
| $R_p$             | Pressure ratio ( $= (dp/dz)_c / (dp/dz)_f$ )                                 |
| $R_v$             | Velocity ratio ( $= V_c / V_{av}$ )  |
| S                 | Arc length   |
| V                 | Velocity   |
| $V_c$             | Capsule Velocity   |

---

\*Such common abbreviations as cp for centipoise and sp. gr. for specific gravity, etc. have also been used.

|   |  |
|---|--|
| W | Weight of the Capsule                              |
| Z | Complex variable in the x-y plane ( $Z = x + iy$ ) |

### Lower Case

|       |   |
|-------|---|
| a     | Clearance   |
| c     | Half of the distance between the two poles of a bi-polar coordinate system. |
| d     | Capsule diameter  |
| dp/dz | Axial pressure gradient   |
| e     | Eccentricity  |
| f     | Friction factor (of Darcy-Weisbach form)                                    |
| k     | Diameter ratio  |
| r     | Distance in the radial direction  |
| s     | Distance between the pipe and capsule centres                               |
| x     | Cartesian coordinate  |
| y     | Cartesian coordinate  |
| w     | Velocity in the axial direction   |
| z     | Distance in the axial direction   |
| $w_z$ | Half of the capsule velocity ( $w_z = V_c/2$ )                              |

### Greek Symbols

|            |  |
|------------|--|
| $\epsilon$ | Surface roughness height   |
| $\zeta$    | Complex variable in the $\xi$ - $\eta$ plane ( $\zeta = \xi + i\eta$ ) |
| $\eta$     | Bipolar coordinate for annular geometry                                |
| $\theta$   | Angle  |
| $\mu$      | Fluid dynamic viscosity  |

|                       |   |
|-----------------------|---|
| $\nu$                 | Fluid kinematic viscosity               |
| $\xi$                 | Bipolar coordinate for annular geometry |
| $\pi$                 | The constant 3.14159.....               |
| $\rho$                | Fluid density                           |
| $\sigma$              | Capsule density                         |
| $\sum_{l=1}^{\infty}$ | Summation of terms from 1 to $\infty$   |
| $\tau$                | Shear stress                            |
| $\phi$                | Angle or some function                  |

### Subscripts

|        |  |
|--------|--|
| ann    | Annulus  |
| av     | Average value                                      |
| c      | Referenced to a capsule-pipe system                |
| f      | Referenced to a free pipe                          |
| Loc    | Local value  |
| m      | At the line of maximum velocities in Pressure flow |
| max    | Maximum value                                      |
| min    | Minimum value                                      |
| T      | Total value  |
| $\eta$ | $\eta = \text{constant}$                           |
| $\xi$  | $\xi = \text{constant}$                            |
| 1      | Refers to capsule                                  |
| 2      | Refers to pipe                                     |

## Superscripts

- \* Refers to shear velocity ( $w^* = \sqrt{\tau/\rho}$ )
- + Refers to dimensionless velocity or distance ratio in velocity profiles for turbulent flow

## 1. INTRODUCTION

In recent years considerable interest has developed in the problem of fluid flow through both concentric and eccentric annuli (Ref. 1 to 17 being some of the relevant ones). Amongst numerous other applications, flow in an annulus has also proved useful as a model for pipeline transportation of capsules. The word 'capsule' in this context has come to mean a large regularly shaped body whose minor axis is comparable to the diameter of the pipe through which it is travelling. A capsule may be hollow or solid, cast or extruded, coated or uncoated, rigid or non-rigid and cylindrical or spherical in shape.

A series of tests on capsule pipelining have been conducted at the Research Council of Alberta in the past few years. The capsules used in such tests have been cylindrical (8, 9, 12, 13, 14)\* or spherical (8, 10, 12, 13), hollow or solid, and of a wide range of densities and capsule/pipe diameter ratios; the cylindrical ones having a variety of lengths and end shapes. The tests have also included experimentation on short trains of spherical and cylindrical capsules. A variety of theoretical investigations have also

---

\* Numbers in parentheses designate references listed at the end of the dissertation.

been made (7, 11, 14).

However, all this work has been mainly concerned with laminar flow in the space surrounding the capsule. Though experimental tests in which there was turbulent flow in the annulus (12, 13, 16) have also been conducted, no theoretical analysis has yet been developed except a somewhat unsatisfactory\* outline (17) for such an approach. The following study thus essentially consists of theoretical predictions of the behaviour of various parameters governing the free flow of a very long cylindrical capsule in a horizontal pipe.

In order that the equilibrium velocity of such a capsule may be determined, a proper balance of the forces acting on it must be obtained. Due to some of the assumptions made in this study, such a force balance requires that the thrust due to pressure force must counterbalance the drag due to shear force on the capsule. Since the former is given by the product of capsule cross sectional area and the applied pressure gradient, and since shear force at a wall in fluid flow is given by  $\mu \frac{dw}{dy}$ , the problem is reduced in effect to finding the velocity gradient at the capsule surface.

For this purpose, suitable velocity profiles were developed depending on the nature of fluid flow in the eccentric annular space. A bipolar coordinate system was used to describe the flow field geometry. Once the capsule velocity corresponding to a given applied pressure gradient

---

\*Reasons for this are given in chapter 2, page 10.

was found, the other parameters such as average velocity, pressure and velocity ratios together with energy requirements were easily calculated. Due to the extremely complicated and lengthy nature of calculations involved, the analysis was performed numerically using a CDC 6400 digital computer.

## 2. LITERATURE SURVEY

The concept of capsule pipelining emerged from an investigation of two-phase flow of water and an immiscible oil conducted by Charles, Govier and Hodgson (18). Following this work, further studies were carried out almost exclusively at the Research Council of Alberta to determine the characteristics of a flow system in which the observed slugs of oil in water were replaced by capsules of cylindrical or spherical shape. These experiments were later extended to cover a wide variety of capsule shapes, sizes and densities in a variety of pipes and liquid carriers. This work has been reported in a series of papers, Part 1 to Part 9 (6 to 14 incl.). This series having the general title 'The Pipeline Flow of Capsules' together with references (15, 16, 17) presents the basic research done to date in this field.

For concentric capsule flow, Charles, in Part 2 of the series (7) proposed four models to describe all the possible flow regimes in a capsule pipeline. These models are:

- i) Laminar flow both in the annulus and in the free pipe.
- ii) Turbulent flow both in the annulus and in the free pipe.
- iii) Laminar flow in the annulus but turbulent flow in

the free pipe.

- iv) Turbulent flow in the annulus but laminar in the free pipe.

Charles pointed out that an unstable region near Reynolds number of 1000 would be expected until either turbulent flow was stable in the annulus and model 4 applied or laminar flow became stable when model 1 applied. However, extremely doubtful of the applicability of model 4 even in the small region at Reynolds numbers below 2000 and diameter ratios between 0.4 and 0.7, he suggested that models 1, 2 and 3 are the only realistic ones which would have wide application in practice.

In Part 3 (8) Ellis investigated experimentally the transport of single, equal density, cylindrical and spherical capsules in a water carrier. He also performed a dimensional analysis of the variables involved in the general case of a capsule flowing in a pipeline and obtained

$$V_c \text{ or } \left(\frac{dp}{dz}\right)_c = \phi_1(V_{av}, \sigma, \rho, \mu, L_c, d, D, \text{end shape}, j, \epsilon_1, \epsilon_2)$$

where  $j$  = factor to take into account the lubricating quality of carrier liquid and the friction between capsule and pipe surfaces

$\epsilon_1$  = capsule roughness height

$\epsilon_2$  = pipe roughness height

By dimensional analysis

$$R_V = \frac{V_c}{V_{av}} = \phi_2 \left( \frac{V_{av} D \rho}{\mu}, \frac{\sigma^{-\rho}}{\rho}, \frac{d}{D}, \frac{L_c}{d}, \text{end shape}, \frac{\epsilon_1}{d}, \frac{\epsilon_2}{D} \right) \quad (2.1)$$

or using  $\left(\frac{dp}{dz}\right)_c$ ,  $\frac{V_c}{V_{av}}$  is replaced by the friction factor

$$\left(\frac{dp}{dz}\right)_c \frac{D}{\rho V_{av}^2}$$

This experimental work was limited to equal density capsules thus eliminating the parameter  $\left(\frac{\sigma^{-\rho}}{\rho}\right)$  as an independent variable. The effects of  $\frac{V_{av} D \rho}{\mu}$ ,  $\frac{d}{D}$ ,  $\frac{L_c}{d}$  and end shape on  $R_V$  were found to be as follows:

- i) The velocity ratio,  $R_V$ , was independent of pipe Reynolds number. A region of instability was, however, noted at Reynolds numbers of approximately  $10^4$  when the value of  $V_c$  changed sharply from a minimum to a maximum value. This instability was attributed by Ellis to a possible displacement of the point of separation of the boundary layer to the rear of the capsule.
- ii)  $R_V$  increased with decreasing  $d/D$ .
- iii)  $R_V$  increased with increasing  $L_c/d$ .
- iv) The effect of end shape was limited for large  $d/D$  but not so for small  $d/D$ .

In Part 7 (12) Ellis and Bolt repeated the experiments using water with equal density capsules in an oil carrier and found generally the same effects as noted with the water carrier. However, the region of instability observed in water (8) at

Reynolds numbers of  $10^4$  did not appear in the oil experiments. Also, data taken in the laminar range with the oil showed good agreement with the laminar flow prediction of Charles (7).

Parts 4 and 5 (9, 10) deal with cylinders and spheres denser than the water carrier while Part 8 (13) deals with cylinders and spheres denser than an oil carrier. In Part 4, a discussion of the various forces involved in the case of an eccentric annulus was presented but no quantitative theory was attempted.

Observations made in Part 4 regarding the presence of a liquid film between the capsule and pipe bottoms are of particular importance. For small diameter ratio capsules and in laminar flow conditions, it was observed by Ellis (9) that the capsules lifted clear off the pipe bottom, first in a tail-up position and at a higher velocity, in a nose-up position. It was also noted that at sufficiently high velocities, this visible lift-off could occur for larger diameter ratio and even for heavier capsules. However, it was pointed out that the geometry of the capsule-pipe system precluded any rigorous application of lubrication theory even when the capsule was fully supported by the liquid film beneath it.

In Part 6 (11), Newton, Redberger and Round used a numerical technique to investigate the effect of clearance, end configuration and length of the capsule, deformations of the capsule cross section and frictional effect between the

capsule and pipe wall for laminar flow in the annulus. A significant effect on capsule behaviour was found for all the above variables except for capsule end configuration and length.

The effect of increasing clearance was to increase the velocity ratio but to decrease the pressure ratio -- the ratio of the pressure gradient in the capsule-pipe system  $(dp/dz)_c$  to that for the free pipe  $(dp/dz)_f$  at the same average velocity. A study of the moments acting on the capsule indicated that smaller diameter ratio capsules would lift off the pipe bottom relatively earlier i.e. at lower velocities. As expected, increasing frictional forces decreased the capsule velocity and consequently the velocity ratio. The effect of other variables have no relevance to the present study.

In Part 9 (14) Kruyer, Redberger and Ellis solved analytically the case of a free-flowing, infinitely long capsule in laminar flow and at varying clearances. It was shown that the pressure ratio at constant throughput was equal to the flow ratio at constant pressure gradient when the annular flow was laminar.

$$\text{i.e. } R_p = \frac{(dp/dz)_c}{(dp/dz)_f} \bigg|_{Q = \text{const}} = \frac{Q_f}{Q_c + Q_{\text{ann}}} \bigg|_{\frac{dp}{dz} = \text{const}} \quad (2.2)$$

Using this relationship, pressure and velocity ratios were calculated for a range of diameter ratios from 0.25 to 0.97

and capsule positions from concentric to fully eccentric. These calculations gave an almost linear plot of  $R_p$  vs.  $R_v$  for varying clearances. For a number of diameter ratios, clearance was plotted against  $R_v$  and  $R_p$  independently. Experimental data from  $\frac{1}{2}$ ,  $1\frac{1}{4}$  and 4 inch diameter pipelines was found to agree well with the theoretical predictions on a  $R_p - R_v$  basis, though the experimental capsules were finite and of various lengths.

However, large differences did appear when capsules of different lengths were compared with each other on a basis of  $R_p$  or  $R_v$  vs. capsule velocity,  $V_c$ . On this basis, it was found that at a given  $V_c$ , the shorter capsules produced lower  $R_p$  and higher  $R_v$ . It is implicit in the theory that such changes can only be caused by an increase in clearance i.e. nose or tail lift occurring at lower  $V_c$  for the shorter capsules. Agreement with the theory on a  $R_p - R_v$  basis even for short capsules (which were probably not parallel to the pipe length) suggests that the governing parameter may not be primarily the clearance but rather the particular velocity ratio the capsule achieves. The shorter capsules may be able to achieve a higher  $R_v$  possibly because the ends produce a more efficient energy transfer from the fluid to the capsule.

Apart from this series on 'The Pipeline Flow of Capsules', an extensive photographic study of capsule behaviour in a pipeline (17) was carried out by Liddle.

Since his observations were mainly concerned with the orientation of capsule in the pipeline, they are not particularly relevant to the present study. However, Liddle also outlined a theoretical approach for predicting the various parameters governing the flow of a capsule in a pipe. Nevertheless, his analysis is not very convincing at some places.

Following his analysis, one will not only have to make use of a number of experimental results but also of a rather bad assumption. This assumption is regarding turbulent flow in the capsule-pipe annulus when the capsule is moving but there is no pressure gradient. It may be noted that such a situation forms only one part of the complete flow; the other part being the case when capsule is stationary for the applied pressure gradient. According to Liddle's theory, it is easy to see that the velocity profile in such a case is given by the dashed line in Fig. 2.1. The actual velocity profile is, however, approximated by the full line in the same figure. It is clear

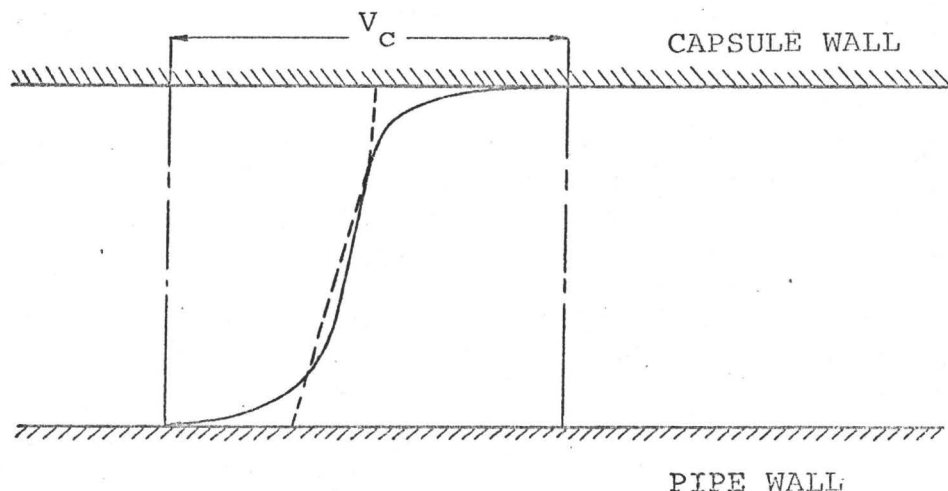


Fig. 2.1 VELOCITY PROFILE IN TURBULENT COUETTE FLOW

then that serious errors in the velocity gradient at the walls and in average velocity calculations would result from such an assumption.

This and a few other minor anomalies in Liddle's suggested outline have been removed in the present study which does not make use of any experimental result for predicting the behaviour of various parameters in a capsule pipeline flow.

### 3. THEORETICAL ANALYSIS

The free flow of a cylindrical capsule in a pipe by means of a fluid carrier is governed by the various forces acting on it. In general, the pipe may not necessarily be horizontal or the capsule parallel to it. Additionally, the density of the capsule may be different from that of the fluid. Whatever the case, a proper balance of the forces acting on the capsule determines its equilibrium velocity. These forces are summarized pictorially in Fig. 3.1 as:

- i) The weight  $W$  of the capsule acting vertically downwards.
- ii) The pressure forces  $P^*$  in the fluid acting perpendicular to the capsule surface at every point.
- iii) The shear forces  $\tau$  due to the fluid acting parallel to the capsule surface at every point.
- iv) Any frictional force  $F$  caused by contact between the pipe and the capsule.

#### 3.1 End Effects

For a capsule of finite length, there will also be end effects, particularly at the capsule nose, that is, the

---

\*  $P$  is varying both in the axial and radial directions in a more complicated manner than that indicated by Fig. 3.1.

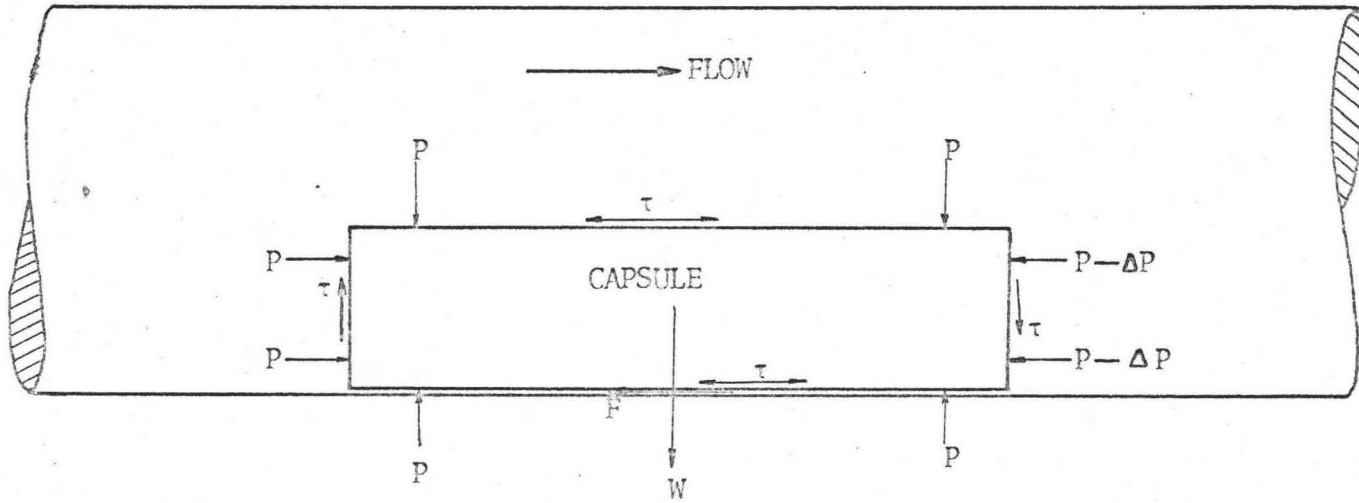


Fig. 3.1 FORCES ACTING ON A CAPSULE IN A PIPE

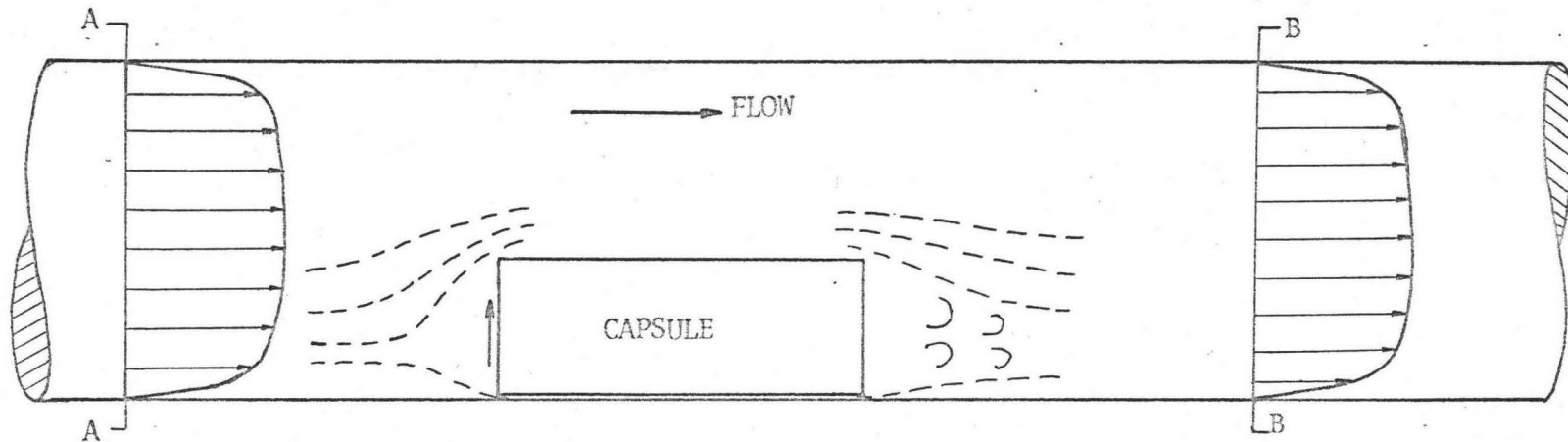


Fig. 3.2 END EFFECTS DUE TO THE CAPSULE

upstream end of the capsule. Examining the velocity profile in the free pipe, it is clear that the capsule is encountering slower moving fluid in the lower portion of the turbulent free pipe flow (Fig. 3.2). This fluid must be displaced in an upward direction into velocity deficient areas in front of the capsule or into the upper regions of the annular area. This movement of the fluid must produce an upward shear force on the capsule nose, thereby lifting it up about a fulcrum at the tail of the capsule.

The velocity profile must again return to a free pipe turbulent profile, thus producing a net downward shear force. However, this transference must occur primarily in the wake of the capsule where pressure forces are small compared to those at the nose. Note that the sections A-A and B-B in Fig. 3.2 are far removed from the capsule ends.

The end effects, therefore, make their presence felt through a proper modification of the pressure and shear forces. These forces can be resolved into components parallel and perpendicular to the capsule length plus a nose or tail-up moment on the capsule.

### 3.2 Force Balance

For a horizontal pipe and a capsule denser than the fluid, vertical components of the pressure and shear forces generally decrease the force on the pipe bottom due to the capsule weight. The resultant force multiplied by the

coefficient of friction determines the frictional force. This force decreases, with improved lubrication of the surface, as the capsule tends to lift from the pipe bottom at higher fluid velocities.

The horizontal component of pressure forces always constitutes a thrust force on the capsule, and the frictional force is always a drag force. The horizontal component of shear force can either be a thrust or a drag force, and can even be both on different parts of the capsule. This may be better understood by considering the flow in the annulus of a capsule filled pipe to be composed of two parts

- i) A pressure flow due to the applied pressure gradient, that is, when the capsule is fixed, and
- ii) A Couette flow due to the motion of capsule alone, that is, when there is no applied pressure gradient.

Examining the nature of velocity profile in the vicinity of the capsule wall (Fig. 3.3, 3.4), it is clear that the shear force exerts a thrust force  $\tau_p$  on the capsule in pressure flow but a drag force  $\tau_c$  in Couette flow. If the two types of flow can be superimposed linearly on each other to represent the total flow, the net shear force at any point on the capsule surface is the algebraic sum of  $\tau_p$  and  $\tau_c$ . This assumption of linear superposition is, of course, valid for laminar flow. But even when the annular flow is turbulent, good agreement between theory and experiment, though over a small range only, leaves little doubt about the validity of this assumption.

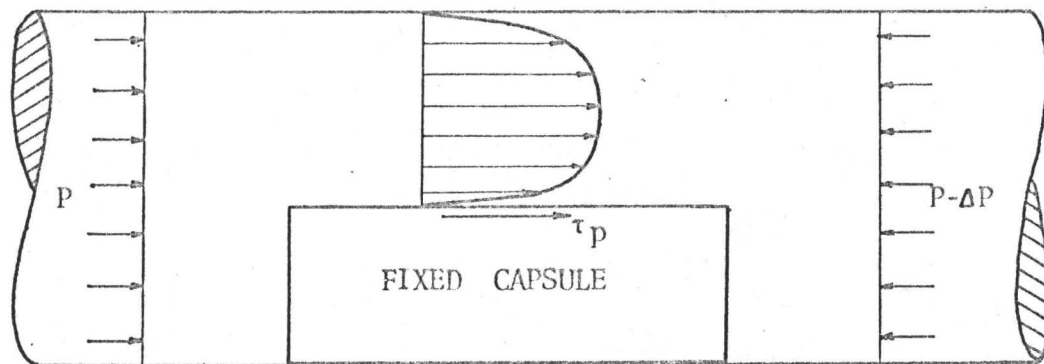


Fig. 3.3 SHEAR STRESS ON A FIXED CAPSULE

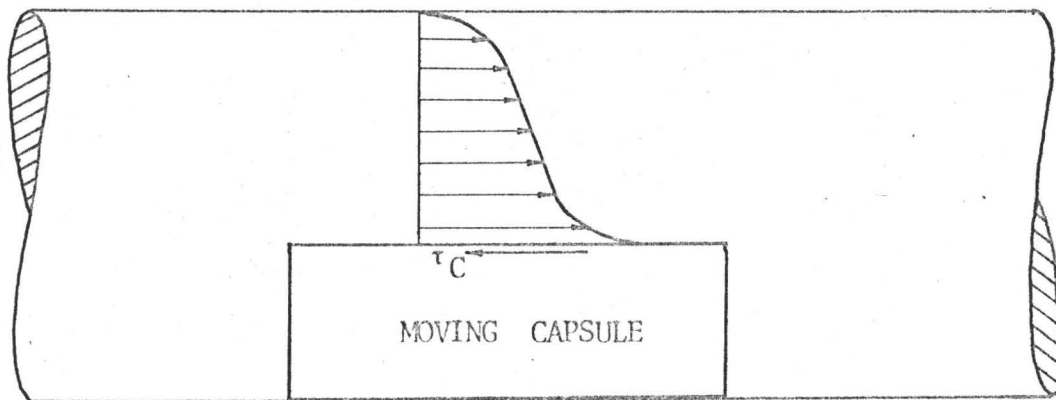


Fig. 3.4 SHEAR STRESS ON A MOVING CAPSULE

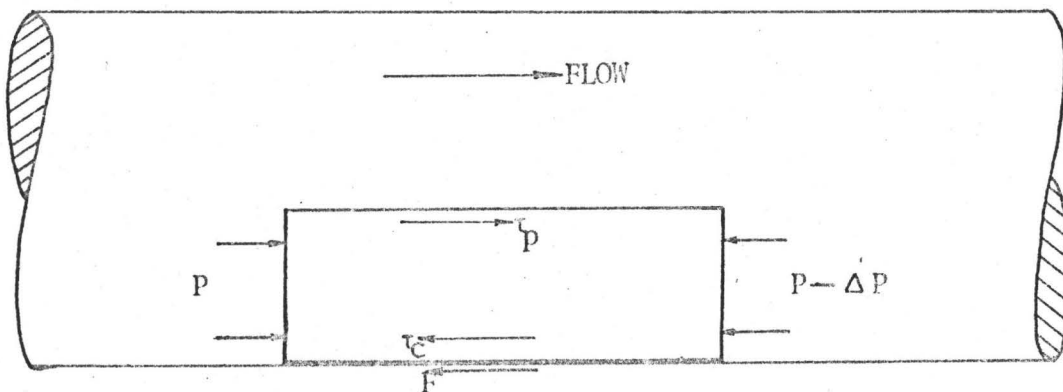


Fig. 3.5 THRUST AND DRAG FORCES ON A CAPSULE

At very low fluid velocities, a cylindrical capsule denser than the fluid will remain stationary on the pipe bottom; the thrust due to the horizontal components of pressure and shear forces being insufficient to overcome the static friction between the capsule and the pipe bottom. As the fluid velocity is increased, the static friction will eventually be overcome and the capsule will slide. This fluid velocity, at which the capsule starts to slide, is commonly known as the threshold velocity. For the capsule to move with a uniform velocity corresponding to an applied pressure gradient, the thrust forces must equal the drag forces, that is, considering Fig. 3.5,

$$\Delta P + \tau_p = F + \tau_c \quad (3.1)$$

### 3.3 Assumptions

For a very long capsule implied by this study, it is reasonable to assume that end effects as well as the tail or nose-up moments are negligible. Also, such a capsule, if denser than the fluid, will only rest on the pipe bottom should the capsule and pipe surfaces be rough since the threshold velocity of such a long capsule will approach infinity as the capsule length approaches infinity. It was, therefore, essential to assume that the surfaces were perfectly smooth. Moreover, for reasons which follow\*,

---

\* c.f. Chapter 4, Section 4.1

a fully eccentric position of the capsule could not be considered. A thin layer of fluid between the capsule and pipe bottom was therefore assumed.

Furthermore, it has been assumed that the pipe is horizontal and the fluid incompressible. Also, any adverse effect of secondary flow in the annulus has been neglected. It has been indicated in Refs. 3 and 4 that such a flow is only encountered in annuli of diameter ratio less than about 0.5. Under these assumptions, the force balance gives

Thrust due to pressure forces = drag due to shear forces

Since end effects are negligible, flow around a capsule is entirely in the axial direction so that, the pressure gradient being constant throughout, the thrust due to pressure force across the ends of the capsule is simply  $A_1 (dp/dz)_c$  per unit length of the capsule.

Further, assuming that the fluid is Newtonian, drag per unit length due to shear force is given by

$$\int \tau \, ds = \int \mu \left( \frac{dw}{dy} \right)_1 \, ds \quad (3.2)$$

where  $ds$  is an elemental arc length on the capsule surface. This integral has been evaluated numerically in the present study. In this perspective, it becomes apparent that the basic problem is the determination of velocity gradient  $(dw/dy)_1$  at a discrete number of points on the capsule surface. However, before attempting to indicate how this was

determined, an essentially physical argument will be given as a basis for the remainder of the analysis.

### 3.4 Nature of Flow in the Annulus

It is reasonable to assume that unless very high velocities with or without very low viscosities are obtained, laminar flow conditions will prevail in the small clearance between the capsule and pipe bottom when the capsule is denser than the fluid. Thus, even though the free pipe flow may be highly turbulent, it is unlikely that flow in the capsule-pipe annulus will be totally turbulent. Then, based on a previous argument that total flow in the annulus consists of a pressure and a Couette flow, three regimes (Fig. 3.6) can be defined

- a) Where both pressure and Couette flows are individually laminar
- b) Where one is turbulent while the other is laminar, and
- c) Where both are individually turbulent

While the presence of region 'a' is mandatory, that of 'b' and 'c' depends on the annular geometry, fluid characteristics and the average flow velocity.

In the light of this argument, it is necessary to formulate a criterion for determining the point of change from laminar to turbulent conditions, that is, the extent of regions 'a', 'b' and/or 'c' in the annulus. It may be pointed

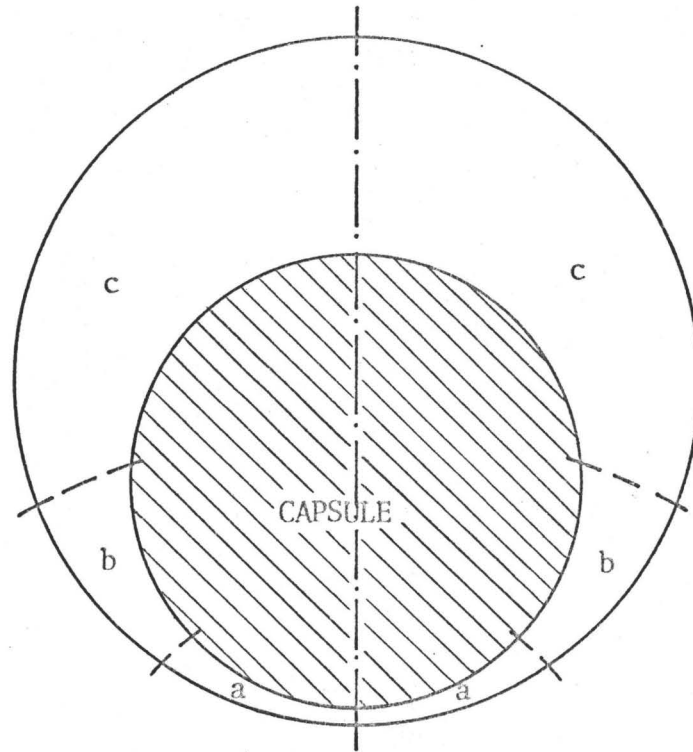


Fig. 3.6 NATURE OF FLOW IN THE ANNULUS

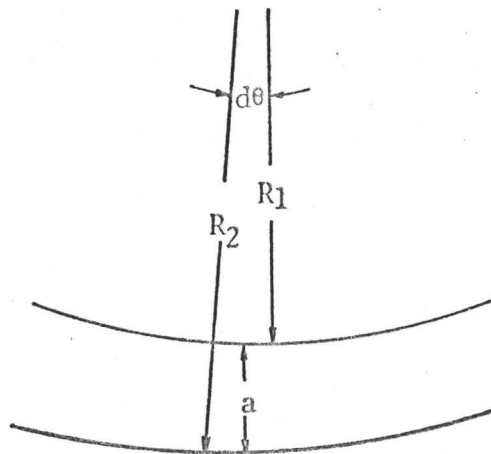


Fig. 3.7 PART OF AN ANNULUS

out that such a transition is gradual in practice, that is, the boundaries of regions a, b or c are not well defined. However, for theoretical considerations, change from laminar to turbulent flow has been assumed to be initiated as the local Reynolds number exceeds a certain critical value.

Hydraulic diameter is conventionally used as the length dimension in Reynolds number calculations. Considering a section of the annulus (Fig. 3.7), we have

$$\text{Area of the section} = \frac{R_1 + R_2}{2} d\theta \cdot a$$

$$\text{Wetted Perimeter} = (R_1 + R_2) d\theta$$

$$\therefore \text{Hydraulic diameter} = D_h = \frac{4 \times \text{area of section}}{\text{wetted perimeter}}$$

$$= 2a$$

$$\text{Then} \quad \text{Re}_{\text{Loc}} = \frac{2a w_{\text{av}}}{\nu} \quad (3.3)$$

where  $w_{\text{av}}$  the average velocity in the section, was determined from the laminar flow relations.

The critical Reynolds number for pressure flow in a pipe is conventionally taken as 2100 while for Couette flow, it has been taken as 2400. Couette (19) found transition to turbulent flow at a Re of 460 for plane Couette flow but he used a Reynolds number criterion of  $\frac{a w_{\text{av}}}{2\nu}$ . Reichardt, using the same definition as of Couette, found the critical Reynolds number to be 750. According to our definition, it, therefore, suggests a range of transition from 1840 to 3000; somewhat

similar to that encountered in free pipe flow. A value of 2400 was finally selected.

### 3.5 Velocity Profiles

In order to determine the velocity gradient at the capsule wall, a knowledge of the velocity profile in the annulus is essential. Since the total flow has already been divided into pressure and Couette flows, and since it can be both laminar and turbulent in different parts of the annulus, the complete velocity profile has been developed in the following three sections.

#### 3.5.1 Laminar Flow:

For laminar flow in a pipe with an eccentric fixed core, Heyda (2) obtained the following exact solution for the point velocity

$$w(\xi, \eta) = -\frac{1}{4\mu} \frac{dp}{dz} \left[ \frac{2c^2 \cosh \eta (1 - \coth \eta_1 \tanh \eta)}{\cosh \eta + \cos \xi} - 2cs \left( \frac{\eta_1 - \eta}{\eta_1 - \eta_2} \right) - 4cs \sum_{n=1}^{\infty} (-1)^n \frac{e^{-n\eta_2} \sinh n(\eta_1 - \eta)}{\sinh n(\eta_1 - \eta_2)} \cos n\xi \right] \quad (3.4)$$

Here,  $(\xi, \eta)$  are the coordinates of a point in the bi-polar coordinate system. Both  $\xi = \text{constant}$  and  $\eta = \text{constant}$  represent two orthogonal families of circles with  $\eta_1$  and  $\eta_2$  representing the capsule and pipe wall respectively. The bi-polar system has been discussed at length in Appendix AI.

The exact relation for total throughput (1) in such

a case is given by

$$Q = - \frac{\pi}{8\mu} \frac{dp}{dz} [R_2^4 - R_1^4 + \frac{4 s^2 c^2}{\eta_2 - \eta_1} - 8 s^2 c^2 \sum_{n=1}^{\infty} \frac{n e^{-n(\eta_1 + \eta_2)}}{\sinh n(\eta_1 - \eta_2)}].$$

(3.5)

Both the eqns. (3.4) and (3.5) are in open form, the nature of which is such that convergence becomes very slow as eccentricity approaches unity. For example, it was found by the author that at least 4000 terms were required to be summed for an eccentricity of 0.9999 and a diameter ratio of 0.9. Realizing that the velocity gradient has to be determined at a number of points on the capsule surface, the exact solution will take a considerably long time even on a high speed computer. It was, therefore, both desirable and necessary to develop an approximate method which would not only be simpler to use but also agree closely with the exact solution as far as velocity gradient and total throughput are concerned.

It was believed that a good starting point would be to use the laminar velocity profile for concentric annular flow in some suitable manner for the eccentric annulus too. A study of the annular geometry revealed that finite but small sections of the annulus such as PQRS (Fig. 3.8) could be considered to be concentric with respect to the centre O. In Fig. 3.8  $O_1$  and  $O_2$  are the centres of capsule and pipe respectively and O is the mid-point of the straight line  $O_1O_2$ ; A and B are the mid-points of arcs PS and QR

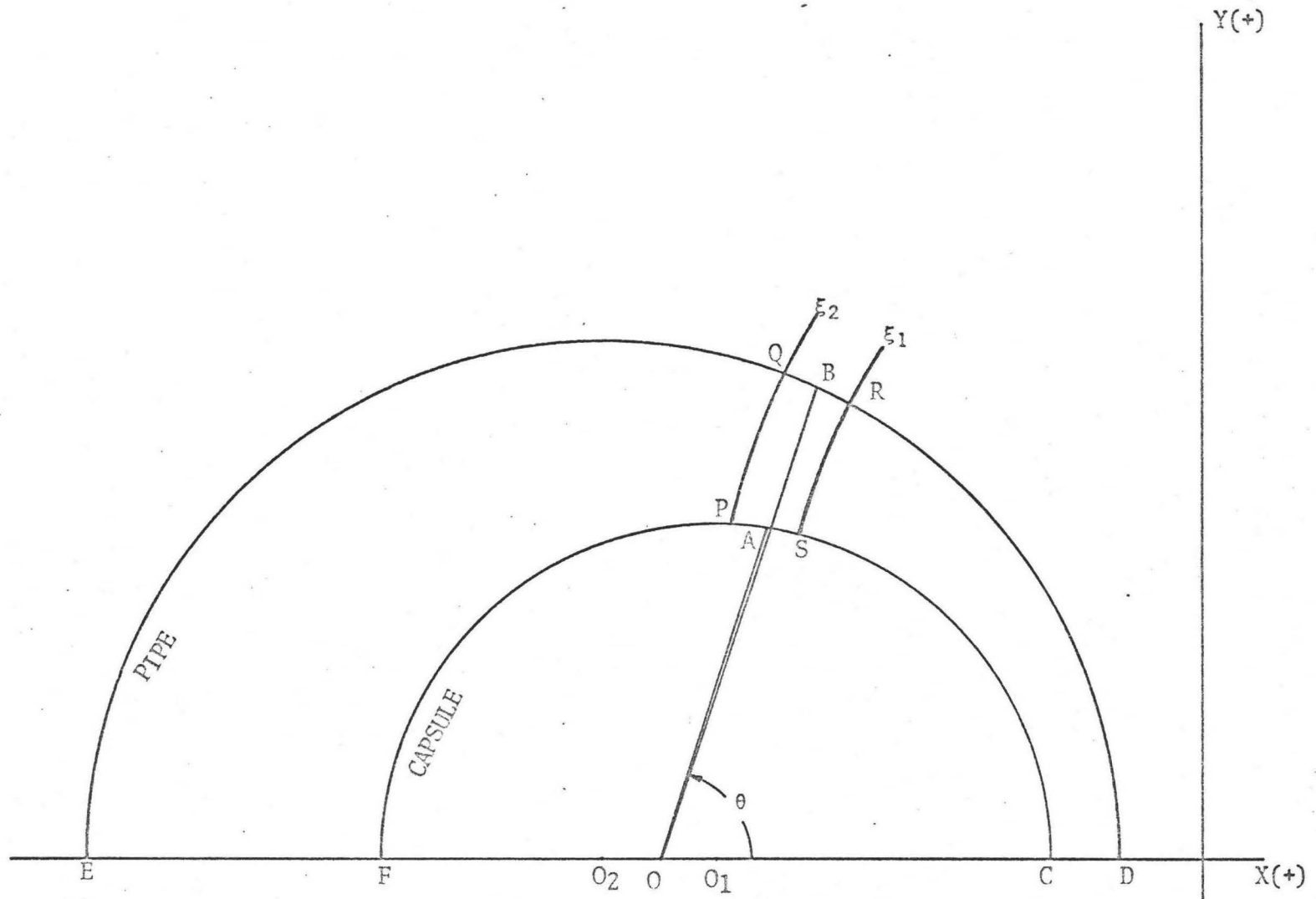


Fig. 3.8 LOCALLY CONCENTRIC ELEMENTS OF THE ANNULUS

respectively. It was found that, for the range of diameter ratios and pipe diameters studied, the maximum value of angle AOB was only about  $0.02^\circ$ . Thus, from the geometrical point of view, small sections of the annulus could be considered to be locally concentric with inner and outer radii OA and OB respectively. Note that OA and OB vary with the angular position  $\theta$ .

To justify physically the assumption of locally concentric elements, eqns. (3.8) and (3.7) were used to evaluate average velocity and velocity gradient at the capsule wall for each of 120 equally spaced elements in the annulus. Flow rate through the annulus was determined by summing the product of average velocity and corresponding cross-sectional area for all the 120 elements. When this total flow rate was compared to that obtained from eqn. (3.5), a maximum error of only 0.2% was found. Comparing the velocity gradients with those obtained by a proper use of eqn. (3.4), it was found that the errors, the maximum of which was even less than 0.5%, were both positive and negative for different elements, so that there was negligible error in the total shear force on the capsule. The approximate method is, therefore, both reliable and simpler to use. It may, however, be pointed out that for an eccentricity approaching unity, the errors may increase if diameter ratios far less than 0.9 were used.

Similar results were found for Couette flow.

Therefore, velocity profiles, that were used, are

For pressure flow:

$$w = -\frac{1}{4\mu} \frac{dp}{dz} \left[ \frac{(r_2^2 - r_1^2) \ln\left(\frac{r}{r_1}\right)}{\ln\left(\frac{r_2}{r_1}\right)} - (r^2 - r_1^2) \right] \quad (3.6)$$

so that the velocity gradient at any point is

$$\frac{dw}{dr} = -\frac{1}{4\mu} \frac{dp}{dz} \left[ \frac{r_2^2 - r_1^2}{r \ln\left(\frac{r_2}{r_1}\right)} - 2r \right] \quad (3.7)$$

and the average velocity is

$$w_{av} = -\frac{1}{8\mu} \frac{dp}{dz} \left[ (r_2^2 + r_1^2) - \frac{r_2^2 - r_1^2}{\ln\left(\frac{r_2}{r_1}\right)} \right] \quad (3.8)$$

For Couette flow:

$$w = V_c \frac{\ln\left(\frac{r_2}{r}\right)}{\ln\left(\frac{r_2}{r_1}\right)} \quad (3.9)$$

so that velocity gradient at any point is

$$\frac{dw}{dr} = -\frac{V_c}{r \ln\left(\frac{r_2}{r_1}\right)} \quad (3.10)$$

and average velocity is

$$w_{av} = V_c \left[ \frac{0.5}{\ln\left(\frac{r_2}{r_1}\right)} - \frac{r_1^2}{r_2^2 - r_1^2} \right] \quad (3.11)$$

In the above relations,  $r_1$  and  $r_2$  are the radii OA and OB respectively (Fig. 3.8) and so are different for each elementary section of the annulus. Also  $r_1 \leq r \leq r_2$ . These relations have been derived in Appendix AII.

### 3.5.2 Turbulent Pressure Flow

Turbulent flow is too complicated to be amenable to exact theoretical analysis even to this day. Only semi-empirical relations approximate the various flow fields in such a case. Eccentric annular flow is no exception to this fact at present. While investigators (4) believe that the defect law is a better approximation to the actual velocity profile than the law of the wall for an eccentric annulus, they also point out that even the defect law breaks down completely for the inner profile at low diameter ratios (3,4). Velocity profile in the region between the capsule wall and locus of maximum velocity is usually referred to as the inner profile. The defect law is

$$\frac{w_{\max} - w}{w^*} = -2.44 \ln \frac{y}{y_{\max}} + 0.8 + h\left(\frac{y}{y_{\max}}\right) \quad (3.12)$$

where  $w$  - point velocity at any angle  $\theta$  (Fig. 3.8)

$w^*$  - shear velocity =  $\sqrt{\tau/\rho}$

$y$  - distance measured outward from the capsule or pipe wall

$y_{\max}$  -  $y$  at which  $w = w_{\max}$

$h\left(\frac{y}{y_{\max}}\right)$  - correction factor (see Ref. 20)

Obviously, a prior knowledge of  $w_{\max}$  is essential for using the defect law. To author's knowledge, however, there is no way of finding  $w_{\max}$  beforehand except by making use of the universal law (law of the wall) given by the equations

$$w^+ = y^+ \quad y^+ < 5 \quad (3.13a)$$

$$w^+ = -3.05 + 5.0 \ln y^+ \quad 5 \leq y^+ \leq 26 \quad (3.13b)$$

$$w^+ = 3.8 + 2.78 \ln y^+ \quad y^+ > 26 \quad (3.13c)$$

where  $w^+ = \frac{w}{w^*}$ ,  $y^+ = \frac{yw^*}{\nu}$ ,  $w^* = \sqrt{\tau/\rho}$

The average velocity at some sections of the annulus was calculated from both the eqns. (3.12) and (3.13) when  $w_{\max}$  to be used in eqn. (3.12) was obtained from eqn. (3.13c). It was found that the average velocity calculated from eqn. (3.12) was higher than that obtained from eqn. (3.13) by about 0.5%. It is known, however, that the universal law, itself, gives a higher average velocity than the actual one (21). Thus, the universal law was finally adopted for the velocity profile in preference to the defect law.

Heyda (2) has performed a rigorous analysis to determine the locus of maximum velocities in the annulus. This analysis is for laminar flow only. Nevertheless, starting with eqn. (35) in Heyda's paper (2), reproduced as eqn. (AI-27) in Appendix AI, it is possible to calculate two values of velocity at the position of maximum velocity for each section of the annulus; one refers to the capsule wall

and the other to the pipe wall. The condition, that these two velocities must be equal, may then be used to determine the correct location of maximum velocity by changing  $\eta_m$  in a trial and error procedure and recalculating the shear velocity on the walls for the new value of  $\eta_m$ .

Shear stress at the wall in turbulent flow is also given by Newton's viscosity law

$$\tau = \mu \frac{dw}{dy}$$

since laminar sub-layer exists very close to the wall. In this sub-layer, velocity is directly proportional to the distance from the wall

$$\text{i.e. } \frac{w}{w^*} = \frac{yw^*}{\nu}$$

$$\text{or } \frac{w}{y} (= \frac{dw}{dy}) = \frac{(w^*)^2}{\nu}$$

$$\text{so that } \tau = \rho (w^*)^2 \quad (3.14)$$

This result can also be obtained by the definition of shear velocity  $w^* = \sqrt{\tau/\rho}$ .

The average velocity for any elementary section of the annulus was calculated by integrating numerically the velocity profile over the central line of the section using Simpson's and Newton's 3/8 rules described in Appendix AIII.

### 3.5.3 Turbulent Couette Flow

Even plane Couette flow, though easy to contemplate

theoretically, is very difficult to achieve in practice. It is not surprising, therefore, that no universally accepted velocity profile exists at present for such a flow. Couette flow in an eccentric annulus is further complicated by the curvature of pipe and capsule walls.

Robertson (22) has performed experimental tests on plane Couette flow. He has also compared his solutions with those obtained by other researchers (23, 24, 25, 26).

Following a basically empirical approach, Robertson found that the velocity profile in the core was very satisfactorily described by the relation

$$1 - \frac{w}{w_z} = 4.1 \sqrt{\frac{C_f}{2}} \left(1 - \frac{y}{b}\right) \quad (3.15)$$

with

$$\sqrt{\frac{C_f}{2}} = \frac{0.19}{\log_{10} \text{Re}} \quad (3.16)$$

where

$$\text{Re} = \frac{w_z b}{\nu}, \quad b = a/2, \quad w_z = \frac{V_c}{2}$$

As part of his unified theory of turbulent flow, Squire (27) has theoretically analysed plane Couette flow, deriving expressions for velocity in both logarithmic and square root form. He found that neither expression completely agreed with the experimental data of Reichardt or Robertson.

However Robertson's recent data on plane Couette flow (28) agrees well with eqn. (3.15) in the core region. Nevertheless, it is easy to see that eqn. (3.15) gives a linear velocity profile. Now the fact that the wall effect

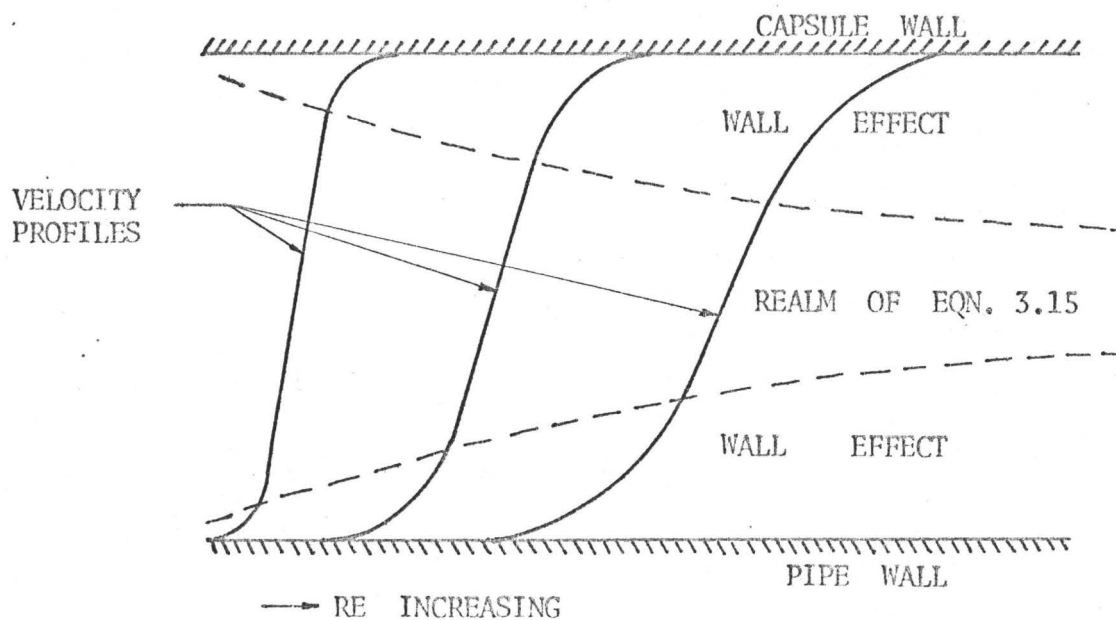


Fig. 3.9 VELOCITY PROFILES IN TURBULENT COUETTE FLOW

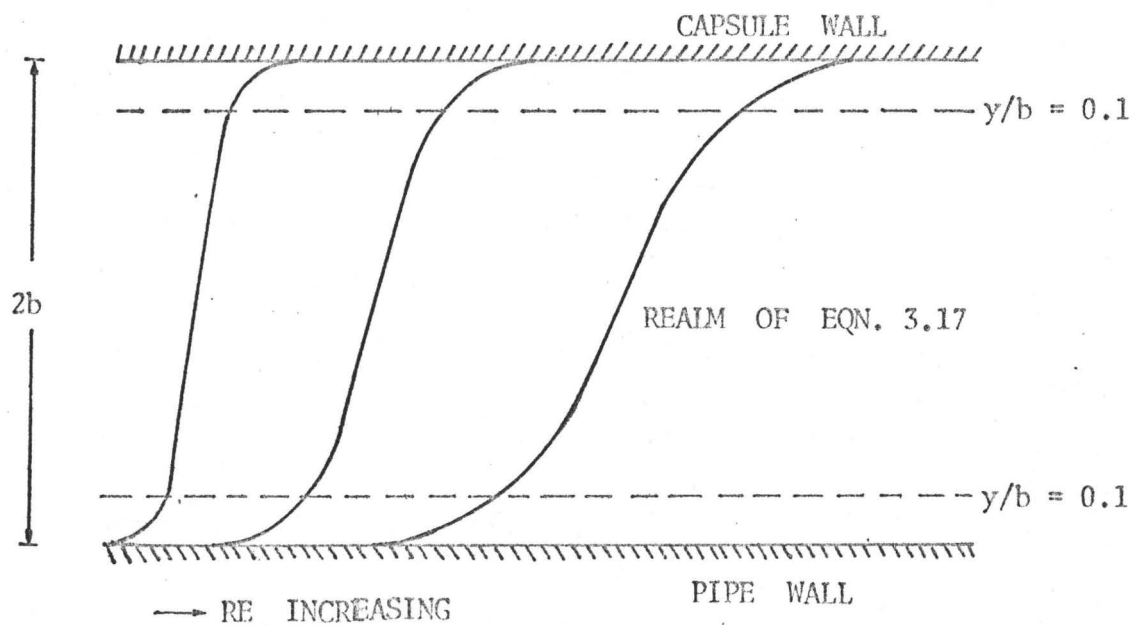


Fig. 3.10 VELOCITY PROFILES IN TURBULENT COUETTE FLOW

creeps more and more into the core (Fig. 3.9) with increasing Reynolds number, is indirectly mentioned in reference (22) but is very clear from Fig. 4 in the same reference. Thus the extent of application of eqn. (3.15) decreases as Reynolds number increases. Since in the present case, a range of Reynolds number from a little over 2400 (the critical value) to about  $10^6$  was feasible for turbulent Couette flow, it was desired to obtain some relation which may cover this range satisfactorily over a fixed core region (Fig. 3.10).

Assuming Robertson's data (22) to be the most reliable of all those presently available, the relation developed to fit the data best over a region of flow from  $y/b = 0.1$  to the point where  $w = V_c/2$  is

$$\frac{w}{w_z} = C_1 + C_2 \sqrt{y/b} \quad (3.17)$$

with 
$$1/C_1 = 2.671 - 0.119 \ln \text{Re} \quad (3.18)$$

where 
$$\text{Re} = \frac{w_z b}{\nu}$$

Also since  $w = w_z$  at  $y = b$ , eqn. (3.17) gives

$$C_2 = 1 - C_1 \quad (3.19)$$

Following Ross (29) and after a careful study of Robertson's data (22), velocity profiles developed for the wall region ( $y/b < 0.1$ ) are:

$$w = 5.6 w^* (1 + \log_{10} y^+) \quad y^+ \geq 15 \text{ and } \frac{y}{b} < 0.1 \quad (3.20a)$$

$$w = 0.8 w^* y^+ \quad 10 < y^+ < 15 \quad (3.20b)$$

$$w = w^* y^+ \quad y^+ \leq 10 \quad (3.20c)$$

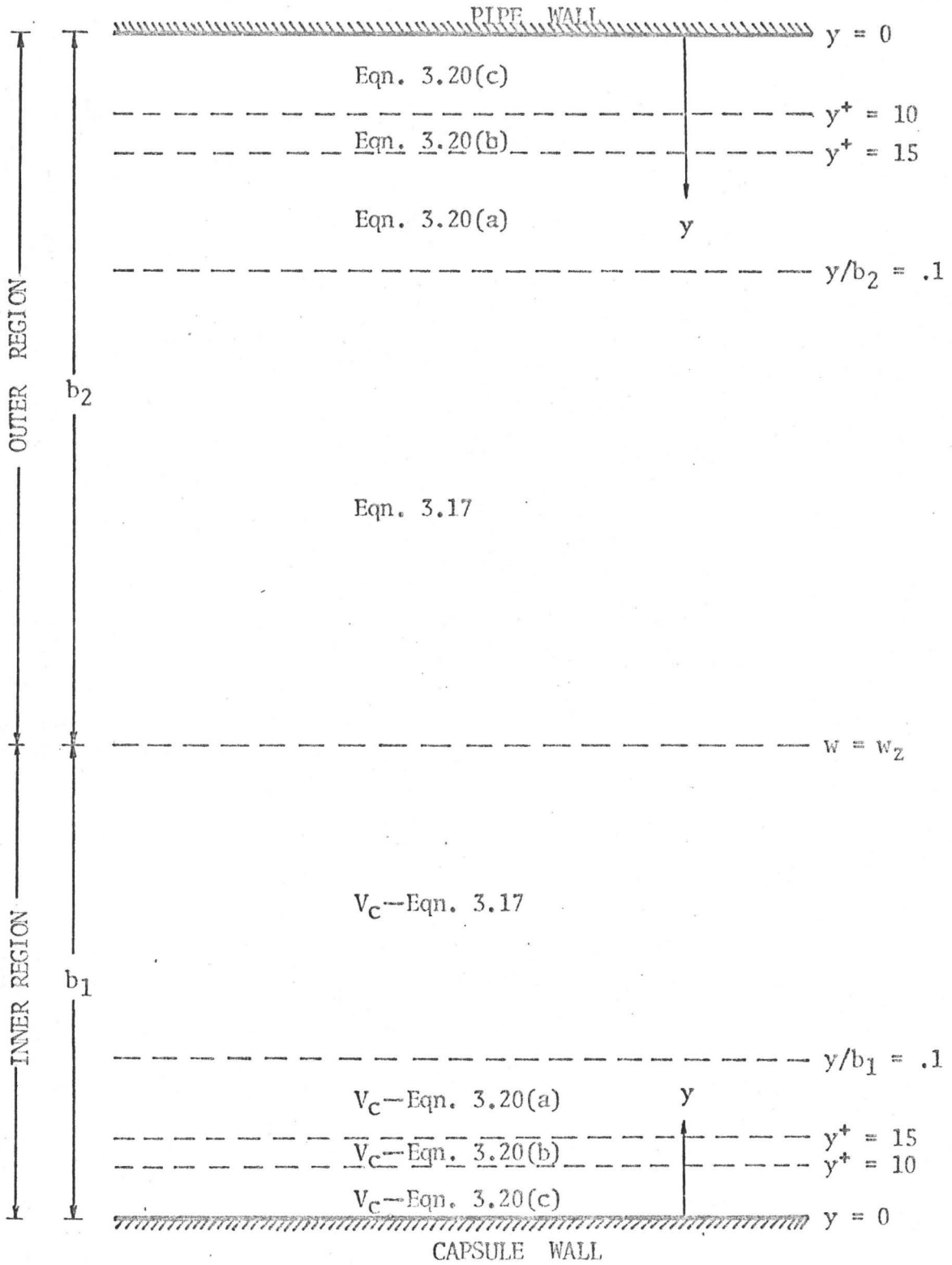


Fig. 3.11 VARIOUS REGIMES FOR VELOCITY PROFILE CALCULATION IN TURBULENT COUETTE FLOW

with  $y^+ = \frac{yw^*}{\nu}$

and  $w^* = \sqrt{\tau/\rho} = \frac{0.19 w_z}{\log_{10} Re}$  ( $\because \tau = \frac{1}{2} \rho C_f w_z^2$  where  $C_f$  is given by eqn. (3.16)).

Needless to say, eqns. (3.17) and (3.20) actually give the velocity deficiency ( $V_c - w$ ) for the inner region from the capsule wall to the point where  $w = w_z$ . Fig. 3.11 is an illustrative representation showing the various velocity profiles used for different regions.

Nothing has been said yet about the point where  $w = V_c/2$ . For a plane Couette flow, it is obviously at the mid-point of the distance between the plates. Such is not the case, however, in the present situation since the surfaces are curved. The capsule and pipe have different curved surface areas; the ratio between the two being the same as the diameter ratio  $k$ . Since in Couette flow, the shear stress on both the boundary walls is equal, the unit shear stress intensity on the pipe wall must be less than that on the capsule wall.

The shear stress is given by

$$\tau = \frac{1}{2} \rho C_f w_z^2$$

Since  $\rho$  and  $w_z$  are constant for the two walls,  $C_f$  must be different on the walls.

But

$$0.5 C_f = \left( \frac{0.19}{\log_{10} Re} \right)^2 = \frac{0.0361}{\left( \log_{10} \frac{bw_z}{\nu} \right)^2}$$

Clearly then the only variable is  $b$ . Considering Fig. 3.8, if  $S_1$  and  $S_2$  represent the arc lengths PS and QR respectively, the relation for determining  $b$  for any section of the annulus is

$$\frac{\log_{10} \left( b_2 \frac{w_z}{v} \right)}{\log_{10} \left( b_1 \frac{w_z}{v} \right)} = \sqrt{\frac{S_2}{S_1}} = E \text{ (say)}$$

Then since  $b_1 + b_2 = a = \text{clearance}$ , the above equation may be written as

$$\frac{(b_1)^E}{a - b_1} = \left( \frac{w_z}{v} \right)^{1-E} \quad (3.21)$$

This equation can only be solved for  $b_1$  by a trial and error procedure. It may be inferred from previous arguments that  $b_1$  is less than  $b_2$ . Actually, it was found that for a diameter ratio of 0.9 and an eccentricity of 0.999, the minimum value of  $b_1$  was only about  $a/4$ . From eqn. (3.17), it is clear that the velocity gradient,  $dw/dy$ , depends on the value of  $b$ ; the dependence is rather complicated since  $C_1$  and  $C_2$  are also functions of  $b$ . Then since  $b_1 \neq b_2$ , it is obvious that the slope of the velocity profile changes suddenly at the point where  $w = w_z$ , that is, it represents a point of discontinuity. In reality, however, the velocity profile should be mathematically smooth.

Let us consider Fig. 3.12 in order to see how such a discrepancy in the velocity profile could be accepted without

seriously affecting the results of this study. In this figure, the dashed line indicates the probable true velocity profile which could not be predicted at present. The full line shows the predicted velocity profile with B as the point of discontinuity while the chain-line represents the velocity profile if the pipe and capsule surfaces were plane.

Now the two important factors that would affect the results of such a study are:

- i) the velocity gradient at the walls -- increasingly so at the capsule wall, and
- ii) the average velocity given by a velocity profile.

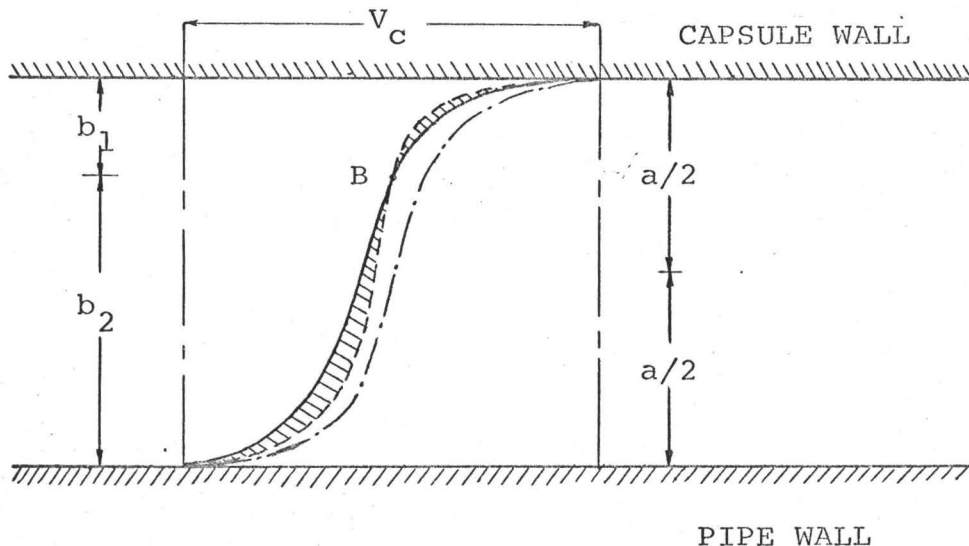


Fig. 3.12 ACTUAL AND PREDICTED VELOCITY PROFILES  
IN TURBULENT COUETTE FLOW

Examination of Fig. 3.12 shows that the predicted velocity gradient at the capsule wall is closer to the probable true one than that obtained in the case of plane-parallel plates. However,

at the pipe wall, the velocity gradient calculated from plane-parallel plate assumption is closer to the probable true one than that given by the predicted velocity profile. Thus while  $b_1$ , calculated by use of eqn. (3.21), was used for  $(dw/dy)_1$ , the value of  $b$  for determining  $(dw/dy)_2$  was taken as  $a/2$ .

It is hard to say what percentage error is involved in the velocity gradients so predicted but it is a fact that the error increases as diameter ratio decreases and as the pipe diameter increases. This observation implies that the maximum error for any capsule-pipe configuration lies at the widest gap such as region EF of Fig. 3.8. For a pipe diameter of 2 ft., an eccentricity of 0.999, and a diameter ratio of 0.9, an estimate of this error may be as high as 10-20% at the widest gap. However, since the error decreases as one proceeds from the region EF to the region CD in the annulus (Fig. 3.8) and is zero for the laminar region if any around CD, the overall error in the total shear force on the capsule may only be 3-6%.

Since this figure is usually accepted in engineering applications and since there does not seem to be any way of improving upon it at present, the velocity profile developed in eqns. (3.17) and (3.20) was accepted. For this very reason, diameter ratios less than 0.9 were not considered.

As far as average velocity is concerned, it will not be affected much since hatched areas (Fig. 3.12) tend to

cancel out each other considerably. Also, such discontinuities as may arise from the use of different equations for different regimes (Fig. 3.11) have negligible effect on the average velocity calculation. Needless to say, they have no effect on the velocity gradient at the walls.

The calculations of shear stress at the walls and average velocity for any section of the annulus were carried out in much the same way as for turbulent pressure flow.

#### 4. NUMERICAL TECHNIQUE

Before the velocity profiles developed in the previous chapter can be used to find the capsule velocity and other parameters, the plane geometry of the flow field must be described by a suitable coordinate system. Such a system requires that lines along which a velocity distribution is assumed to apply are orthogonal to both the inner and outer walls. To facilitate this, Heyda (2) developed the bipolar coordinates  $(\xi, \eta)$  of a point with respect to the Cartesian coordinates  $(x, y)$  referred to an origin on the common annular diameter to the right of the pipe wall (Fig. 4.1). The  $\eta$  coordinate family, of which the capsule and pipe walls are two members, consists of a set of circles with centres on the  $x$ -axis and the  $\xi$  family, orthogonal to the  $\eta$  family, is a set of circles with centres on the  $y$ -axis. The  $(\xi, \eta)$  system has been developed in detail in the Appendix AI.

##### 4.1 Clearance

From this development, it can be seen that the bipolar system degenerates for an eccentricity of unity. But for a very long capsule implied by this study, a position tending towards an eccentricity of one is the obvious situation. From these arguments, it is clear that a value for eccentricity

should be taken very close to unity. That a value of 0.999 was finally selected for it is based on one more argument which follows.

As explained previously, diameter ratios below 0.9 could not be considered at present without involving a considerable error in the parameters calculated. Eight diameter ratios between and including 0.9 and 0.99 were used. Defining clearance as the ratio of minimum thickness of the liquid layer under the capsule surface to the pipe diameter, the following relation for it may be developed

$$\text{clearance} = \frac{a_{\min}}{D} = \frac{1}{2}(1 - k)(1 - e) \quad (4.1)$$

Thus for an eccentricity of 0.999 the above equation gives values of clearance varying from  $5 \times 10^{-5}$  to  $5 \times 10^{-6}$  as diameter ratio,  $k$ , varies from 0.9 to 0.99. Also, the relative roughness usually ascribed to a 24 in. commercial steel pipe is  $7.5 \times 10^{-5}$ , and it increases as the pipe diameter decreases. Since pipe diameters of 4, 6, 12 and 24 in. were considered for this study, it would mean that the clearance obtained was always less than the relative roughness of a commercial steel pipe. This is not to suggest, however, that the capsule and pipe are in contact at the bottom since their surfaces have already been assumed to be perfectly smooth.

The numerical integration of eqn. (3.2) may now be considered. The product of a finite incremental arc length on the capsule surface and the velocity gradient at the mid point of that arc must be calculated at a number of points

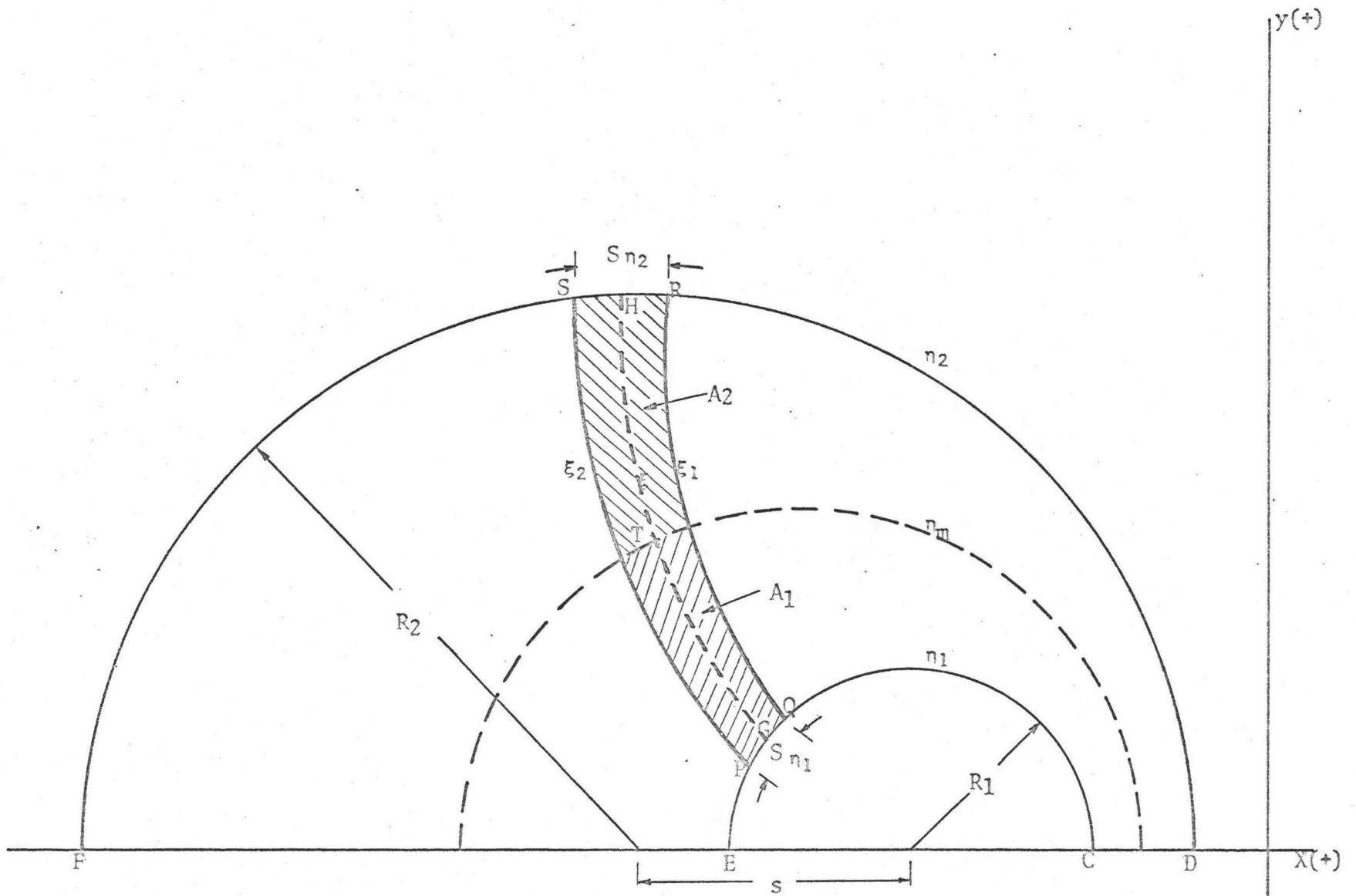


Fig. 4.1 DIVISION OF ANNULUS

all along the outside circumference of the capsule. Such products should then be summed algebraically and the sum multiplied by the coefficient of viscosity,  $\mu$ , to give the net shear force on the capsule. It may be noted that it is sufficient to consider only half of the flow field since it is symmetrical about the common annular diameter passing through the centres of pipe and capsule. The technique used to divide the annulus into a number of finite incremental divisions is described below.

#### 4.2 Division of Annulus

Briefly, the pipe circumference was divided into 120 equal parts, one of which is shown enlarged as arc RS in Fig. 4.1. For each of these parts, values were calculated for the  $\xi_1$ ,  $\xi_2$  and  $\xi$  curves passing through the points R, S and H respectively where H is the mid point of arc RS. Note that  $\xi_1$  for one element is  $\xi_2$  for the adjacent element and vice-versa, so that the first value of  $\xi_1$  on straight line CD is zero and the last value of  $\xi_2$  on EF is equal to  $\pi$ . Also it may be noted that the  $\xi$  curve will bisect the arc PQ on the capsule surface at the point G and that, in general,  $\xi \neq (\xi_1 + \xi_2)/2$  for an element. The arc lengths PQ, GT and TH, and the areas  $A_1$  and  $A_2$  were then calculated.

Within this general context, Fig. 4.2 may be considered to see how a  $\xi$  value can be calculated once the

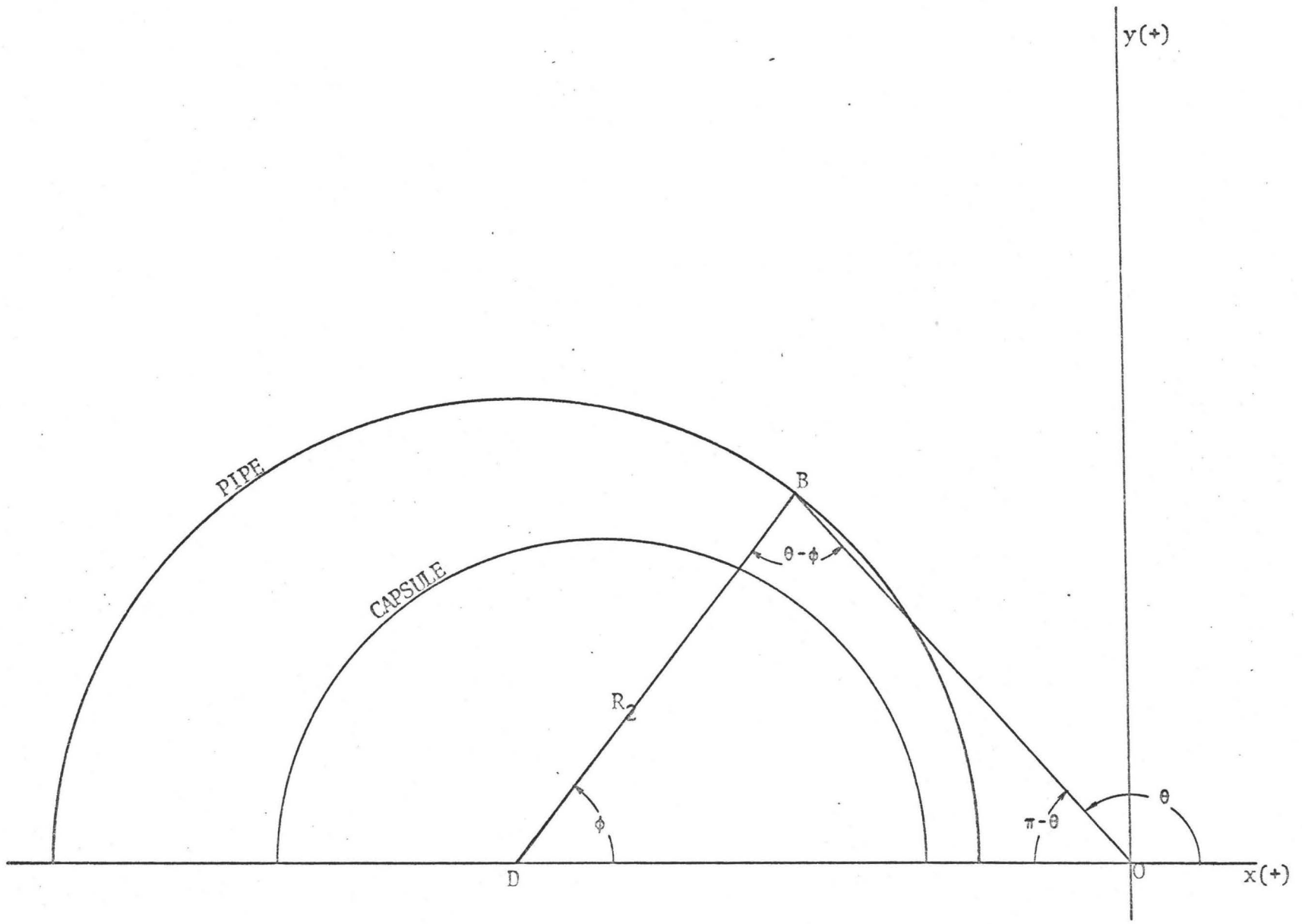


Fig. 4.2 DETERMINATION OF  $\xi$  VALUES OF ELEMENTAL SECTIONS

angular position of a point on the pipe surface is known. B is such a point in this figure while D is the centre of pipe. Since the incremental arc lengths on the pipe surface are all equal, the value of angle  $\phi$  is known. Then applying the sine law to the triangle OBD, we get

$$\frac{BD}{\sin(\pi-\theta)} = \frac{OD}{\sin(\theta-\phi)}$$

Simplifying, we obtain

$$\tan \theta = \frac{\sin \phi}{\cos \phi - \frac{OD}{BD}} \quad (4.2)$$

Also from eqn. (AI-21),

$$\tan \theta = \frac{\sin \xi}{\sinh \eta_2} \quad (4.3)$$

Then from eqns. (4.2) and (4.3),

$$\sin \xi = \frac{-\sin \phi \sinh \eta_2}{\cos \phi - \frac{OD}{BD}} \quad (4.4)$$

While BD is the pipe radius in eqn. (4.4), OD is given by  $c \coth \eta_2$  (from eqn. (AI-8)). The values of  $c$ ,  $\eta_1$  and  $\eta_2$  are given by eqns. (AI-15) to (AI-17).

### 4.3 Calculation of Geometrical Constants

After calculating the  $(\xi, \eta)$  coordinates of points such as P, Q, etc. (Fig. 4.1), the  $(x, y)$  coordinates of these points by use of eqns. (AI-18) and (AI-19) may be calculated. Then, as indicated in Appendix AI, the arc length PQ can be calculated using eqn. (AI-26).

To find the arc lengths GT and TH, and areas  $A_1$  and

$A_2$ , the value of  $\eta_m$  should be known. This was found by use of eqn. (AI-27). But since this equation holds only for laminar pressure flow, the exact value of  $\eta_m$  for any element in turbulent pressure flow was calculated by the trial and error procedure outlined in the previous chapter (Sec. 3.5.2). Calculation of GT, TH,  $A_1$  and  $A_2$  was carried out, therefore, in a different subroutine in the computer programme included in Appendix AIII. While arc lengths GT and TH were calculated in a way similar to that of PQ, the areas  $A_1$  and  $A_2$  were calculated by numerical integration of eqn. (AI-24) using a Gauss integration technique.

Considering Fig. 4.1 again, it is clear that areas  $A_1$  and  $A_2$  are changing from a minimum value around CD to a maximum value around EF. Also, this change is brought about by a continuous change in the arc lengths such as GT and TH while arc lengths such as RS are constant. Therefore, while the Gaussian integration employed in the  $\xi$  direction was a fixed 6-point one, it was varied all along the annulus from a minimum of 2-points near CD to a maximum of 16-points near EF; the variation affected by an increase of 2-points after every 15 elements.

It may be mentioned that when the total annular area obtained by a summation of incremental areas  $A_1$  and  $A_2$  was compared to that given by  $\pi(R_2^2 - R_1^2)$ , complete agreement was found up to at least the eighth significant figure; the maximum error being only  $5 \times 10^{-7}\%$ . Also the incremental arc

lengths on the capsule surface were almost equal to each other for the geometries studied.

## 5. RESULTS AND DISCUSSION

The results of numerical computations are presented in Figs. 5.1 to 5.10. Considering these figures, it may be observed that these results were obtained for average velocities of approximately 1 to 10 ft/sec in pipes of diameters 4, 6, 12 and 24 inches with capsule-to-pipe diameter ratios of 0.9 to 0.99. For a fixed eccentricity of 0.999, the computations were carried out for two liquid carriers -- one being water and the other an oil with a specific gravity of 0.85 and dynamic viscosity of 10 cp. A few general remarks, not observable from these figures, will be made first before discussing the results as such.

It was found that if the pressure flow in the annulus was turbulent, the point of maximum velocity was nearer to the inner wall than in the case of laminar flow; the deviation decreasing as the diameter ratio was increased. Similar observations were made experimentally by Brighton and Jones (3). Furthermore, it was observed that the eccentricity and diameter ratio could not be combined into one parameter -- clearance. The reason is contained within eqn. (4.1); one value of clearance can be associated with different combinations of eccentricity and diameter ratio. However, since the annular geometry changes with such combinations, the various parameters governing the capsule flow will be seriously affected. Also, it is implied that, unless otherwise

specified, eccentricity of the capsule-pipe system is constant for whatever follows in this chapter.

### 5.1 f-Re Plot (Fig. 5.1)

Now consider Fig. 5.1 illustrating the variation of friction factor with Reynolds number. For the capsule-pipe system, Reynolds number was based on hydraulic diameter and average annulus velocity while the friction factor was calculated in the standard Darcy-Weisbach form. The relations are

$$\text{Re} = \frac{(D-d) V_{\text{ann}}}{\nu} \quad (5.1)$$

and

$$f = \left( \frac{dp}{dz} \right)_c \frac{2D}{\rho V_{\text{ann}}^2} \quad (5.2)$$

Fig. 5.1 also shows a similar variation in the case of a perfectly smooth free-pipe flow for comparative purposes. It may be noted, however, that the average velocity has to be used for the free-pipe case together with pipe diameter instead of hydraulic diameter as before for Reynolds number calculation. The relations this time are

$$\text{Re}_f = \frac{D V_{\text{av}}}{\nu} \quad (5.3)$$

and

$$f_f = \left( \frac{dp}{dz} \right)_f \frac{2D}{\rho V_{\text{av}}^2} \quad (5.4)$$

Any discontinuities in the plots are due to transition from laminar to turbulent flow.

### 5.1.1 Effect of $d/D$ on $f$

It may be observed from Fig. 5.1 that with increasing diameter ratio the friction factor increases at a fixed Reynolds number. The reasons for such a behaviour are rather complex. Firstly, for a fixed pipe diameter, the cross-sectional area of the capsule increases with the square of diameter ratio thus requiring a higher pressure gradient for its movement. Secondly, as the diameter ratio increases, the annular area decreases so that at least the same change of velocity has to take place over a shorter distance between two points. The velocity gradients and hence the shear stresses are larger on the capsule surface. This increase in drag force has to be counterbalanced by a further increase in the pressure gradient. Thirdly as given by Eqn. (5.1), the Reynolds number is directly proportional to  $V_{ann}$  and  $(D-d)$ . With an increase of  $d/D$ , the hydraulic diameter,  $(D-d)$  or  $D(1-d/D)$ , decreases so that in order to keep the same value of  $Re$ , a higher  $V_{ann}$  will be required. It will further require a higher pressure gradient though not necessarily a higher friction factor since the latter is directly proportional to  $dp/dz$  but inversely to  $V_{ann}^2$ . It seems, however, that the first two factors outweigh the third even if it is in opposition to them.

### 5.1.2 $f-Re$ in Comparison to $f_f-Re_f$

It is clear from Fig. 5.1, that the whole pattern

of variation of  $f$  with  $Re$  in a capsule-pipe system is similar to that in a free pipe. For laminar flow in the annulus, the relation between  $f$  and  $Re$  is not only linear but the straight line is also parallel to that in the case of a free pipe suggesting thereby that, within the range of investigation, the product of  $f$  and  $Re$  is a constant that varies only with the diameter ratio. It may be recalled that this product is equal to 64 for flow in a free pipe. The following table gives the value of this constant for different  $d/D$  in a capsule-pipe system.

| Diameter<br>Ratio ( $d/D$ ) | The Product<br>$f \cdot Re$ |
|-----------------------------|-----------------------------|
| 0.9                         | 259.2                       |
| 0.93                        | 320.5                       |
| 0.95                        | 380.6                       |
| 0.96                        | 419.9                       |
| 0.97                        | 468.3                       |
| 0.98                        | 529.3                       |
| 0.985                       | 566.1                       |
| 0.99                        | 608.6                       |

The above values are for an eccentricity of 0.999. When the annular flow is turbulent, it seems that the friction factor decreases and reaches an asymptotic value at some high enough Reynolds number -- much the same as in free pipe flow. The

various curves for different diameter ratios will become parallel and almost horizontal.

Another significant point is that the  $f$  vs.  $Re$  curve for free pipe flow crosses over those for the capsule-pipe system in the turbulent region. Such a crossover occurs at relatively high average velocities which increase rapidly as the diameter ratio changes from 0.9 to 0.99. Once in this region, the pressure gradient required to obtain a certain average velocity in the capsule-pipe system will be lower than that required for the same average velocity in a free pipe. However, in practice for a finite capsule, some of the basic assumptions underlying this study will be violated at the high velocities required for such an advantage. For example, the axis of a finite capsule will no longer be parallel to the pipe axis due to nose or tail-up moments. This changed capsule attitude will markedly affect the various parameters. It is, therefore, doubtful to say at this stage whether such an advantageous situation is practicable. Experimental tests at such high velocities should be able to clarify this position.

### 5.1.3 Critical Reynolds Number

Another point which may be noted from Fig. 5.1 is with regard to the critical Reynolds number where transition from laminar to turbulent flow takes place in the capsule-

pipe system. At a first glance, it may appear that this critical Re range (approximately 1000 to 1500 for different diameter ratios) is far less than the usually accepted value of 2100 for a free pipe flow. It should be noted, however, that the parameters for the length dimension and velocity used for the Reynolds number calculation are different in the two cases. While Re for the capsule-pipe system is based on  $(D-d)$  and  $V_{ann}$ , it is based on  $D$  and  $V_{av}$  for the free pipe flow (eqns. 5.1 and 5.3). The ratio of  $(D-d)$  to  $D$  is  $(1-k)$  which obviously decreases with increasing diameter ratio and for a value of  $k$  equal to 0.9, this ratio is 0.1. Also when the velocity ratio,  $R_v$ , is greater than 1.0,  $V_{ann}$  is less than  $V_{av}$ . For  $R_v$  less than 1.0, however,  $V_{ann}$  is greater than  $V_{av}$ . But since  $R_v$  was never less than 0.92 in the present investigation, the maximum ratio of  $V_{ann}$  to  $V_{av}$  was only 1.35. Obviously then at a  $V_{av}$  that nearly corresponds to the critical Reynolds number in a capsule-pipe system, the corresponding Re in a free pipe would be far greater than 2100, that is, well into the turbulent region.

For example, with water flowing in a 4 in. diameter pipe having a capsule of diameter ratio 0.97, the flow is laminar at a  $V_{av}$  of 2 ft/sec but if there were no capsule in the pipe, the flow would be turbulent; the free-pipe Re at that  $V_{av}$  being about  $6 \times 10^4$ . This fact that the presence of a capsule in a pipe suppresses turbulence has also been experimentally observed by many researchers. But up until

now, due to uncertainty about the knowledge of critical Reynolds number for a capsule-pipe system, various methods have been used to classify the flow as either laminar or turbulent. Some research workers have even refrained from making such a classification. It may, however, be mentioned that Ellis and Bolt (12) suggested a critical Re of about 1000 similar to that observed in Fig. 5.1.

## 5.2 $R_p$ - $R_v$ Plot (Fig. 5.2)

This figure can be best discussed in three stages. To start with, the flow is laminar both in the annulus and in the free pipe at low enough velocities so that it falls somewhere in the linear portion of the  $f$ -Re plot in Fig. 5.1. Now since

$$f \propto \frac{dp/dz}{V^2}$$

it may be seen that from eqns. (2.2), (5.2) and (5.4),  $R_p$  may also be defined as

$$R_p = \frac{f}{f_f} \left( \frac{V_{ann}}{V_{av}} \right)^2 \quad (5.5)$$

In laminar flow,  $V_{ann} \propto V_{av}$  and since the ratio  $f/f_f$  is also constant for any diameter ratio (Fig. 5.1), there will only be one  $R_p$  for any value of average velocity once the diameter ratio is fixed. It may be pointed out at this stage that while the value of  $R_p$  depends on the nature of flow both in the annulus and in the free pipe,  $R_v$  is independent of the

nature of free pipe flow since it is a ratio of  $V_c$  to  $V_{av}$ . For laminar annular flow because  $V_c$  is directly proportional to  $V_{av}$ ,  $R_v$  will also be independent of  $V_{av}$  at a fixed  $d/D$ . Obviously then, for a fixed diameter ratio and eccentricity, there is only one point on a  $R_p - R_v$  plot for any  $V_{av}$  as long as the resulting flow is laminar both in the annulus and in the free pipe. Considering Fig. 5.2, this point is the starting point of the vertical linear portion at the top of the curves. Note that this point could be included in Fig. 5.2 only by making the  $R_p$ -axis discontinuous at some point in between.

Consider now an increase in  $V_{av}$  so that the flow in the annulus is still laminar but in a free pipe, it is turbulent for the same total flow rate. That such a situation is possible has already been explained in the discussion on the  $f-Re$  plot. Obviously then  $R_v$  will still be constant and the same as in the previous case since it is independent of the nature of free-pipe flow.  $R_p$ , on the other hand, will decrease with increasing  $V_{av}$  since the friction factor  $f_f$  in eqn. (5.5) is higher for turbulent flow in the free pipe than that if the flow were laminar at the same Reynolds number. On Fig. 5.2, therefore, the  $R_p - R_v$  plot will be a vertical straight line the position of which varies with the diameter ratio.

When  $V_{av}$  is increased further so that flow in the annulus also becomes turbulent, the value of velocity ratio

will change since  $V_c$  is no longer proportional to  $V_{av}$ . It has been observed that the velocity ratio increases with the average velocity till it tends to become constant -- a stage which, for its accomplishment, requires a lower  $V_{av}$  for a higher diameter ratio capsule. Thus while the velocity ratio for a capsule of diameter ratio 0.99 is almost always constant with the average velocity, that for a 0.9 diameter ratio capsule is changing widely over the range of investigation.

In this region, the pressure ratio is also continuously decreasing with increasing  $V_{av}$  though at a lower rate than that in the second case when flow is laminar in the annulus but turbulent in the free pipe. The reason for this change in rate lies in the plots of Fig. 5.1 for turbulent flow. When the nature of annular flow changes from laminar to turbulent, the slope of the  $f$ - $Re$  plot decreases in much the same fashion as for free-pipe flow. The rate of change of slope in the two cases is different, so much so that while the curve for the capsule-pipe system is over that for free pipe to start with, the two curves cross over each other eventually and change respective positions at high Reynolds numbers. As explained previously, the value of  $R_p$  will drop below unity but will eventually become constant at some value between 0 and 1 since the  $f$ - $Re$  curves for the free pipe and the pipe with a capsule in it tend to become horizontal at quite high Reynolds numbers. As mentioned earlier, however,

the practicability of such a case is doubtful at the high average velocities involved.

It may also be noted that for the most part in Fig. 5.2, the velocity ratio is greater than unity which implies that the average velocity in the capsule-pipe system is less than the capsule velocity. The reason for this is that under conditions of high velocity ratio, at most only a small proportion of the fluid around the top of the capsule will have a velocity greater than that of the capsule. The fluid between the bottom of pipe and capsule and that around the sides will be moving relatively slowly. The total effect can result in an average velocity falling short of the capsule velocity thereby resulting in a velocity ratio greater than unity.

#### 5.2.1 Effect of $d/D$ and $V_{av}$ on $R_v$

Another important result, inherent in Fig. 5.2, is the effect of diameter ratio on the velocity ratio. At low average velocities, the velocity ratio increases with diameter ratio increasing up to 0.97 beyond which it starts to decrease. As the average velocity rises, however, the curves for the smaller diameter ratio capsules overtake those of the larger. This observation can be made from the blend of curves near the  $R_v$ -axis in Fig. 5.2 together with Figs. 5.3 and 5.4. The reason for such a behaviour of  $R_v$  with

increasing diameter ratio and at varying average velocity lies in the change of position of the capsule relative to the velocity distribution in the pipe as the capsule diameter increases. A small diameter capsule, occupying as it does the lower part of the pipe, is situated in a relatively low velocity region; as the capsule diameter increases, the capsule finds itself in a region of increasing mean local velocity. Then as explained earlier during the discussion of Fig. 5.1 (Sec. 5.1.1), the drag force on the capsule due to shear stresses will increase with the diameter ratio. However, since the cross-sectional area of the capsule increases with the square of its diameter, the thrust force due to the pressure gradient will increase. Also the weight per unit length of a capsule increases with the square of its diameter so that this increase in the weight to be moved would tend to reduce the velocity ratio as the diameter ratio increases. The net result will, of course, depend on a proper balance of these opposing effects. It is not surprising, therefore, that at low  $V_{av}$ , the velocity ratio reaches a maximum at a diameter ratio of 0.97.

Such a behaviour would also be expected from the fact that at a  $d/D$  of 1.0, the capsule would be a piston and the velocity ratio would be unity. Since the velocity ratio has already become  $> 1$  for a  $d/D = 0.95$ , it would be expected that a trend toward lower  $R_v$  must ensue from a diameter ratio somewhere between 0.95 and 1.0. It has been

suggested (9) that for very long cylinders or trains of cylinders, the maximum velocity ratio may be obtained at a  $d/D$  ratio of about 0.95. The present observation is thus close to this suggestion. Lastly, it may be noted that the  $R_p$ - $R_v$  plots in Fig. 5.2 are not affected by the pipe diameter and fluid properties.

### 5.3 $R_p$ - $V_{av}$ Plots (Fig. 5.3, 5.4)

The concept of pressure ratio is relatively recent compared with that of velocity ratio. Accordingly, the behaviour of this ratio has been studied in more detail than that observable from Fig. 5.2. While Fig. 5.3 shows the variation of  $R_p$  with  $V_{av}$  for different pipe diameters and  $d/D$  ratios when the liquid carrier is water, Fig. 5.4 shows a similar variation for an oil as the liquid carrier. The curves are all similar though suitably displaced as the diameter ratio, pipe diameter or the liquid carrier changes.

#### 5.3.1 Effect of $d/D$ on $R_p$

As explained in the discussion of Fig. 5.1 (Sec. 5.1.1) a greater pressure gradient is required to move a higher diameter ratio capsule at a given  $V_{av}$  once the pipe diameter and fluid carrier are fixed. However, since the pressure gradient required for the same flow rate through a free pipe is

independent of diameter ratio,  $R_p$  would increase with an increase in diameter ratio (see eqn. (2.2)).

### 5.3.2 Effect of $V_{av}$ on $R_p$

It has already been explained while discussing Fig. 5.2 (Sec. 5.2) that as  $V_{av}$  increases the pressure ratio decreases at a faster rate in the beginning but tends to become constant later on at high average velocities. From Fig. 5.3 and 5.4 it is clear that this condition of near constancy of  $R_p$  is accomplished at a relatively lower average velocity for a less viscous liquid carrier. The explanation of this behaviour lies in Fig. 5.1. Since with all parameters except viscosity held constant, a more viscous liquid will result in a lower Reynolds number at a given  $V_{av}$ , the nature of the turbulent portion of  $f$ - $Re$  plot in Fig. 5.1 suggests that to get to the nearly horizontal part of the curve a higher  $V_{av}$  is required for a more viscous liquid. It should be noted that operation in this portion of Fig. 5.1 is essential for attaining a nearly constant value of  $R_p$ .

### 5.3.3 Effect of $D$ on $R_p$

Inherent in Figs. 5.3 and 5.4 is also the effect of pipe diameter on pressure ratio. With other parameters held constant, a larger pipe diameter will result in a greater

annulus area as well as greater capsule cross-sectional area. At a given  $V_{av}$ , the velocity gradients at the capsule wall will be smaller since about the same change of velocity from one point to another will take place over a greater distance. The drag force due to shear stresses will, therefore, be lower on a capsule in a larger diameter pipe. Since for an equilibrium velocity of the capsule this drag force has to be counterbalanced by the thrust force due to pressure gradient, it is clear that a lower  $(dp/dz)_c$  will be required. Moreover, since the thrust force is given by the product of  $(dp/dz)_c$  and the cross-sectional area of the capsule (which increases with  $D^2$  for a fixed diameter ratio), it follows that the pressure gradient required for a given  $V_{av}$  will be still lower. An increase in pipe diameter, therefore, results in a marked decrease in  $(dp/dz)_c$  required to attain a certain  $V_{av}$ . For example, at a  $V_{av}$  of about 10 ft/sec for water in a 4 inch diameter pipe, the value of  $(dp/dz)_c$  was found to be at least 14 times as much as that in a 24 inch diameter pipeline at the same  $V_{av}$ ; the ratio increased to about 36 for a  $V_{av}$  of nearly 1 ft/sec.

However, with an increase in pipe diameter, the free pipe Reynolds number increases and, therefore from Fig. 5.1, the friction factor  $f_f$  decreases. Since  $dp/dz$  is in general proportional to  $f/D$ , the pressure gradient  $(dp/dz)_f$  will also decrease with an increase in pipe diameter. This change in  $(dp/dz)_f$ , though in the same direction as that for  $(dp/dz)_c$ ,

will in any case be relatively smaller in magnitude since  $(dp/dz)_f$  is almost inversely proportional to  $D$ ; the effect of decrease in  $f_f$  with  $D$  being very small. Since  $R_p$  is a ratio of  $(dp/dz)_c$  to  $(dp/dz)_f$ , the net effect will be to decrease  $R_p$  as the pipe diameter increases. An observation of Figs. 5.3 and 5.4 will, however, reveal that the rate of decrease of pressure ratio with  $D$  declines appreciably as the pipe diameter continues to increase.

#### 5.3.4 Effect of Fluid Characteristics on $R_p$

A comparison of the results in Fig. 5.3 with those in Fig. 5.4 indicates that  $R_p$  increases as the fluid carrier becomes more viscous. The reason for this behaviour is perhaps not immediately apparent and follows similar conflicting arguments as for the effect of  $D$  on  $R_p$ . As the fluid viscosity increases, the drag force due to shear stresses on the capsule also increases since  $\tau = \mu \frac{dw}{dy}$ . To counter-balance this increased drag force, a higher pressure gradient  $(dp/dz)_c$  will obviously be required. Additionally as  $v$  increases, the free pipe Reynolds number decreases and so the friction factor  $f_f$  increases. However, since  $dp/dz$  is in general proportional to the product  $\rho \cdot f$  and since the density,  $\rho$ , of oil was taken as 0.85 times that of water, the value of  $(dp/dz)_f$  will, if at all, increase only very little in comparison to that of  $(dp/dz)_c$ . The pressure ratio

will, therefore, increase as the viscosity of the fluid increases.

#### 5.4 Energy Requirements vs. $V_{av}$ (Fig. 5.5, 5.6)

Fig. 5.5 and 5.6 show the variation of  $(\text{hp}/\text{ft})/(\text{ft}^3/\text{sec})$  with various variables such as average velocity, diameter ratio, pipe diameter and the fluid properties. The energy requirements in capsule-pipeline work have been generally expressed in the past in terms of hp-hr/ton-mile but these units could not be used in the present study since this study holds for any density of the capsule provided that a proper clearance is obtained along with other pertinent factors. The energy per unit length of pipe hp/ft, was therefore divided by the volumetric flow rate  $Q_c$  due to the movement of the capsule alone to get the parameter  $(\text{hp}/\text{ft})/(\text{ft}^3/\text{sec})$ .

It may be noted that this ratio can be converted easily into the conventional form of hp-hr/ton-mile by dividing by the capsule density and a proper conversion factor. Additionally, hp/ft is given by the relation

$$\text{hp}/\text{ft} = (\text{dp}/\text{dz})_c \frac{Q_T}{550}$$

so that expressing  $Q_T$ , the total volumetric flow rate through the pipe, in terms of  $V_{av}$ , we get after dividing by  $Q_c$  that

$$(\text{hp}/\text{ft})/(\text{ft}^3/\text{sec}) = \frac{1}{550} (\text{dp}/\text{dz})_c \left(\frac{V_{av}}{V_c}\right) \left(\frac{D}{d}\right)^2 \quad (5.6)$$

#### 5.4.1 Effect of $V_{av}$ on the Energy Requirements

Fig. 5.5 and 5.6 indicate that  $(hp/ft)/(ft^3/sec)$  increases with the average velocity. It has been noted already that a greater pressure gradient is required to attain a higher  $V_{av}$  but the velocity ratio  $(V_c/V_{av})$  also increases with  $V_{av}$ . The increase in  $R_v$  is, however, very small. Within the entire range of investigation, the velocity ratio only increased from a minimum of 0.92 to a maximum of nearly 1.06. On the other hand, the increase in  $(dp/dz)_c$  required for a higher  $V_{av}$  is comparatively large. Thus while in laminar annular flow  $(dp/dz)_c$  is directly proportional to  $V_{av}$ , in turbulent flow,  $(dp/dz)_c$  has to be more than doubled for twice the  $V_{av}$ . Eqn. (5.6) will, therefore, give a higher value of energy required for a larger  $V_{av}$ . The rate of increase of  $(hp/ft)/(ft^3/sec)$  with  $V_{av}$  is maximum to start with and decreases to a nearly constant value at high  $V_{av}$ .

#### 5.4.2 Effect of $d/D$ on the Energy Requirements

With an increase in diameter ratio,  $d/D$ , one may expect from eqn. (5.6) that  $(hp/ft)/(ft^3/sec)$  will decrease. This is not so, however, since  $(dp/dz)_c$  increases with an increase in  $d/D^*$ . Though the ratio  $V_{av}/V_c$  also decreases

---

\*c.f. Section 5.1.1 for an explanation of this.

with  $d/D$  increasing up to 0.97 at least, it appears that the increase in  $(dp/dz)_c$  offsets all the opposing effects. This is not difficult to understand once it is realized that for a  $d/D$  ratio of 0.99, the pressure gradient required for a given  $V_{av}$  is at least 36 times as much as for a  $d/D$  of 0.9 with the same pipe diameter.

#### 5.4.3 Effect of D and Fluid Properties on the Energy Requirements

Again with an increase in pipe diameter, it may seem from eqn. (5.6) that the energy required will increase. However since the ratios,  $d/D$  and  $V_c/V_{av}$ , are constant, a lower  $(dp/dz)_c$  required with a larger pipe diameter will result in a lower value of  $(hp/ft)/(ft^3/sec)$ . Considerable economics in power requirements can, therefore, be effected by using a larger diameter pipe. Also with other parameters held constant, a more viscous liquid carrier will need a higher energy input since a larger pressure gradient is required.

#### 5.5 Solution of a Problem in General

At this stage, it may be proper to point out that Figs. 5.1 to 5.6 have been drawn not only with a view to enable the effect of various parameters on important variables to be studied but also to enable the problem of capsule-pipeline flow to be solved completely should the

main parameters lie within the range of investigation. For example, if in a particular problem, the liquid carrier is neither water nor the oil specified in this study or the eccentricity is not 0.999, etc., the computer programme included in Appendix AIII will have to be run. The approach to an arbitrary problem with the use of Figs. 5.1 to 5.6 will be demonstrated using a 10 in. diameter pipe through which a capsule of diameter ratio 0.92 has to be carried by water at a  $V_{av}$  of 5 ft/sec; the minimum distance between the capsule and pipe surfaces being  $4 \times 10^{-4}$  inches.

The eccentricity of the given capsule-pipe system is first calculated. Since the pipe diameter is 10 inches, the clearance, as defined in eqn. (4.1), will be  $4 \times 10^{-5}$ . For a diameter ratio of 0.92, eqn. (4.1) will then give the value of eccentricity as 0.999 -- the one used for this study. Since the fluid carrier is water, Figs. 5.4 and 5.6 will not be used at all for the solution.

The pressure ratio  $R_p$  can be obtained from Fig. 5.3, but not directly since none of the four plots in this figure is for a pipe diameter of 10 inches and because there is no curve for a  $d/D$  ratio of 0.92 on these plots. It will be necessary, therefore, to plot  $R_p$  vs.  $D$  for a  $V_{av}$  of 5 ft/sec and  $d/D$  varying from say, 0.9 to 0.97. For each diameter ratio, there will be one curve passing through 4 points corresponding to pipe diameters of 4, 6, 12 and 24 inches. There will thus be five curves on this  $R_p$ - $D$  plot corresponding to diameter

ratios of 0.9, 0.93, 0.95, 0.96 and 0.97. Taking points off these curves for a pipe diameter of 10 in., a plot of  $R_p$  vs.  $d/D$  can be drawn. The value of  $R_p$  can then be taken from this plot for a  $d/D$  of 0.92. The energy required, (hp/ft)/(ft<sup>3</sup>/sec), may be found in a similar fashion from Fig. 5.5.

Knowing  $R_p$ , values of  $R_v$  for diameter ratios from 0.9 to 0.97 are obtained from Fig. 5.2. A plot of  $R_v$  vs.  $d/D$  with the aid of these five points enables the value of  $R_v$  corresponding to a diameter ratio of 0.92 to be determined. Since  $R_p$  is a ratio of  $(dp/dz)_c$  to  $(dp/dz)_f$ , the pressure gradient  $(dp/dz)_c$  can be easily calculated once  $(dp/dz)_f$  is known from the curve for free pipe flow in Fig. 5.1. Also, the capsule velocity can be easily calculated from a known  $R_v$  and  $V_{av}$ . If the value of  $V_{ann}$  is desired as well, the relation

$$V_{ann} = \frac{V_{av} - k^2 V_c}{1 - k^2} \quad (5.7)$$

may be used.

### 5.6 Velocity Distribution (Figs. 5.7, 5.8)

Before comparing the theoretical results with the experimental ones available in the literature, it is pertinent to look at some typical velocity distributions in Figs. 5.7 and 5.8. These velocity distributions have been drawn for the widest and the smallest gaps between the capsule and

pipe surfaces for water flowing at average velocities of approximately 2, 4, 6, 8 and 10 ft/sec in pipes of diameters 4, 6, 12 and 24 in. having a capsule of diameter ratio 0.9 for Fig. 5.7 and 0.99 for Fig. 5.8. The factors by which the widest and the smallest gaps have been enlarged are 1.25 and 2500 respectively for Fig. 5.7, and 12.5 and 25000 for Fig. 5.8. It may be noted that there is solely laminar Couette flow in the smallest gap of the annulus. From eqn. (3.9), one may expect the velocity profile to be logarithmic in this case. However, because of the very small distance over which the velocity is distributed, it is linear for all practical purposes as shown in Figs. 5.7 and 5.8. Realising the large factors by which the smallest gap has been enlarged in these figures, it may be concluded that the velocity gradients are very high.

Both the pressure and Couette flows are turbulent in the widest gap for a diameter ratio of 0.9 (Fig. 5.7). Starting from the top of this figure, it can be seen that the velocity gradient at the capsule wall is changing direction as either the average velocity or the pipe diameter increases. For example, at a  $V_{av}$  of 2 ft/sec in pipes of diameters 4 and 6 in., the velocity gradient is such that the shear stress at the top of the capsule (where the widest gap occurs) produces a thrust force on it. For practically all other cases, the shear stress produces a drag force on the capsule. Now since the shear force at the bottom of the capsule is

invariably a drag force, it follows that for these two cases, there is a transition point where the drag force changes into a thrust force as one proceeds from the bottom to the top of the capsule along its surface.

Fig. 5.8 shows that the shear stress always produces a drag force on the capsule both at the top and at the bottom. In this figure, a marked change in the velocity profiles can be seen because the flow in the widest gap changes from a totally laminar flow to partially laminar or totally turbulent flow. For example, at a  $V_{av}$  of 2, 4 and 6 ft/sec in a 4 in. diameter pipe, a  $V_{av}$  of 2 and 4 ft/sec in a 6 in. diameter pipe and at a  $V_{av}$  of 2 ft/sec in a 12 in. diameter pipe, the flow is totally laminar. As either the average velocity or pipe diameter increases beyond these values, the flow first becomes a turbulent Couette and laminar pressure flow, and finally a completely turbulent flow in the widest gap. There is, thus, a transition from laminar to turbulent flow both in the horizontal and vertical directions in Fig. 5.8. The associated changes in shear stress at the top of the capsule can be easily contemplated by the nature of velocity profiles.

### 5.7 Comparison with Experiment (Figs. 5.9, 5.10)

It may be pointed out at the outset that a comparison of theoretical results was possible only with the experimental

data in Part 9 (14) of the series on 'The Pipeline Flow of Capsules'; the main reason being that the experimental data elsewhere does not indicate the clearance. As given by eqn. (4.1), clearance depends not only on the diameter ratio but also on the eccentricity of a capsule-pipe system. All the available experimental results, except those in Part 9, mention only the diameter ratio since the clearance, and indirectly the eccentricity, is rather difficult to measure experimentally; it being non-uniform over the capsule length in most cases and varying from a maximum at the nose to a minimum at the tail. Nevertheless, it is a very important factor that determines the annular geometry and hence the behaviour of various variables.

During the comparison of results, it was observed that the experimental data in Part 9 (14) corresponds only to laminar flow conditions in the annulus though at the average velocities encountered, the free pipe flow is both laminar and turbulent. However, on the basis of the discussion of the  $R_p - R_v$  plot (Sec. 5.2, Fig. 5.2), it follows that the experimental curve in Fig. 12 of Part 9 can be extended fairly accurately up to a velocity ratio of about 1.1. It then provides some points for comparison even when the flow in the annulus is turbulent. The present theory could, therefore, be tested both for laminar as well as turbulent flow in the annulus. It would of course be desirable to test the theory over a wide range of capsule-pipe configurations

with turbulent annular flow. However, there is a paucity of the necessary data and consequently the data of Part 9 (14) was relied upon exclusively.

#### 5.7.1 Laminar Flow in the Annulus

Fig. 8 of Part 9 contains experimental data for laminar flow both in the annulus and in the free pipe at the corresponding  $V_{av}$ . This data pertains to a 24 in. long, 0.824 diameter ratio capsule flowing in lubricating oil ( $\mu = 36$  cp and sp. gr. = 0.86) in a 0.532 in. diameter pipeline. The hollow cylindrical capsule was loaded to different specific gravities thereby giving different clearances at the same capsule velocity. The relationship between the capsule velocity and clearance is given in Fig. 13 of Part 9. For a few clearances, the computer programme developed in Appendix AIII was run with appropriate changes for the various parameters such as  $d/D$ ,  $D$ ,  $\mu$ ,  $\nu$  and  $\rho$  pertinent to the experimental data. The results obtained from these computations are plotted in Fig. 5.9.

Three axes are used in this figure to represent a number of variables simultaneously. Arrows on the curves refer to the axes used to represent the variables. The dependence of one variable on the other may be understood by following the dashed lines in Fig. 5.9. The nearly straight line represents the theoretical prediction of the

$R_p - R_v$  relationship while the other two curves show the theoretical variation of  $R_p$  with  $V_c$  for different capsule densities; the specific gravity of capsule for the upper curve being 11.75 while for the lower, it is 2.03. It may be recalled that the present theoretical analysis can only distinguish between two capsule densities by means of different clearances at the same capsule velocity. Also these clearances have to be supplied to the computer programme in terms of different eccentricities and/or diameter ratios. Moreover, it may be noted that since the diameter ratio is fixed in the present case, the eccentricity or, in other words, the clearance for the capsule-pipe system is continuously varying from one point to another on all the curves in Fig. 5.9.

The circled points shown in Fig. 5.9 correspond to the experimentally determined results in Fig. 8 of Part 9. It is obvious that a good agreement exists between the analytical prediction and experimental data as long as liquid in the capsule-pipe annulus is in laminar flow. It is also clear that the end effects do not cause much deviation from the theoretical prediction for very long capsules probably because the experimental capsule had a rather high length to diameter ratio;  $L_c/d$  being 55 in the present case. Nevertheless, one may doubt the validity of a previous statement (Chapter 3, Sec. 3.5.3) that the present study may hold good only for diameter ratios of 0.9 or over since for the results in Fig. 5.9, the diameter ratio is only 0.824. It may be recalled,

however, that the only reason for making such a limitation was the lack of a satisfactory velocity profile for turbulent Couette flow. Since there is only laminar flow in the annulus for the results in Fig. 5.9, we are no longer bounded by this limit. Whether the present theory is really subjected to such a limit could not be detected due to lack of pertinent experimental data for turbulent annular flow.

### 5.7.2 Turbulent Flow in the Annulus

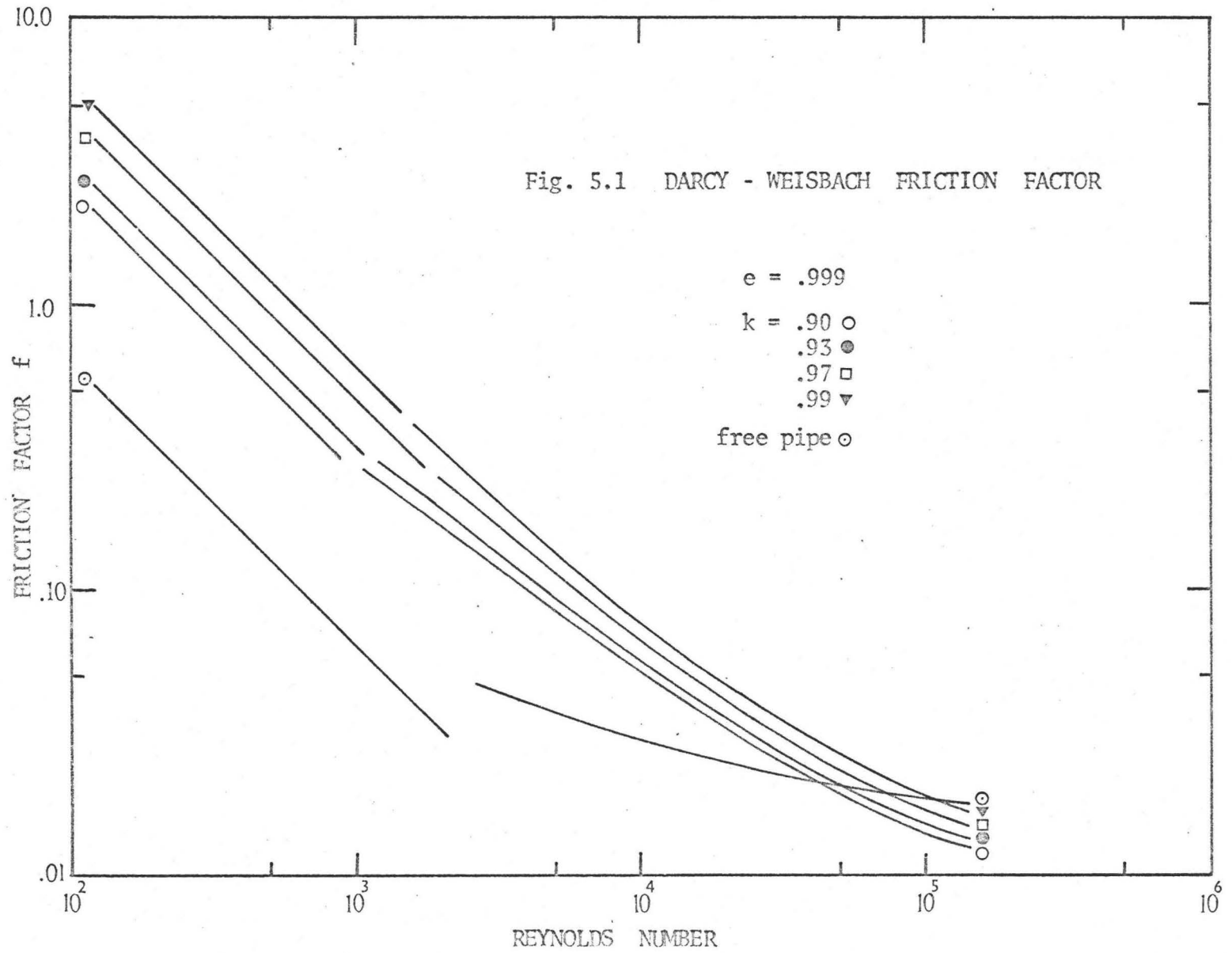
Turning now to the case when the annular flow is turbulent, observe that, as indicated already, the data in Fig. 12 of Part 9 can be hopefully used for comparison. This data corresponds to a 48 in. long, 0.9 diameter ratio aluminium (sp. gr. = 2.71) cylindrical capsule flowing in transformer oil ( $\mu = 16.7$  cp, sp. gr. = 0.853) in a 4.03 in. diameter pipeline. Fig. 5.10 shows the theoretical prediction of  $R_p - R_v$  relationship for this capsule-pipe system. As before, eccentricity is again varying all along the curve in Fig. 5.10 which for the most part corresponds to laminar flow in the annulus but turbulent in the free pipe. The annular flow is also turbulent, however, for the lower part of the curve. The circled points shown in Fig. 5.10 pertain to the experimental data in Fig. 12 of Part 9. The agreement between the theory and experiment is again good though the length to diameter ratio of the experimental capsule is only about 13.2.

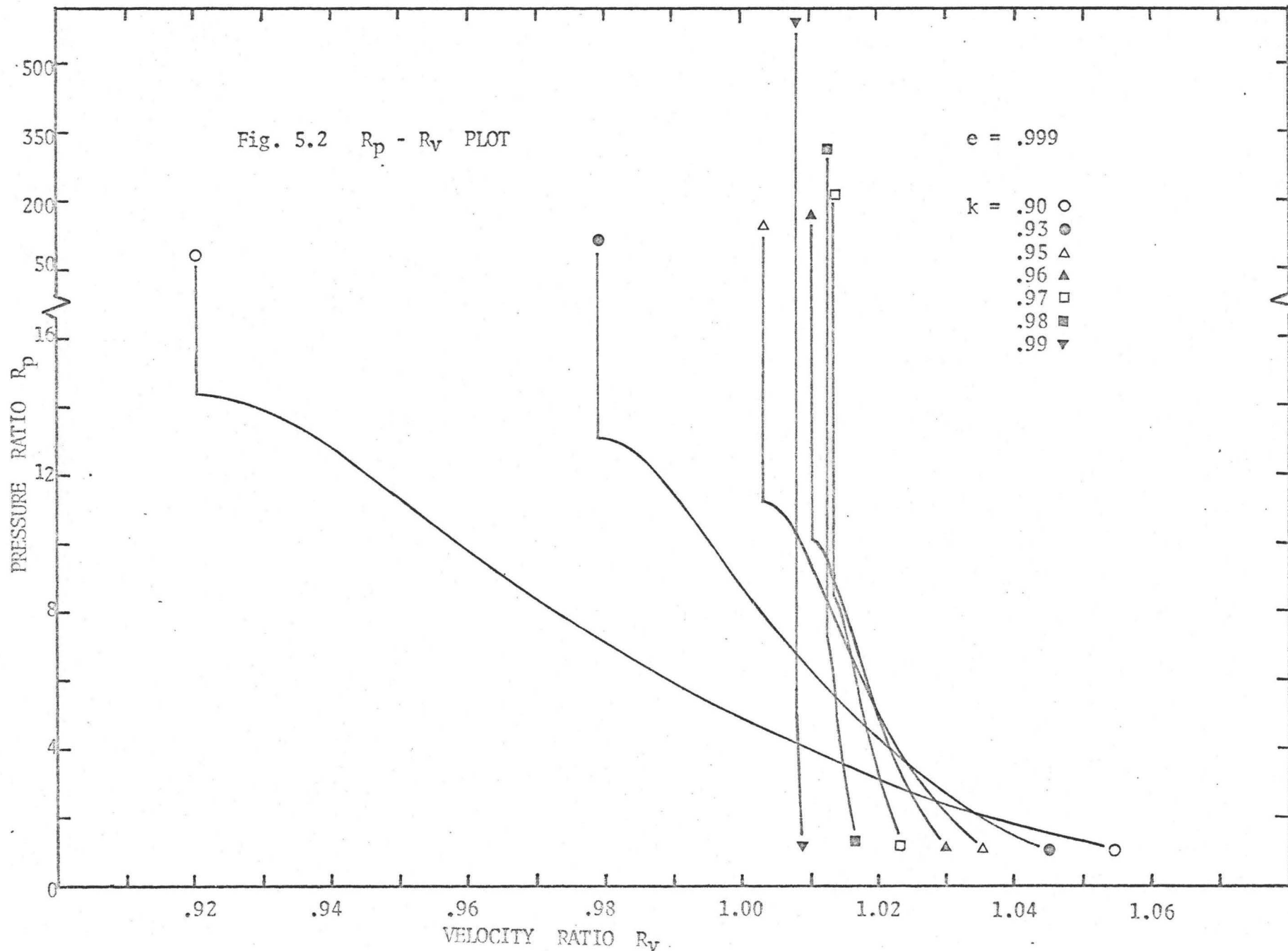
Three possible reasons may be cited for any discrepan-

cies between data from cylindrical capsules and the theoretical predictions:

- i) The experimental capsule is finite and may display end effects.
- ii) The capsule axis is not parallel to the pipe axis in most cases, and
- iii) When the capsule moves at very small clearances, a frictional force between the pipe wall and the capsule is introduced.

Any one of these three conditions invalidates the analytical model of a very long, free-flowing, cylindrical capsule in a pipe. It is also possible that these three causes of deviation may at times compensate one another to give experimental data closer to the prediction than warranted. Additionally, reading the values from figures in Part 9 may constitute another factor contributing to the discrepancies, the maximum of which is about 5%.





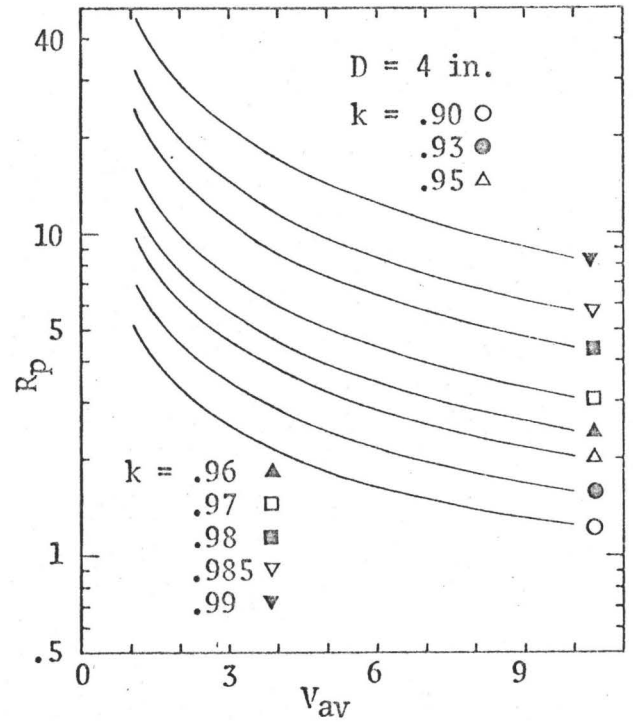
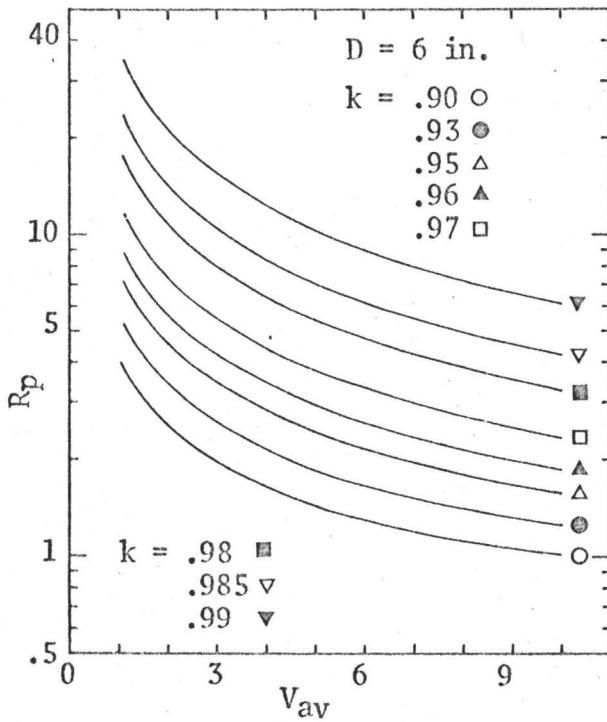
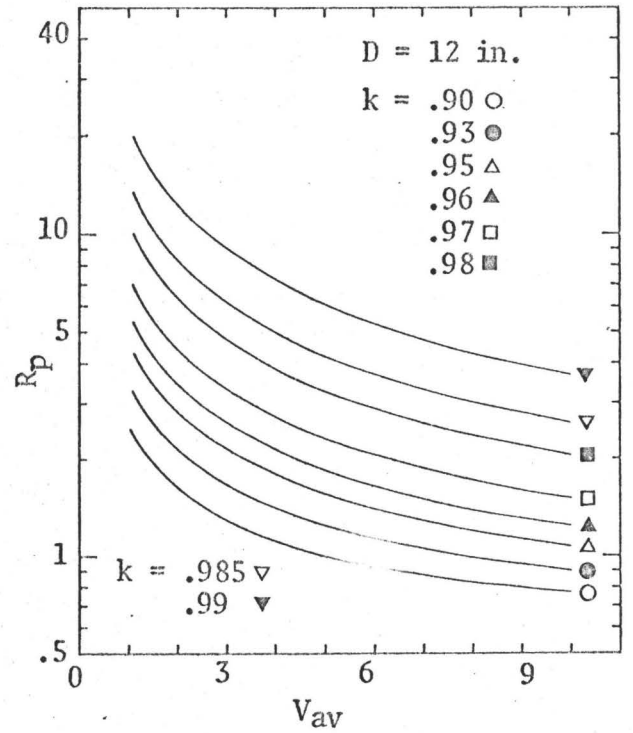
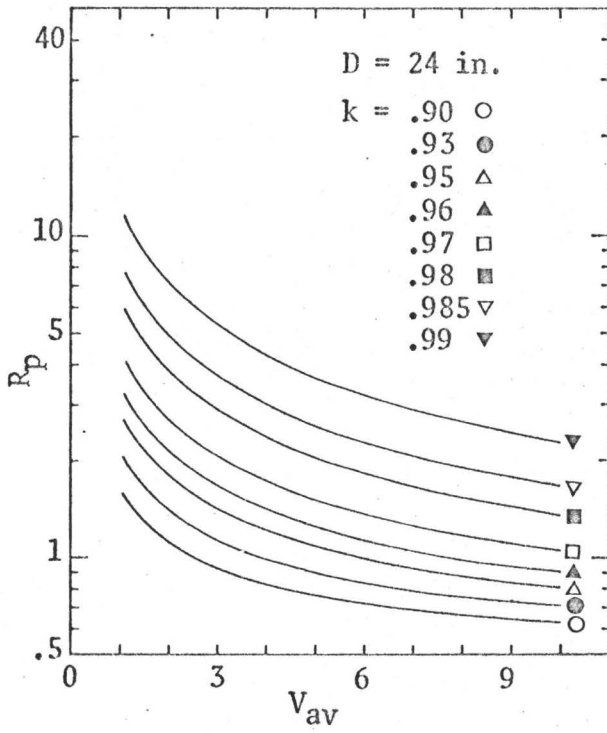


Fig. 5.3 VARIATION OF PRESSURE RATIO WITH AVERAGE VELOCITY, PIPE DIAMETER AND DIAMETER RATIO FOR WATER AS THE LIQUID CARRIER (  $e = .999$ ,  $\mu = 1$  cp, sp. gr. = 1.0 )

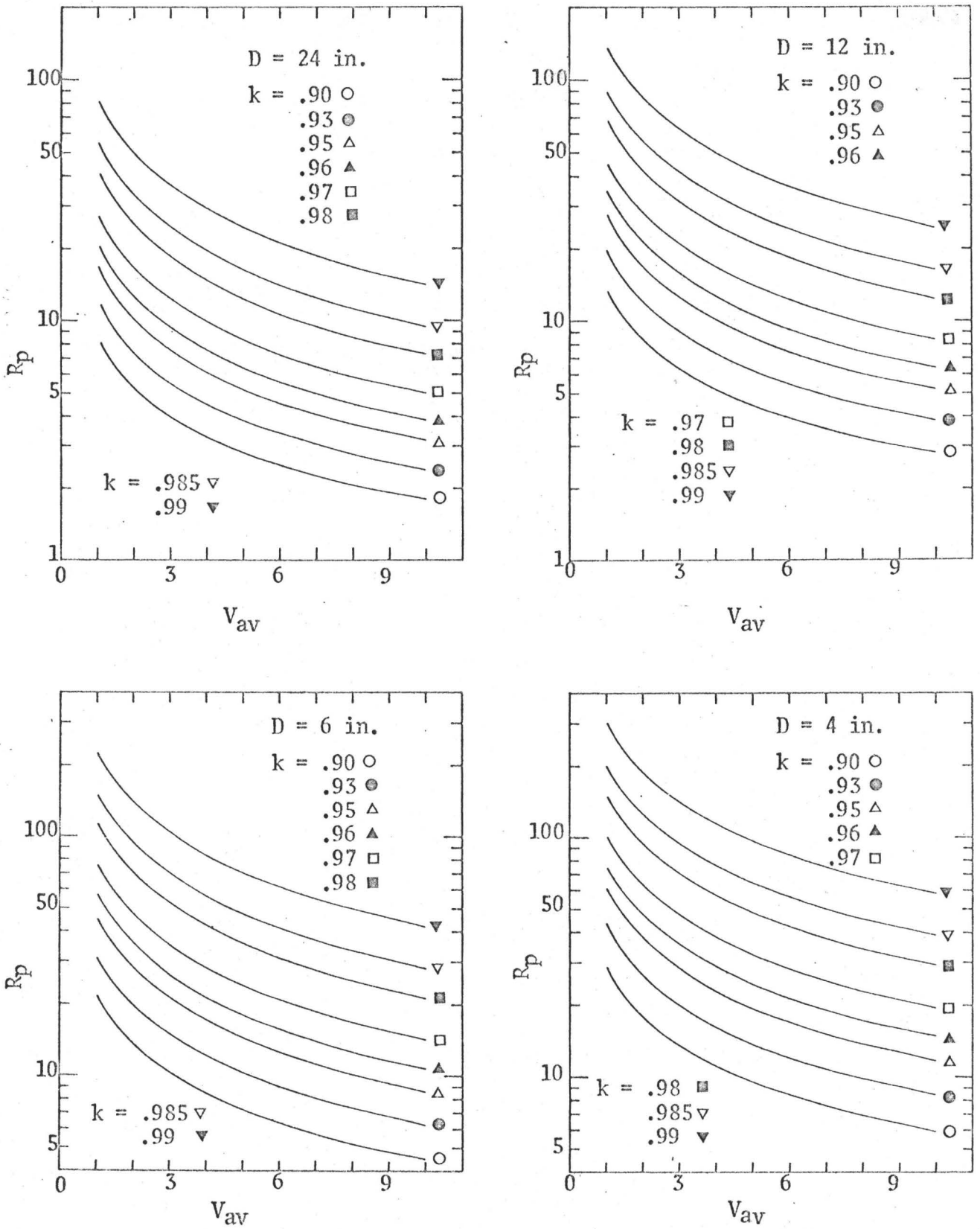


Fig. 5.4 VARIATION OF PRESSURE RATIO WITH AVERAGE VELOCITY, PIPE DIAMETER AND DIAMETER RATIO FOR AN OIL AS THE LIQUID CARRIER (  $e = .999$ ,  $\mu = 10$  cp, sp. gr. = .85 )

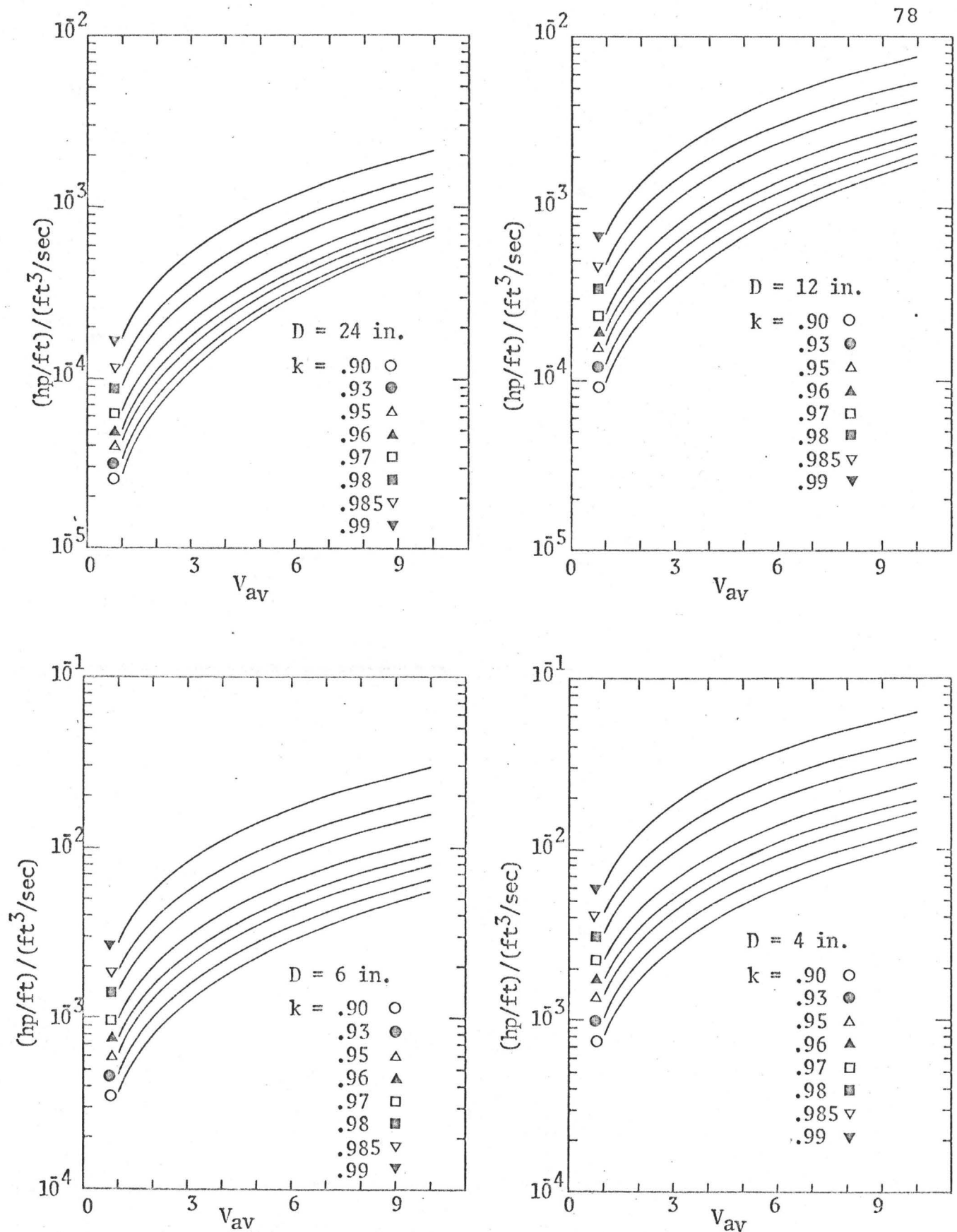


Fig. 5.5 VARIATION OF ENERGY REQUIRED WITH AVERAGE VELOCITY, PIPE DIAMETER AND DIAMETER RATIO FOR WATER AS THE LIQUID CARRIER (  $e = .999$ ,  $\mu = 1$  cp, sp. gr. = 1.0)

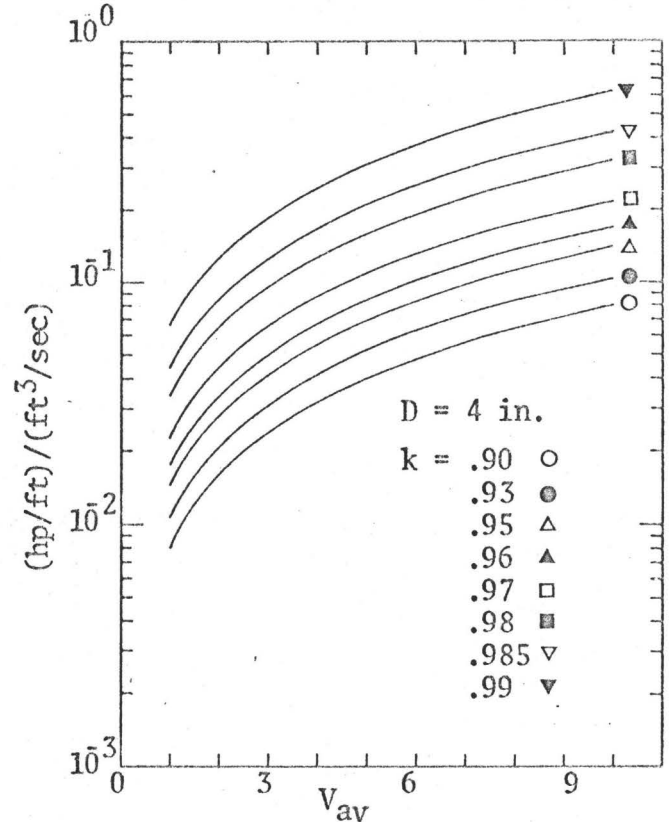
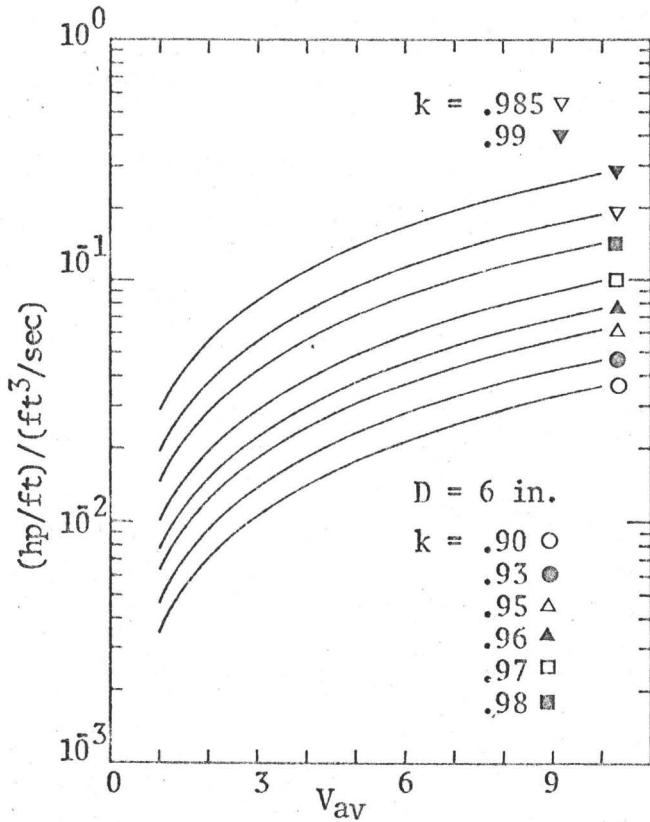
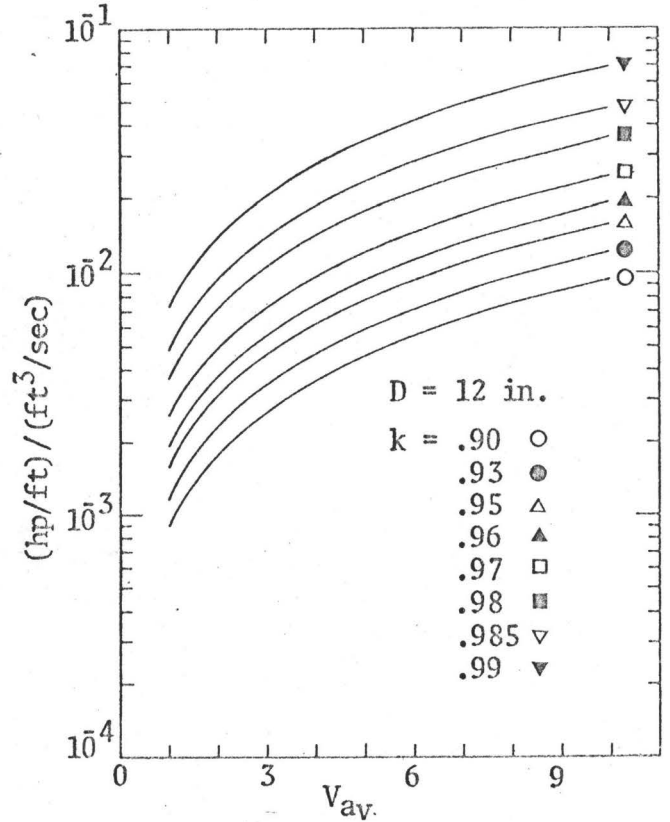
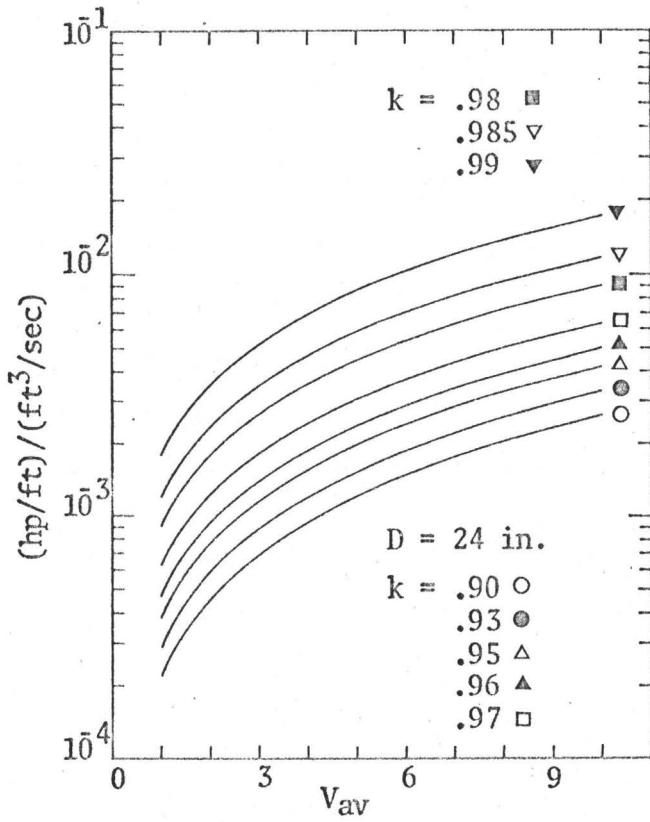


Fig. 5.6 VARIATION OF ENERGY REQUIRED WITH AVERAGE VELOCITY, PIPE DIAMETER AND DIAMETER RATIO FOR AN OIL AS THE LIQUID CARRIER ( $e = .999$ ,  $\mu = 10 \text{ cp}$ ,  $\text{sp. gr.} = .85$ )

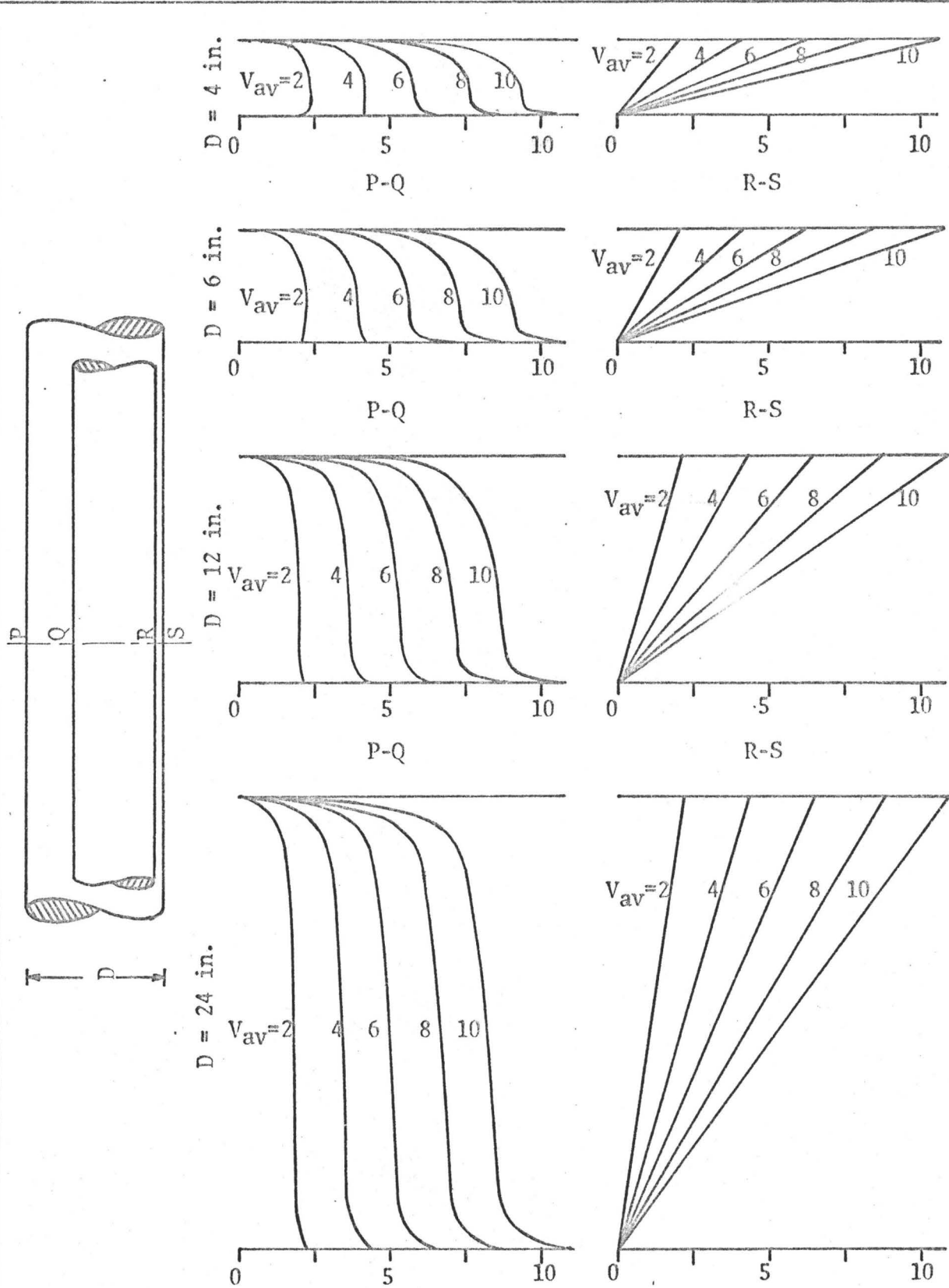


Fig. 5.7 VELOCITY DISTRIBUTION IN THE SMALLEST AND WIDEST GAPS FOR WATER FLOWING AT AVERAGE VELOCITIES OF 2, 4, 6, 8 AND 10 ft/sec IN PIPES OF 4, 6, 12, 24 in. DIAMETERS HAVING A FREELY FLOWING CAPSULE OF DIAMETER RATIO 0.9

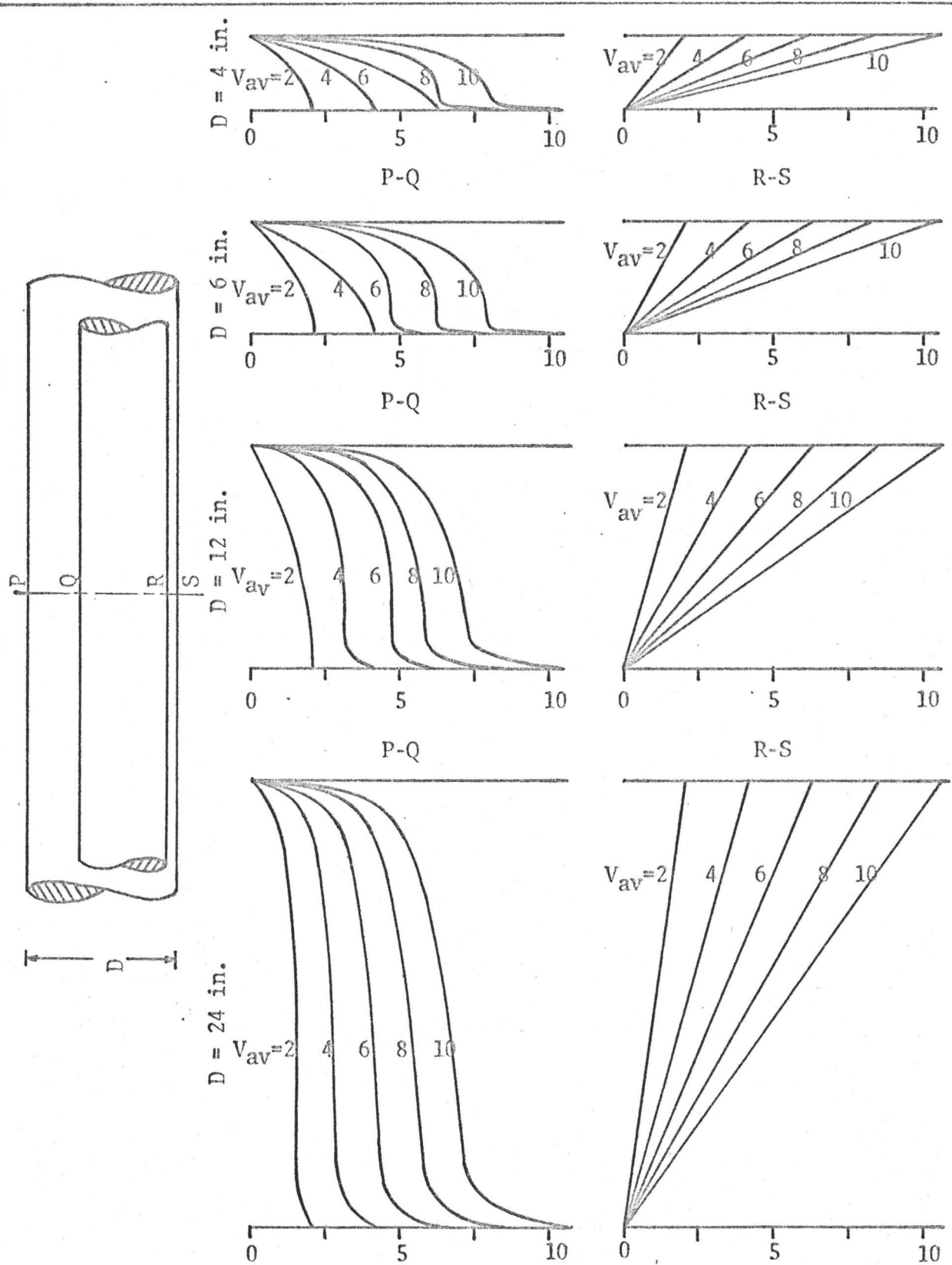


Fig. 5.8 VELOCITY DISTRIBUTION IN THE SMALLEST AND WIDEST GAPS FOR WATER FLOWING AT AVERAGE VELOCITIES OF 2, 4, 6, 8 AND 10 ft/sec IN PIPES OF 4, 6, 12, 24 in. DIAMETERS HAVING A FREELY FLOWING CAPSULE OF DIAMETER RATIO .99

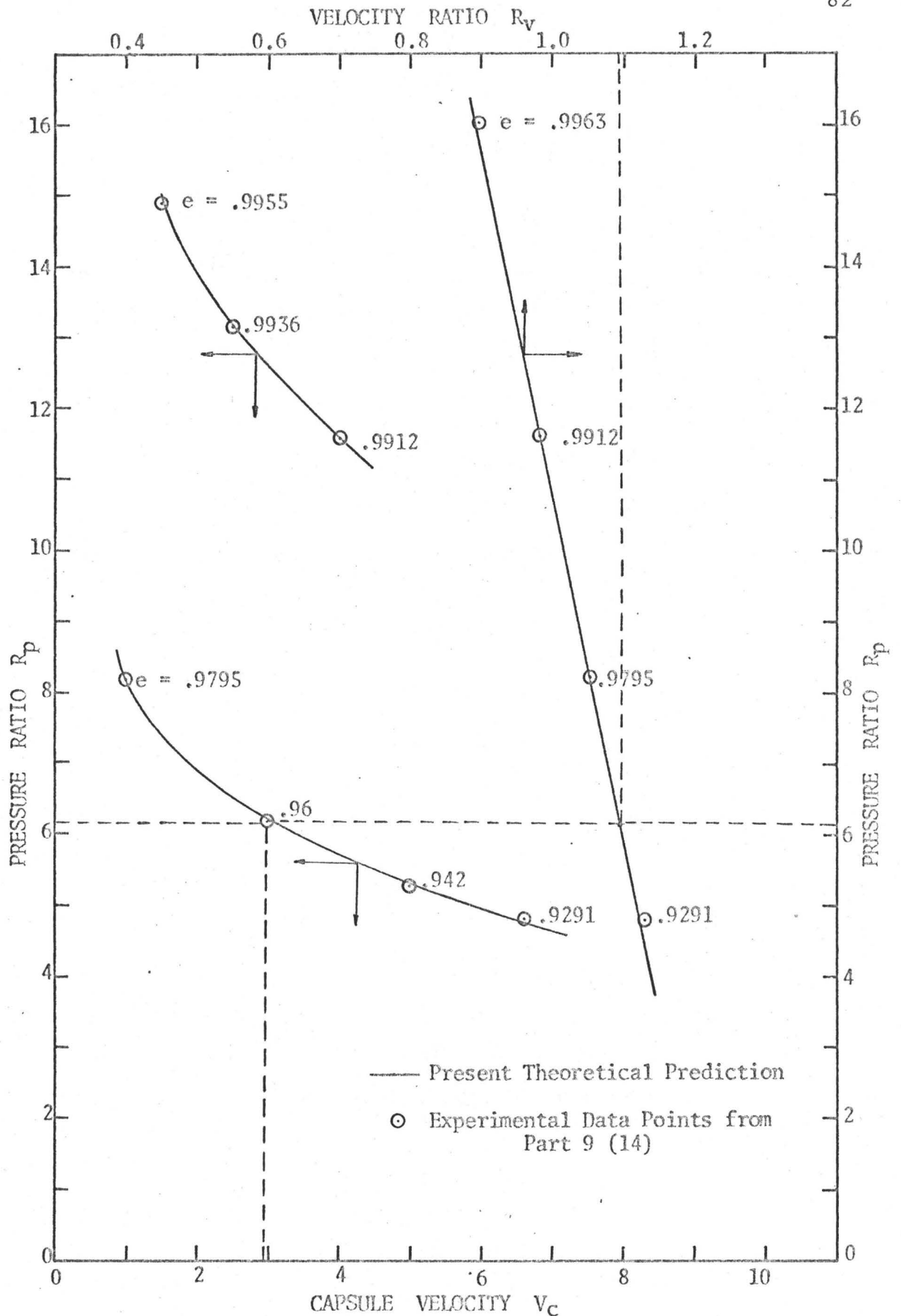
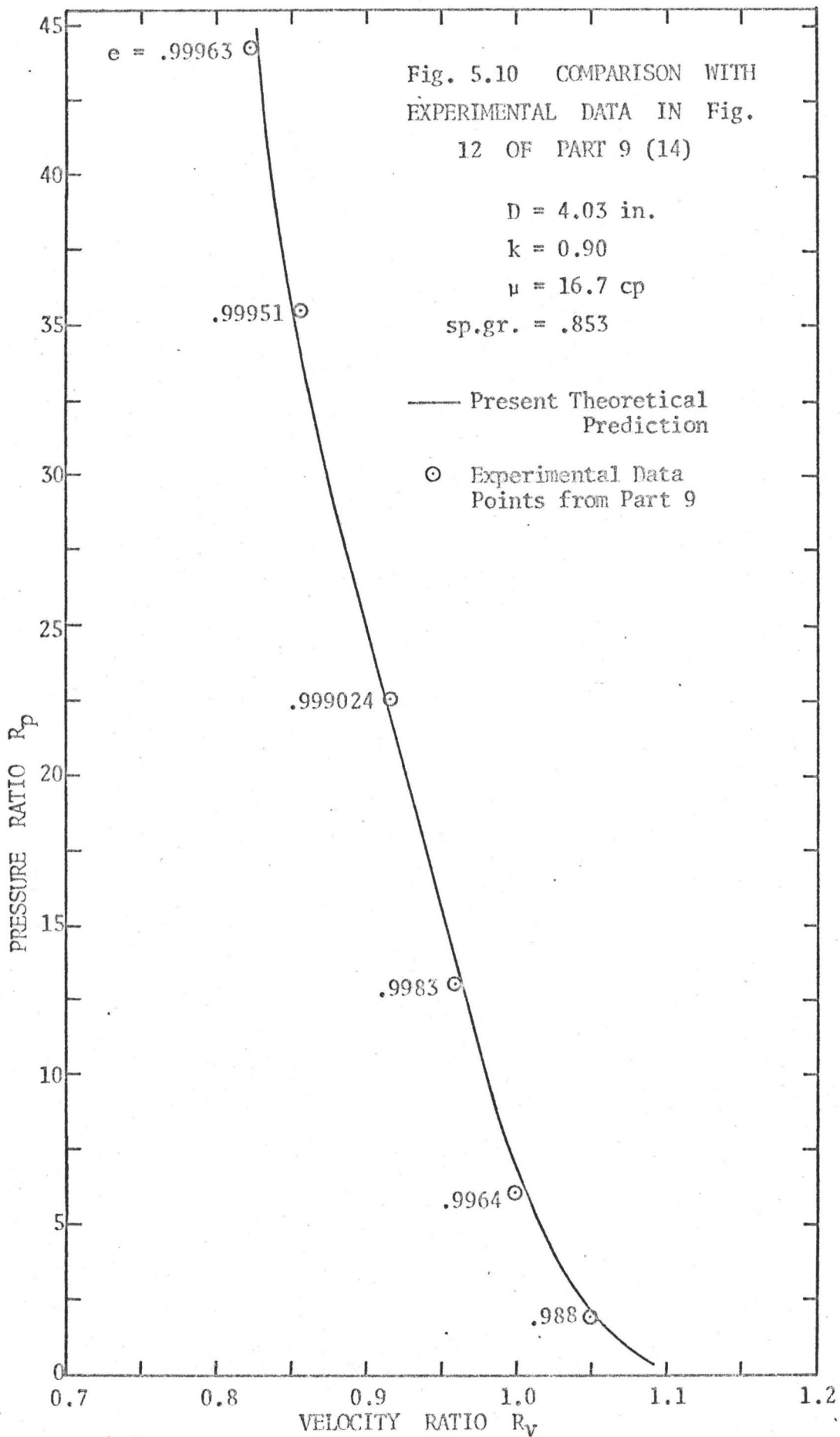


Fig. 5.9 COMPARISON WITH EXPERIMENTAL DATA IN Fig. 8 OF PART 9(14)  
 (  $D = .532$  in.,  $k = .824$ ,  $\mu = 36$  cp, sp. gr. = .86 )



## 6. CONCLUSIONS

The theoretically predicted effect of various parameters on velocity ratio, pressure ratio and energy requirements can be summarised as follows:

- i) The average flow velocity does not affect the velocity ratio as long as the annular flow is laminar. In turbulent flow, however, velocity ratio increases with the average velocity.
- ii) The velocity ratio increases with the diameter ratio up to 0.97 beyond which it starts to decrease. The effect of a higher  $V_{av}$  is, however, to result in a higher  $R_v$  for a lower  $d/D$ .
- iii) There is no effect of average velocity on the pressure ratio when the annular as well as free-pipe flow is laminar. As either of the two flows becomes turbulent,  $R_p$  decreases with an increase in  $V_{av}$ .
- iv) The pressure ratio increases with a decrease in pipe diameter and an increase in diameter ratio and liquid viscosity.
- v) The effect of an increase in  $V_{av}$ ,  $d/D$  and liquid viscosity is to result in a higher energy requirement in terms of (hp/ft)/(ft<sup>3</sup>/sec) or conventionally in terms of hp-hr/ton-mile. A decrease in pipe diameter results in a similar effect.

It was also observed that the laminar flow regime applies to a far wider range of Reynolds numbers when a capsule is present in a pipe (the range depending on the annular geometry) than for the fluid flowing alone. Moreover, the locus of maximum velocities for turbulent pressure flow in the annulus is closer to the capsule wall than that for laminar pressure flow.

A comparison with experimental data for single capsules run in pipes of  $\frac{1}{2}$  and 4 in. diameters shows that a good agreement exists between the analytical prediction and experimental results. It is hoped that the performance of a single, very long capsule in a pipe may provide a theoretical criterion against which the performance of commercial capsule pipelines, generally employing continuous trains of capsules, can be judged.

It would not be proper, however, to conclude this study without a recommendation for further experimental work on the circular Couette flow in turbulent regime. It may be recalled that the lack of a suitable velocity profile in such a case was the only reason for limiting the application of the present theoretical analysis to the capsule-pipe configurations with diameter ratios equal to or greater than 0.9. Furthermore, it is recommended that a proper velocity profile be found from further experimental tests on turbulent pressure flow in the annulus since the universal velocity profile for free-pipe flow adopted in the present study

deviates more and more from the actual one as the diameter ratio decreases.

## APPENDIX AI

### Geometry of the Eccentric Annulus

Heyda (2) has described the bipolar coordinate system for an eccentric annulus. This system is such that the pipe and capsule walls belong to one of the two families of circles which are orthogonal to each other.

Let the x-y plane in Fig. AI-1 be regarded as the complex Z plane ( $Z = x + iy$ ) and let a new complex variable,  $\zeta$ , be defined by  $\zeta = \xi + i\eta$ . Then starting with the transformation,

$$Z = ic \tan\left(\frac{1}{2}\zeta\right) \quad (\text{AI-1})$$

it is possible to find relations between x, y,  $\xi$  and  $\eta$ .

Considering Fig. AI-1, it may be observed that

$$\frac{r_1}{r_2} = \frac{|\vec{P}0 + 0\vec{O}_1|}{|\vec{O}_20 + \vec{O}P|} = \left| \frac{c - Z}{c + Z} \right| \quad (\text{AI-2})$$

$$\text{Also } \theta_2 - (\theta_1 - \pi) = \arg(c + Z) - \arg(c - Z)$$

$$= \arg\left(\frac{c + Z}{c - Z}\right) \quad (\text{AI-3})$$

The transformation in eqn. (AI-1) can also be written as

$$\frac{c + Z}{c - Z} = e^{i\zeta}$$

$$\text{or } \left| \frac{c + Z}{c - Z} \right| \arg\left(\frac{c + Z}{c - Z}\right) = e^{i(\xi+i\eta)}$$

$$= e^{-\eta} \cdot e^{i\xi}$$

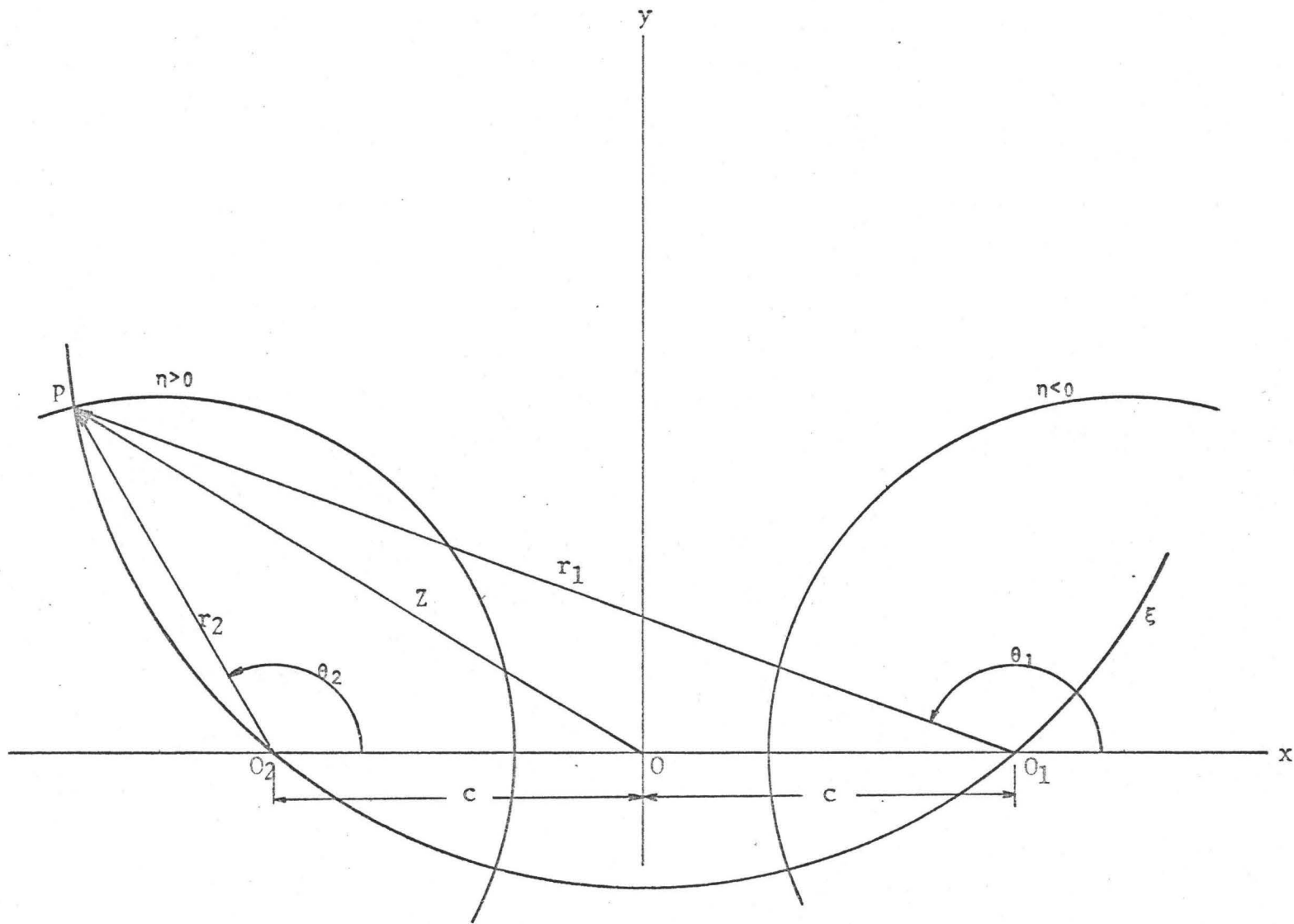


Fig. AI-1 COMPLEX  $Z$  PLANE

$$\therefore e^{-\eta} = \left| \frac{c + z}{c - z} \right| = \frac{r_2}{r_1} \quad (\text{due to eqn. (AI-2)})$$

$$\text{or } \eta = \ln \frac{r_1}{r_2} \quad (\text{AI-4})$$

$$\begin{aligned} \text{Also } \xi &= \arg \left( \frac{c + z}{c - z} \right) \\ &= \theta_2 - (\theta_1 - \pi) \quad (\text{due to eqn. (AI-3)}) \end{aligned}$$

$$\text{or } \xi = \pi - (\theta_1 - \theta_2) \quad (\text{AI-5})$$

In the  $z$ -plane,  $r_1$ ,  $r_2$ ,  $\theta_1$  and  $\theta_2$  may be expressed as

$$r_1 = \sqrt{(x - c)^2 + y^2}$$

$$r_2 = \sqrt{(x + c)^2 + y^2}$$

$$\theta_1 = \tan^{-1} \left( \frac{y}{x - c} \right)$$

$$\theta_2 = \tan^{-1} \left( \frac{y}{x + c} \right)$$

Hence from eqns. (AI-4) and (AI-5), it follows that

$$\eta = \ln \sqrt{\frac{(x - c)^2 + y^2}{(x + c)^2 + y^2}} \quad (\text{AI-6})$$

$$\text{and } \xi = \pi - \left( \tan^{-1} \frac{y}{x - c} - \tan^{-1} \frac{y}{x + c} \right) \quad (\text{AI-7})$$

Writing eqn. (AI-6) in the exponential form and then squaring both sides, it follows that a constant  $\eta$  line in the  $z$  plane is transformed into the circle

$$(x + c \coth \eta)^2 + y^2 = c^2 \operatorname{csch}^2 \eta \quad (\text{AI-8})$$

in the Z-plane, with centre on the x-axis. For  $\eta < 0$ , the circle lies in the right-half plane and encloses  $0_1$  while for  $\eta > 0$ , the circle lies in the left-half plane and encloses  $0_2$  (Fig. AI-1).

Taking tangents of both sides of eqn. (AI-7) and simplifying, it can be shown that a constant  $\xi$  line in the  $\zeta$  plane is transformed into the circle

$$x^2 + (y + c \cot \xi)^2 = c^2 \csc^2 \xi \quad (\text{AI-9})$$

in the Z-plane, with centre on the y-axis. This constant  $\xi$  circle is orthogonal to the constant  $\eta$  circle. Also, the  $\xi$ -values for points on the circle segments below the x-axis are  $\pi$  more than the  $\xi$ -values for points on the corresponding circle segments above the x-axis.

Taking the pipe and capsule surfaces to belong to the family of circles for which  $\eta = \text{constant}$ , eqn. (AI-8) gives

$$R_1 = c \operatorname{csch} \eta_1 \quad (\text{AI-10})$$

$$R_2 = c \operatorname{csch} \eta_2 \quad (\text{AI-11})$$

and 
$$s = c (\operatorname{coth} \eta_2 - \operatorname{coth} \eta_1) \quad (\text{AI-12})$$

In order to solve these equations for  $\eta_1$  and  $\eta_2$ , a diameter ratio,  $k$ , and an eccentricity,  $e$ , may be defined as

$$k = \frac{R_1}{R_2} \quad (\text{AI-13})$$

and 
$$e = \frac{s}{R_2 - R_1} \quad (\text{AI-14})$$

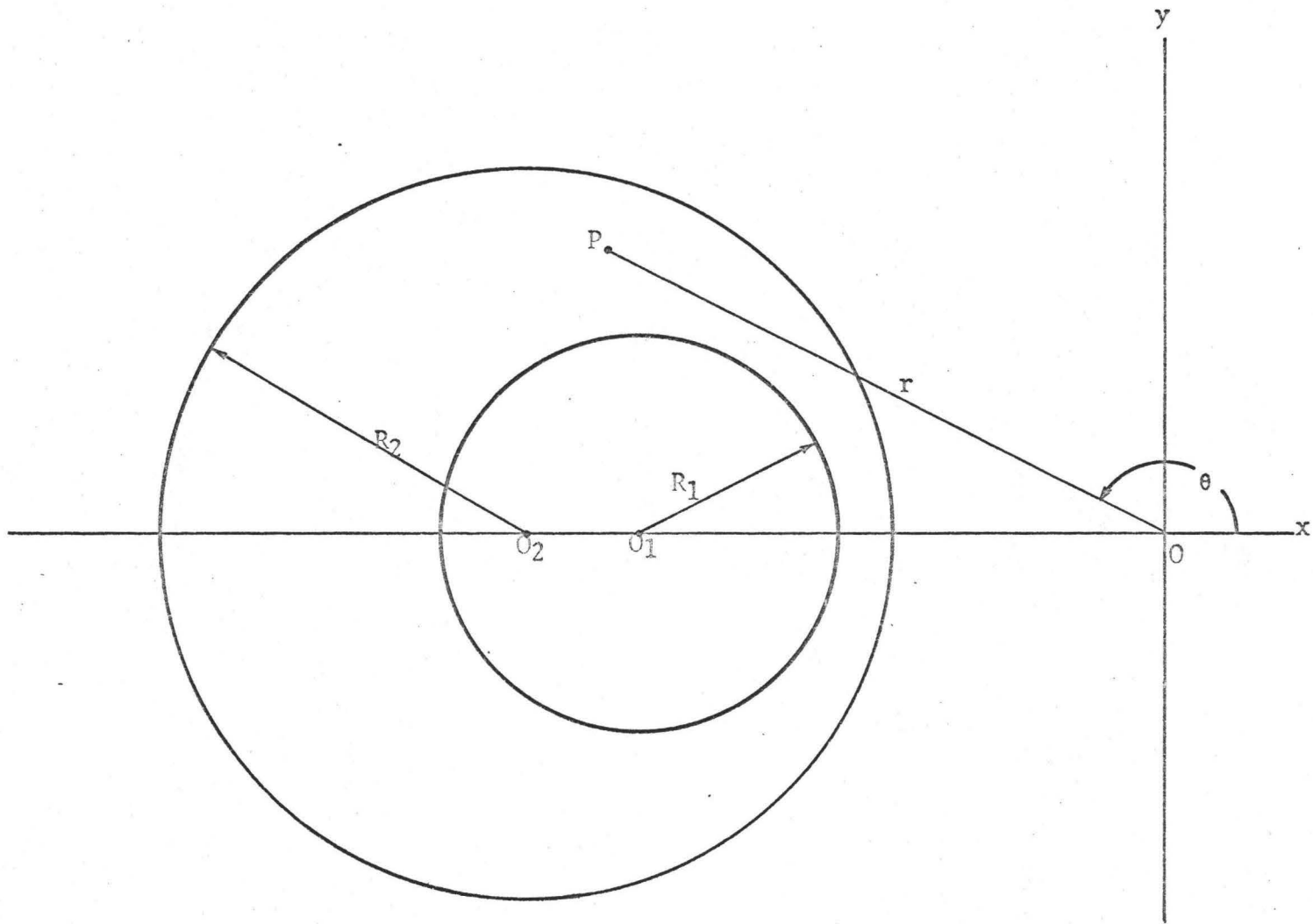


Fig. AI-2 POLAR CO-ORDINATES OF A POINT IN THE ANNULUS

It is, then, possible to show that  $\eta_2$  is given by

$$2 \cosh \eta_2 = \frac{1+k}{e} + (1-k)e \quad (\text{AI-15})$$

Rewriting eqns. (AI-11) and (AI-10) gives

$$c = R_2 \sinh \eta_2 \quad (\text{AI-16})$$

and

$$\sinh \eta_1 = \frac{c}{R_1} \quad (\text{AI-17})$$

From eqn. (AI-1), it is easy to establish the transformation equations:

$$x = \frac{-c \sinh \eta}{\cosh \eta + \cos \xi} \quad (\text{AI-18})$$

and

$$y = \frac{c \sin \xi}{\cosh \eta + \cos \xi} \quad (\text{AI-19})$$

To find the polar coordinates  $(r, \theta)$  of Fig. AI-2 from known values of  $(\xi, \eta)$ , it is easy to show, using eqns. (AI-18) and (AI-19), that

$$\begin{aligned} r^2 = x^2 + y^2 &= c^2 \frac{\sinh^2 \eta + \sin^2 \xi}{(\cosh \eta + \cos \xi)^2} \\ &= c^2 \frac{\cosh^2 \eta - \cos^2 \xi}{(\cosh \eta + \cos \xi)^2} \end{aligned}$$

or

$$r^2 = c^2 \frac{\cosh \eta - \cos \xi}{\cosh \eta + \cos \xi} \quad (\text{AI-20})$$

and

$$\tan \theta = \frac{y}{x} = - \frac{\sin \xi}{\sinh \eta} \quad (\text{AI-21})$$

Also from eqns. (AI-18) and (AI-19), it follows that arc length,  $ds_{\xi}$ , along a constant  $\xi$  curve is given by

$$ds_{\xi} = \frac{-c}{\cosh \eta + \cos \xi} d\eta \quad (\text{AI-22})$$

the minus sign indicating that  $\eta$  decreases as  $s_{\xi}$  increases.

Similarly, the arc length,  $ds_{\eta}$ , along a constant  $\eta$  curve is given by

$$ds_{\eta} = \frac{c}{\cosh \eta + \cos \xi} d\xi \quad (\text{AI-23})$$

And the area,  $dA$ , of an element is

$$dA = \frac{-c^2 d\eta d\xi}{(\cosh \eta + \cos \xi)^2} \quad (\text{AI-24})$$

To find  $s_{\xi}$ ,  $s_{\eta}$  and  $A$ , these three equations are rather difficult to integrate. Following Wilson (5), eqn. (AI-24) was integrated numerically using Gauss integration technique (30, 31), but a direct geometrical approach was used to replace eqns. (AI-22) and (AI-23).

Considering Fig. AI-3, the chord length between two points  $(\eta_2, \xi)$  and  $(\eta_m, \xi)$  on a constant  $\xi$  curve is

$$L_{\xi} = \sqrt{(x(\eta_2, \xi) - x(\eta_m, \xi))^2 + (y(\eta_2, \xi) - y(\eta_m, \xi))^2}$$

where  $x(\eta, \xi)$  and  $y(\eta, \xi)$  are given by eqns. (AI-18) and (AI-19). Thus, the half angle,  $\phi$ , enclosed by the radii from the centre of the circle  $\xi = \text{constant}$  to the points  $(\eta_2, \xi)$  and  $(\eta_m, \xi)$  is

$$\phi = \sin^{-1} \left( \frac{L_{\xi} \sin \xi}{2c} \right)$$

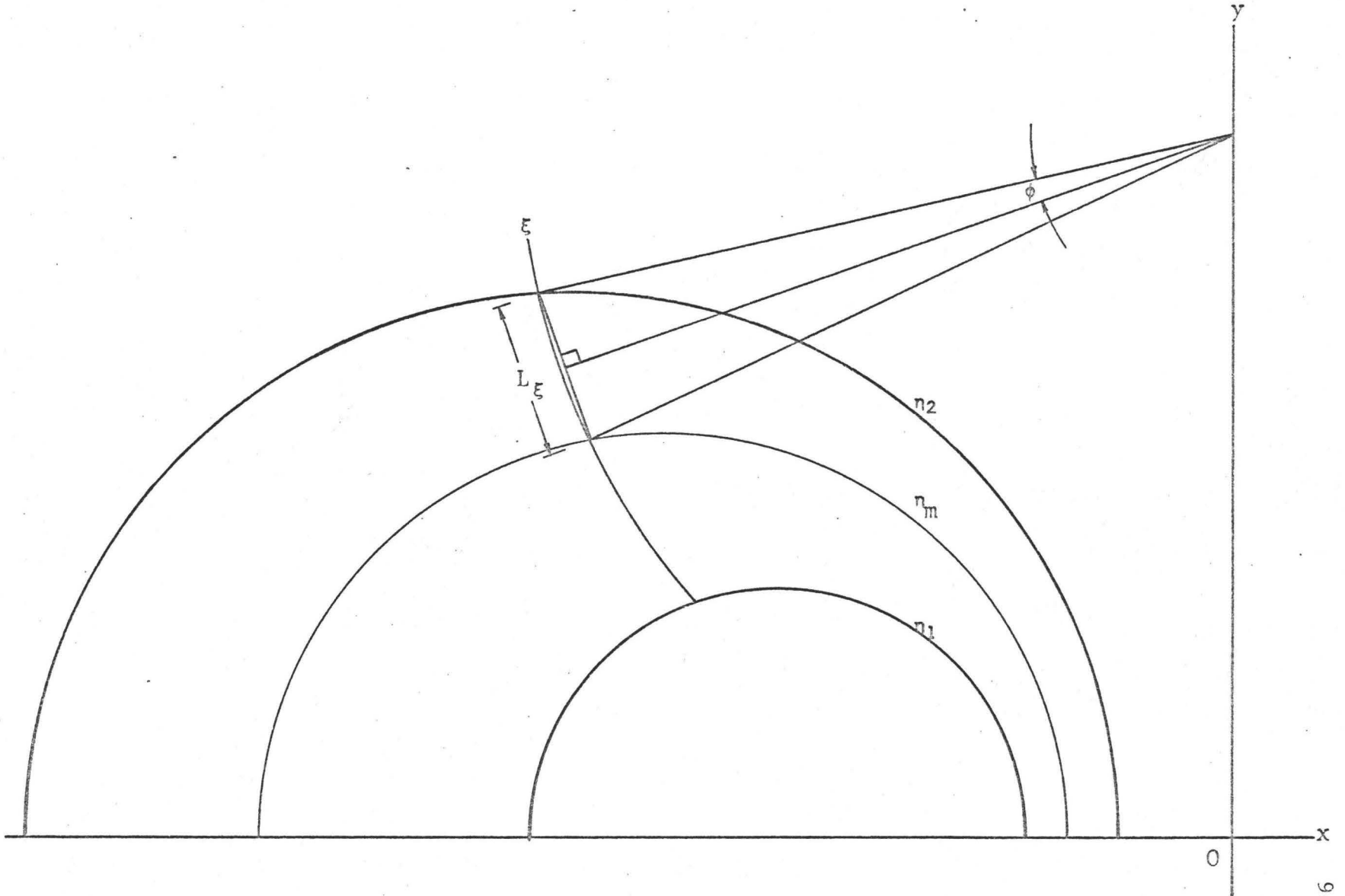


Fig. AI-3 ARC LENGTH DETERMINATION

Therefore, the arc length,  $s_\xi$ , along the constant  $\xi$  curve between the two points is given by

$$s_\xi = \frac{2c}{\sin \xi} \sin^{-1} \left( \frac{L_\xi \sin \xi}{2c} \right) \quad (\text{AI-25})$$

Similarly, the arc length,  $s_\eta$ , along a constant  $\eta$  line between two points  $(\eta, \xi_1)$  and  $(\eta, \xi_2)$  is given by

$$s_\eta = \frac{2c}{\sinh \eta} \sin^{-1} \left( \frac{L_\eta \sinh \eta}{2c} \right) \quad (\text{AI-26})$$

where  $L_\eta$  is given by

$$L_\eta = \sqrt{(x(\eta, \xi_1) - x(\eta, \xi_2))^2 + (y(\eta, \xi_1) - y(\eta, \xi_2))^2}$$

The approximate relation to find  $\eta_m$  in laminar flow, given in (2), is

$$\eta_m = \operatorname{sech}^{-1} \frac{1}{2} \left[ \sqrt{(1 - \tanh \eta_1)(1 + \tanh \eta_2)} + \sqrt{(1 + \tanh \eta_1)(1 - \tanh \eta_2)} \right]$$

(AI-27)

## APPENDIX AII

### Laminar Velocity Profile in a Concentric Annulus

The velocity profile for laminar flow in a concentric annulus can be easily obtained by the application of Navier-Stokes equation in cylindrical coordinates.

For fully developed incompressible, laminar flow due to a constant pressure gradient, the Navier-Stokes equation reduces to

$$\frac{1}{\mu} \frac{dp}{dz} = \frac{d^2 w}{dr^2} + \frac{1}{r} \frac{dw}{dr}$$

where  $r$  is the radial direction and  $w$  is the point velocity in  $z$  direction (Fig. AII-1)

The above equation can be written in the form

$$\frac{1}{\mu} \frac{dp}{dz} = \frac{1}{r} \frac{d}{dr} \left( r \frac{dw}{dr} \right) \quad (\text{AII-1})$$

or

$$d \left( r \frac{dw}{dr} \right) = \frac{1}{\mu} \frac{dp}{dz} r dr$$

Since  $\frac{dp}{dz}$  is constant, integrating this equation twice, we get

$$w = \frac{1}{4\mu} \frac{dp}{dz} r^2 + C \ln r + D \quad (\text{AII-2})$$

The constants  $C$  and  $D$  can be evaluated by the boundary conditions

$$w = 0 \quad \text{at} \quad r = r_1, r_2$$

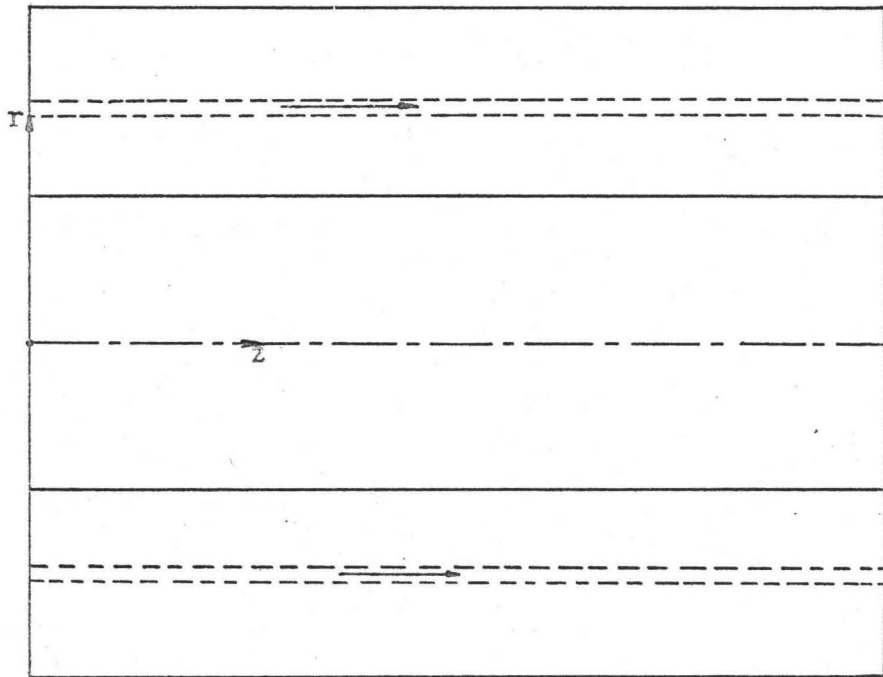
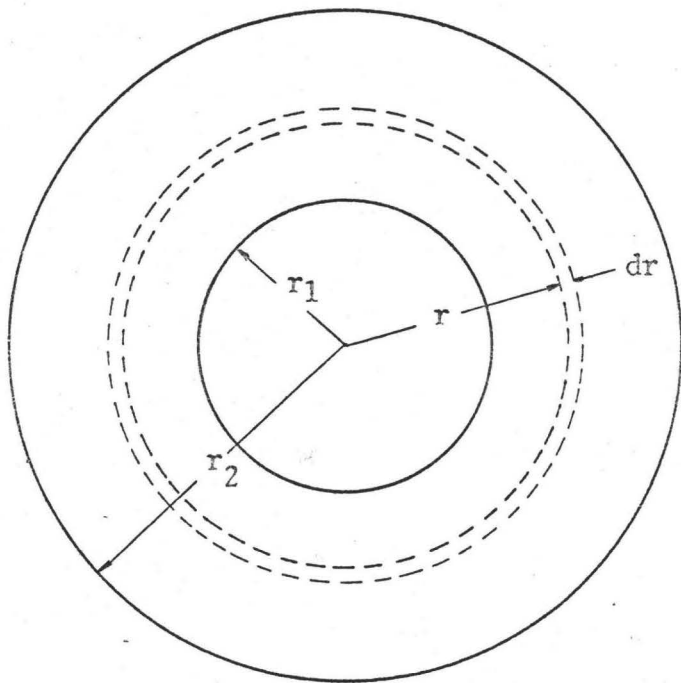


Fig. AII-1 THE CONCENTRIC ANNULUS

to obtain

$$C = \frac{-1}{4\mu} \frac{dp}{dz} \frac{r_2^2 - r_1^2}{\ln \frac{r_2}{r_1}}$$

and

$$D = \frac{-1}{4\mu} \frac{dp}{dz} \left( \frac{r_1^2 \ln r_2 - r_2^2 \ln r_1}{\ln \frac{r_2}{r_1}} \right)$$

Eqn. (AII-2), therefore, becomes after simplification

$$w = \frac{-1}{4\mu} \frac{dp}{dz} \left[ \frac{(r_2^2 - r_1^2) \ln \left(\frac{r}{r_1}\right)}{\ln \left(\frac{r_2}{r_1}\right)} - (r^2 - r_1^2) \right] \quad (\text{AII-3})$$

To obtain an expression for the average velocity, consider an elemental ring of thickness  $dr$  at a radius  $r$  as shown in the Fig. (AII-1). The total volume flow rate through the annulus is then given by

$$\begin{aligned} Q &= \int_{r_1}^{r_2} 2\pi r w dr \\ &= \frac{-2\pi}{4\mu} \frac{dp}{dz} \int_{r_1}^{r_2} \left[ \frac{(r_2^2 - r_1^2) \ln \left(\frac{r}{r_1}\right)}{\ln \frac{r_2}{r_1}} - (r^2 - r_1^2) \right] r dr \\ &= \frac{-\pi}{2\mu} \frac{dp}{dz} \left[ \frac{r_2^2 - r_1^2}{\ln \frac{r_2}{r_1}} \left\{ \frac{r^2}{2} \ln \left(\frac{r}{r_1}\right) - \frac{r^2}{4} \right\} - \frac{r^2}{4} + r_1^2 \frac{r^2}{2} \right]_{r_1}^{r_2} \\ &= \frac{-\pi}{8\mu} \frac{dp}{dz} (r_2^2 - r_1^2) \left[ (r_2^2 + r_1^2) - \frac{r_2^2 - r_1^2}{\ln \left(\frac{r_2}{r_1}\right)} \right] \end{aligned}$$

The average velocity is, therefore, given by

$$\begin{aligned} w_{av} &= Q/\pi(r_2^2 - r_1^2) \\ &= -\frac{1}{8\mu} \frac{dp}{dz} \left[ (r_2^2 + r_1^2) - \frac{r_2^2 - r_1^2}{\ln\left(\frac{r_2}{r_1}\right)} \right] \end{aligned} \quad (\text{AII-4})$$

This development of velocity profile was for the laminar pressure flow. In case the flow is due to the motion of the inner wall rather than due to the pressure gradient as in Couette flow the differential eqn. (AII-1) will be modified as

$$\frac{1}{r} \frac{d}{dr} \left( r \frac{dw}{dr} \right) = 0$$

or

$$d\left(r \frac{dw}{dr}\right) = 0$$

Again integrating twice, we get

$$w = C \ln r + D \quad (\text{AII-5})$$

The boundary conditions are

$$w = 0 \quad \text{at} \quad r = r_2$$

$$w = V_c \quad \text{at} \quad r = r_1$$

From eqn. (AII-5) then, it is easy to obtain

$$C = -\frac{V_c}{\ln\left(\frac{r_2}{r_1}\right)}$$

and

$$D = V_c \frac{\ln \frac{r_2}{r_1}}{\ln \frac{r_2}{r_1}}$$

Eqn. (AII-5) then becomes after simplification

$$w = V_c \frac{\ln \left(\frac{r_2}{r}\right)}{\ln \left(\frac{r_2}{r_1}\right)} \quad (\text{AII-6})$$

To find the average velocity, the total volume flow rate is again given by

$$Q = \int_{r_1}^{r_2} 2\pi r w \, dr$$

Using eqn. (AII-6) and integrating, we get

$$Q = \pi (r_2^2 - r_1^2) V_c \left[ \frac{1}{2 \ln \left(\frac{r_2}{r_1}\right)} - \frac{r_1^2}{r_2^2 - r_1^2} \right]$$

The average velocity is then given by

$$\begin{aligned} w_{av} &= \frac{Q}{\pi (r_2^2 - r_1^2)} \\ &= V_c \left[ \frac{1}{2 \ln \frac{r_2}{r_1}} - \frac{r_1^2}{r_2^2 - r_1^2} \right] \quad (\text{AII-7}) \end{aligned}$$

## APPENDIX AIII

### Computer Solution

The various parameters governing the flow in a capsule-pipeline were calculated by the application of FORTRAN IV language to the equations developed in Chapters 3 and 4 and Appendix AI. The final form of the solution is included in this Appendix. Several appropriately placed comment cards, identified by a letter C in the extreme left hand space, serve to explain the calculations performed in the immediately following portion of the programme. In addition, a summary of the important FORTRAN symbols and a brief description of the programme are included to clarify the solution.

The important symbols are tabulated below with capital lettered word(s) in parentheses, if any, indicating the section(s) of the programme where the symbols appear. Those that have not been so indicated appear in almost all sections of the programme.

| <u>Fortran Symbol</u> | <u>Description</u>  |
|-----------------------|---|
| AC(K,L)               | Inner and outer incremental areas $A_1$ and $A_2$ .   |
| B(K,L)                | Distance from the inner and outer wall ( $b_1$ and $b_2$ ) where $w = \frac{V_c}{2}$ in turbulent Couette flow (VCTAO,VELPCT) |

|         |  |
|---------|--|
| C       | Half of the distance between the two poles of a bipolar coordinate system.   |
| CR(K,L) | Squares of locally concentric radii $r_1$ and $r_2$ for laminar flow in the annulus.   |
| DPDZ    | Pressure gradient applied, $\frac{dp}{dz}$ in $lb_f/ft^3$ .  |
| DR      | Diameter ratio, k.   |
| ECC     | Eccentricity of the annular geometry, e  |
| ETA(1)  | $\eta$ coordinate of the capsule wall, $\eta_1$  |
| ETA(2)  | $\eta$ coordinate of the pipe wall, $\eta_2$   |
| ETAL    | $\eta$ coordinate of the line of maximum velocities for laminar flow -- same for the whole annulus   |
| ETAT    | $\eta$ coordinate of the line of maximum velocities for turbulent flow -- varying with the location of incremental section in the annulus (PRESUR) |
| F       | Friction factor in capsule-pipe system<br>$(f = \frac{2 D}{\rho V_{ann}^2} \frac{dp}{dz})$   |
| FF      | Moody friction factor for the free pipe with the same volume flow as in capsule-pipe system (MAIN)   |
| FSX(L)  | Arc length along a constant $\xi$ curve such as GH in Fig. 4.1   |
| HP      | Horse-power required per foot of pipe length for a unit capsule discharge (MAIN).  |

|       |   |
|-------|---|
| I     | Total number of divisions of the annulus taken as 120   |
| IJ    | The incremental section number after which pressure flow becomes turbulent                              |
| JI    | The incremental section number after which Couette flow becomes turbulent                               |
| K     | Index used to reference inner or outer section. For the inner section, $K = 1$ ; for the outer, $K = 2$ |
| L     | Index used to identify any incremental section -- varies from 1 to I                                    |
| MU    | Dynamic viscosity of the fluid, $\mu$   |
| NU    | Kinematic viscosity of the fluid, $\nu$   |
| OX(K) | Distance of the capsule or pipe centre from the origin (GEOMTR)   |
| PI    | The constant $\pi$  |
| R(1)  | Capsule radius, $R_1$   |
| R(2)  | Pipe radius, $R_2$  |
| RE    | Reynolds number $(\frac{V_{ann} D_h}{\nu})$ in the Capsule-pipe system (MAIN)                           |
| REC   | Reynolds number for Couette flow only in the annulus (VCTAO, VELPCT)                                    |
| REF   | Reynolds number in free pipe $(\frac{V_{av} D}{\nu}) \dots$ (MAIN)                                      |
| REP   | Reynolds number for pressure flow only in the annulus (PRESUR)  |

|          |  |
|----------|--|
| RHO      | Fluid density, $\rho$  |
| RP       | Pressure ratio, $R_p$ (MAIN)   |
| RV       | Velocity ratio, $R_v$ (MAIN)   |
| SE(K,L)  | Incremental arc lengths $s_\eta$ along the capsule and pipe walls                                    |
| SV(K,L)  | Shear velocity, $w^*$ , in pressure flow only  |
| SX(K,L)  | Incremental arc lengths along a constant $\xi$ line such as arcs GT and TH in Fig. 4.1               |
| TAO(K,L) | Total shear stress at the mid points of increment arc lengths along the capsule or pipe wall (VCTAO) |
| TC       | One part of TAO due to Couette flow only (VCTAO)   |
| TP       | The other part of TAO due to pressure flow only (VCTAO)  |
| UT       | Shear velocity, $w^*$ , in Couette flow only (VCTAO,VELPCT)  |
| VAC      | Average velocity for Couette flow only in any incremental section (VELPCT)                           |
| VANN     | Average velocity through the whole annulus (due to fluid alone), $V_{ann}$                           |
| VAP      | Average velocity for pressure flow only in any incremental section (VELPCT)                          |
| VAV(L)   | Average velocity for total flow in any incremental section (VELPCT)                                  |
| VAVG     | Average velocity of flow through the pipe (fluid + capsule), $V_{av}$                                |

|                |  |
|----------------|--|
| VC             | Capsule velocity, $V_c$  |
| VMPT           | Maximum velocity for turbulent pressure flow only in any incremental section<br>( $Re_p > 2100$ ) (PRESUR) |
| W              | Weight coefficient for Gaussian Integration of area (Ref. 31)  |
| XI(L)          | $\xi$ coordinate of the central line through any incremental section                                       |
| XI2(1)         | $\xi_1$ coordinate for any incremental section   |
| XI2(2)         | $\xi_2$ coordinate for any incremental section   |
| X(K,L), Y(K,L) | Coordinates (x,y) of points such as G and H in Fig. 4.1  |
| X1,Y1          | Coordinates (x,y) of points such as Q and R in Fig. 4.1  |
| X2,Y2          | Coordinates (x,y) of points such as P and S in Fig. 4.1  |
| XM,YM          | Coordinates (x,y) of points such as T in Fig. 4.1  |
| YP             | $y^+ = \frac{y w^*}{\nu}$ for turbulent flow (VELPCT)  |
| Z              | Abscissae for Gaussian integration of area (Ref. 31)   |

The complete programme has been divided into 5 sections -- a main programme that calls four sub-programmes for the solution of the problem. The input data for the programme

consists of the weight coefficients  $W$  and abscissae  $Z$  for Gaussian integration (31) of annulus area. Also encountered at a slightly later stage is the input data for pressure gradients required to obtain an average velocity from about 1 ft/sec to 10 ft/sec for all the geometries considered.

After setting the values of a few constants, the main programme calls the subroutine GEOMTR. The first step in this subroutine is to evaluate the  $\eta$  coordinates of the capsule and pipe walls and of the line of maximum velocities for laminar pressure flow. This value is used later in the subroutine PRESUR as a first estimate of  $\eta_m$  for an element in turbulent pressure flow. The next step involves the calculation of  $\xi$  coordinate of the incremental elements in a manner described in Chapter 4 (Sec. 4.2). The rest of the subroutine calculates the incremental arc lengths along the capsule and pipe walls, the coordinates  $(x,y)$  of the mid points of these arcs and the squares of local concentric radii,  $r_1$  and  $r_2$ , required for laminar flow. It may be pointed out that since eqn. (4.4) expresses  $\sin \xi$  in terms of known variables on the right hand side and since, in general,  $\sin(\pi - \theta) = \sin \theta$ , a check had to be provided for the values of XI(L) and XI2(2) till they were individually less than  $\pi/2$ . The details of this check are clear in the subroutine itself.

The calculation of other geometrical constants such as incremental arc lengths along constant  $\xi$  lines for both

inner and outer regions in pressure flow and of areas  $A_1$  and  $A_2$  was carried out in the subroutine PRESUR. The reason for it is that these constants depend on the value of  $\eta_m$  which in turn depends on the nature of pressure flow -- laminar or turbulent -- in the element. Since the number of elements, which may be in turbulent pressure flow, depends not only on the annular geometry but also on the applied pressure gradient, this subroutine has to be called every time the pressure gradient changes even though the annular geometry is same. Such is not the case, however, for calculations performed in the subroutine GEOMTR.

To determine the exact value of  $\eta_m$  for an element in turbulent pressure flow, the subroutine PRESUR first evaluates two incremental areas and two shear velocities for the inner and outer regions. Then the two values of maximum velocity obtained at the estimated value of  $\eta_m$  are matched to within  $10^{-3}\%$  by shifting the value of  $\eta_m$  in a trial and error procedure. It may be mentioned that not more than 2 trials were sufficient to find the exact value of  $\eta_m$  in all the cases encountered.

Subroutine VCTAO calculates the equilibrium velocity of the capsule for the applied pressure gradient. Though only shear force on the capsule needs to be calculated for this purpose, the subroutine also determines the shear stress distribution on the pipe wall. The exact value of capsule velocity is determined by changing  $V_c$  in a trial and error

manner so as to balance the pressure force by the shear force on the capsule. An important variable required for determining the shear stress on the capsule wall is  $b_1$ , the distance from the capsule surface to the point where  $w = V_c/2$  in turbulent Couette flow. This is also given by a trial and error solution of eqn. (3.21).

Having determined the capsule velocity, the subroutine VELPCT calculates the average velocity and volumetric flow rate in the annulus due to the motion of the fluid alone. While determination of average velocity in laminar flow is straightforward by use of eqns. (3.8) and (3.11), it is carried out by numerically integrating the appropriate velocity profile in turbulent flow. Since the distance between the capsule and pipe walls increases from the bottom to the top of the pipe, the number of points at which velocity should be calculated for an element in turbulent flow should also increase. The programme sets this number equal to the number that designates the element so that velocity is calculated at as many as 120 points in the widest gap at the top of the annulus.

Needless to say, the velocity distribution at the central line of the element was assumed to be the same over the whole of the incremental section. The average velocity in each section was then multiplied by its corresponding cross-sectional area and the products were summed for all elements to give the volumetric flow rate. A machine subroutine QSF to be subsequently elaborated, was used for the

numerical integration of the velocity profile by Simpson's and Newton's 3/8 rule.

The various parameters such as  $V_{av}$ ,  $R_v$ ,  $R_p$ ,  $f$ ,  $Re$ , etc. were then calculated in the main programme. For calculation of  $R_p$  in case the fluid flow in the free pipe was turbulent, the curve for smooth pipes in the Moody diagram was approximated by the relation given by Colebrook and White. This relation is

$$\frac{1}{\sqrt{f_f}} = 1.74 - 2 \log_{10} \left( \frac{18.7}{Re_f \sqrt{f_f}} \right) \quad (\text{AIII-1})$$

Knowing  $Re_f$ , this equation was solved for the friction factor  $f_f$  in a trial and error procedure.

All the four trial and error solutions were based on linear approximations meaning thereby that the relation between the two variables concerned was assumed to be linear. Fig. AIII-1 may be considered to understand this concept clearly. Let OG be the starting

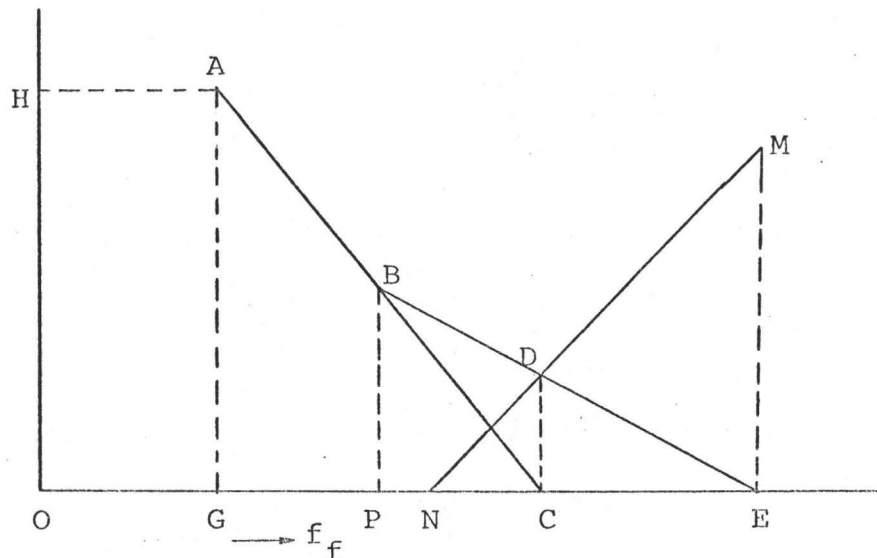


Fig. AIII-1 LINEAR APPROXIMATIONS TO THE TRUE VALUE

value of  $f_f$  for a known  $Re_f$ . Then if OG were the true value of  $f_f$ , the ordinate would have been zero. However, let it be OH so that A represents the starting point. Let the first prediction, which is always arbitrary in such a technique, estimate the value of  $f_f$  to be OP, giving the ordinate equal to PB. Now assuming a straight line relationship, the programme will estimate that for the ordinate to be zero, the value of  $f_f$  should be OC. Starting with OC, let CD be the actual ordinate value instead of zero. The straight line BD will then estimate the value of  $f_f$  to be OE, followed by ON and so on till the ordinate becomes very nearly zero -- less than a preassigned value such as  $10^{-10}$ .

The following is a brief outline of the subroutine QSF called in the subprogramme VELPCT. To compute the vector of integral values:

$$z_i = z(x_i) = \int_a^{x_i} y(x) dx \quad (i = 1, 2, 3, \dots, n)$$

with  $x_i = a + (i - 1)h$

formulae used in QSF are ( $z_1 = 0$  to start with)

$$z_j = z_{j-1} + \frac{h}{3}(1.25 y_{j-1} + 2y_j - 0.25 y_{j+1})$$

$$z_j = z_{j-2} + \frac{h}{3} (y_{j-2} + 4y_{j-1} + y_j) \dots \text{Simpson's Rule}$$

$$z_j = z_{j-3} + \frac{3h}{8} (y_{j-3} + 3y_{j-2} + 3y_{j-1} + y_j) \dots \text{Newton's 3/8 rule}$$

$$z_j = z_{j-5} + \frac{h}{3} (y_{j-5} + 3.875 y_{j-4} + 2.625 y_{j-3} + 2.625 y_{j-2} + 3.875 y_{j-1} + y_j)$$

where  $z_j$  are integral values

$y_j$  are function values

and  $h$  is the size of the interval

In these formulae, the truncation error is of the order of  $h^5$ .

The complete programme that follows is quite general in the sense that appropriate changes need be made only in the main section for any different geometry or a different liquid carrier. The total number of divisions of the annulus can also be changed without any difficulty.

C MAIN SECTION OF THE PROGRAMME

C ALL LINEAR DISTANCES ARE IN INCHES , AREAS IN SQ. INCHES , VELOCITIES  
 C IN FT/SEC. , RHO IN SLUGS/C.FT , NU IN FT\*\*2/SEC , MU IN SLUGS/FT-SEC,  
 C TAO IN LBF/FT\*\*2 , DPDZ IN LBF/C.FT AND HP IN (HP/FT)/(C.FT/SEC) .

C REAL NU,MU  
 DIMENSION Z(16,16),W(16,16),R(2),ETA(2),SE(2,120),CR(2,120),SX(2,1  
 120),AC(2,120),SV(2,120),XI(120),DXI(120),XIA(120),FSX(120),B(2,120  
 2),X(2,120),Y(2,120),DP(10)  
 DATA PI,I,ECC/3.1415926535898,120,.999/  
 READ(5,40) RHO,MU,NU,AUX  
 40 FORMAT(F7.0,2E14.8,F4.0)

C READING THE ABSCISSAE Z AND WEIGHT COEFFICIENTS W FOR GAUSS INTEGRATION

C DO 45 NN=2,16,2  
 N=NN/2  
 DO 45 M=1,N  
 READ(5,46) Z(NN,M),W(NN,M)  
 46 FORMAT(2F20.12)  
 MM=NN+1-M  
 Z(NN,MM)=-Z(NN,M)  
 45 W(NN,MM)=W(NN,M)

C CALLING SUBROUTINES IN ORDER TO CALCULATE VC AND VANN FOR A GIVEN DPDZ

C DO 38 NDIA =1,64  
 READ(5,55) DP,DR,R(2)  
 55 FORMAT(10F6.0,2F5.0)  
 R(1)=DR\*R(2)  
 CALL GEOMTR (C,I,PI,R,DR,ECC,ETA,ETAL,XI,DXI,XIA,SE,X,Y,CR)  
 IF(NDIA-33) 35,36,35  
 36 READ(5,40) RHO,MU,NU,AUX  
 35 AUY=.5\*(1.-DR)\*(1.-ECC)  
 WRITE(6,34) R,DR,ECC,AUY,RHO,MU,NU  
 DO 38 NVC =1,10  
 DPDZ=DP(NVC)\*(1.-DR)\*AUX/.72  
 VC=NVC  
 SOM=PI\*R(1)\*R(1)\*DPDZ/144.  
 CALL PRESUR (C,I,IJ,DPDZ,FSX,W,Z,SX,ETAL,ETA,SE,SV,AC,RHO,MU,NU,XI  
 1,DXI,XIA,X,Y,CR)  
 CALL VCTAO (I,IJ,JI,MU,NU,DPDZ,SV,FSX,VC,SE,CR,RHO,SUM,SOM,B,NTC)  
 CALL VELPCT(I,IJ,JI,CR,DPDZ,MU,NU,SX,FSX,SV,VC,AC,PI,R,VANN,B)

C CALCULATING VELOCITY AND PRESSURE RATIOS AND ENERGY REQUIREMENTS

C VAVG=VANN-(VANN-VC)\*DR\*DR  
 RV=VC/VAVG  
 F=R(2)\*DPDZ/(RHO\*VANN\*VANN\*3.)  
 RE=VANN\*(R(2)-R(1))/NU/6.  
 REF=VAVG\*R(2)/(NU\*6.)  
 IF(REF.LE.2100.) GO TO 17

```

N=0
FF=0.02
28. RH=2.*ALOG10(REF*SQRT(FF))-0.7963-1./SQRT(FF)
   IF(ABS(RH ).LE.1.E-10) GO TO 26
   IF(N.GT.0) GO TO 27
   AF=FF
   AUY=RH
   FF=1.1*FF
   N=1
   GO TO 28
27  AD=RH *(FF-AF)/(RH -AUY)
   AF=FF
   AUY=RH
   FF=FF-AD
   N=N+1
   IF(N.GT.15) GO TO 29
   GO TO 28
29  WRITE(6,30) REF,VAVG
30  FORMAT(1H0,2X,*N OVER 15 FOR RE =*,E10.3,* AND VAVG =*,F7.3)
26  RP=(VANN/VAVG)**2*F/FF
   GO TO 19
17  RP=DPDZ*R(2)*R(2)/(1152.*MU*VAVG)
19  HP=DPDZ/(RV*DR*DR*550.)

```

C

C. WRITING THE RESULTS AND PUNCHING THEM OUT ON COMPUTER CARDS

C

```

WRITE(6,91) VC,DPDZ,VANN,VAVG,RV,RP,HP,RE,F,IJ,JI,SUM,SOM,NTC
WRITE(7,92) R(2),DR,ECC,VC,DPDZ,VANN,VAVG,RV,RP
WRITE(7,95) RE,F,HP,IJ,JI,SOM,SUM,NTC
38  CONTINUE
34  FORMAT(1H1,/,4X,*R(1) =*,F7.3,* INCHES*,5X,*R(2) =*,F5.1,* INCHES
1*,5X,*DIAMETER RATIO =*,F5.3,5X,*ECCENTRICITY =*,F5.3,5X,*CLEARANC
2E =*,E10.3,* DIA*,/,15X,*RHO =*,F7.4,* SLUGS/C.FT*,10X,*MU =*,E13
3.6,* SLUGS/FT-SEC*,10X,*NU =*,E13.6,10H FT**2/SEC,/,5X,*VC*,6X,*
4PSF/FT*,6X,*VANN*,6X,*VAVG*,7X,*RV*,8X,*RP   HP-S/FT3-FT   REY*
5,10X,*F*,8X,*IJ   JI   PIPE SF   CAP SF   NTC*,/)
91  FORMAT(1H0,F8.4,F11.5,2F10.4,F10.5,F10.4,3E12.3,2I6,2E10.2,I4)
92  FORMAT(F4.1,2F5.3,F14.10,F10.6,F14.10,F10.6,F8.6,F10.6)
95  FORMAT(E15.7,2E14.7,2I4,2E13.6,I3)
STOP
END

```

SUBROUTINE GEOMTR (C,I,PI,R,DR,ECC,ETA,ETAL,XI,DXI,XIA,SE,X,Y,CR)

C  
C SUBROUTINE TO CALCULATE A FEW GEOMETRICAL CONSTANTS

C  
C DIMENSION R(2),ETA(2),OX(2),SINH(2),COSH(2),XI2(2),XI(1),DXI(1),XI  
1A(1),SE(2,I),X(2,I),Y(2,I),CR(2,I)

C  
C SETTING ETA VALUES AND LOCATING CENTRES OF PIPE AND CAPSULE

C  
C  
C AUX=(1.+DR)/ECC+(1.-DR)\*ECC  
C ETA(2)=ALOG(AUX/2.+SQRT(AUX\*AUX/4.-1.))  
C C=R(2)\*(EXP(ETA(2))-EXP(-ETA(2)))/2.  
C ETA(1)=ALOG(C/R(1)+SQRT(C\*C/R(1)/R(1)+1.))  
C AUX=.5\*(SQRT((1.-TANH(ETA(1)))\*(1.+TANH(ETA(2))))+SQRT((1.+TANH(ET  
1A(1)))\*(1.-TANH(ETA(2))))))  
C ETAL=ALOG(1./AUX+SQRT(1./AUX/AUX-1.))  
C DO 5 K=1,2  
C OX(K)=-C/TANH(ETA(K))  
C AUX=EXP(-ETA(K))  
C COSH(K)=(1./AUX+AUX)/2.  
5 SINH(K)=COSH(K)-AUX  
C XOX=(OX(1)+OX(2))/2.

C  
C GENERATING VALUES OF ELEMENTAL XI

C  
C  
C PXI=0.0  
C XI2(2)=0.0  
C DO 16 L=1,I  
C TH2=(FLOAT(L)-.5)\*PI/FLOAT(I)  
C XI(L)=ASIN(-SIN(TH2)\*SINH(2)/(OX(2)/R(2)+COS(TH2)))  
C IF(XI(L).LT.PXI) XI(L)=PI-XI(L)  
C IF(XI(L).GT.PI/2.) GO TO 19  
C AUX=C\*SQRT((COSH(2)-COS(XI(L)))/(COSH(2)+COS(XI(L))))  
C AUX=ASIN(AUX\*SIN(ATAN(SIN(XI(L))/SINH(2)))/R(2))  
C IF(ABS(TH2-AUX).GT.1.E-5) XI(L)=PI-XI(L)  
19 PXI=XI(L)  
C XI2(1)=XI2(2)  
C AUX=FLOAT(L)\*PI/FLOAT(I)  
C XI2(2)=ASIN(-SIN(AUX)\*SINH(2)/(OX(2)/R(2)+COS(AUX)))  
C IF(XI2(2).LT.XI2(1)) XI2(2)=PI-XI2(2)  
C N=0

C  
C FINDING ARC LENGTH OF ELEMENTS ALONG THE WALLS

C  
C  
C IF(L.EQ.1) GO TO 25  
C SE(2,L)=SE(2,1)  
C GO TO 23  
25 SE(2,1)=PI\*R(2)/FLOAT(I)  
C X1=-C\*SINH(1)/(COSH(1)+1.)  
C Y1=0.0  
C GO TO 24  
23 X1=X2  
C Y1=Y2

```

24  X2=-C*SINH(1)/(COSH(1)+COS(XI2(2)))
    Y2=-X2*SIN(XI2(2))/SINH(1)
    SE(1,L)=2.*R(1)*ASIN(SQRT((X2-X1)**2+(Y2-Y1)**2)/2./R(1))
    IF(XI2(2).GT.PI/2. .OR. N.EQ.1) GO TO 28
    IF(SE(1,L)/SE(2,1).LT.0.95) XI2(2)=PI-XI2(2)
    N=N+1
    GO TO 24
28  DXI(L)=(XI2(2)-XI2(1))/2.
    XIA(L)=(XI2(2)+XI2(1))/2.

```

C  
C  
C

FINDING LOCAL CONCENTRIC RADII FOR VELOCITY PROFILES IN LAMINAR FLOW

```

DO 16 K=1,2
X(K,L)=-C*SINH(K)/(COSH(K)+COS(XI(L)))
Y(K,L)=-X(K,L)*SIN(XI(L))/SINH(K)
16  CR(K,L)=(X(K,L)-XOX)**2+Y(K,L)**2
    RETURN
    END

```

```

SUBROUTINE PRESUR(C,I,IJ,DPDZ,FSX,W,Z,SX,ETAL,ETA,SE,SV,AC,RHO,MU,
1NU,XI,DXI,XIA,X,Y,CR)

```

```

C
C SUBROUTINE TO FIND THE SHEAR VELOCITY IN TURBULENT REGION AFTER
C LOCATING THE MAX. VELOCITY CURVE PRECISELY IN THE WHOLE ANNULUS
C WHEN THE CAPSULE IS STATIONARY

```

```

C
C CALCULATION OF ELEMENTAL AREAS AND ARC LENGTHS ALONG CONSTANT XI
C LINES IS IMPLICIT FOR THIS PURPOSE

```

```

C
C DIMENSION SE(2,I),SX(2,I),AC(2,I),SV(2,I),FSX(I),W(16,16),Z(16,16)
1,ETA(2),CE(2),FV(2),H(2),VMPT(2),XI(I),DXI(I),XIA(I),X(2,I),Y(2,I)
2,CR(2,I)

```

```

REAL NU,MU

```

```

IJ=0

```

```

N=1

```

```

NN=2

```

```

DO 43 L=1,I

```

```

ETAT=ETAL

```

```

NT=0

```

```

C
C FINDING ARC LENGTHS ALONG THE CENTRAL XI LINES

```

```

54 COSHM=(EXP(ETAT)+EXP(-ETAT))/2.

```

```

SINHM=COSHM-EXP(-ETAT)

```

```

XM=-C*SINHM/(COSHM+COS(XI(L)))

```

```

YM=-XM*SIN(XI(L))/SINHM

```

```

DO 47 K=1,2

```

```

SX(K,L)=2.*C*ASIN(.5*SIN(XI(L))*SQRT((X(K,L)-XM)**2+(Y(K,L)-YM)**2
1)/C)/SIN(XI(L))

```

```

C
C CALCULATING ELEMENTAL AREA BY GAUSS INTEGRATION TECHNIQUE

```

```

BM=(ETAT-ETA(K))/2.

```

```

IF(K.EQ.2) BM=-BM

```

```

BP=(ETAT+ETA(K))/2.

```

```

IF(L-N*15) 25,25,26

```

```

26 NN=NN+2

```

```

N=N+1

```

```

25 AC(K,L)=0.0

```

```

DO 47 M=1,NN

```

```

AUX=BM*Z(NN,M)+BP

```

```

DO 47 NA=1,6

```

```

47 AC(K,L)=AC(K,L)-C*C*BM*DXI(L)*W(NN,M)*W(6,NA)/(((EXP(AUX)+EXP(-AUX
1))/2.+COS(DXI(L)*Z(6,NA)+XIA(L)))**2)

```

```

C
C TESTING FOR TRANSITION FROM LAMINAR TO TURBULENT FLOW WHEN VC=0.0

```

```

FSX(L)=SX(1,L)+SX(2,L)

```

```

IF(L.GT.(IJ+1)) GO TO 51

```

```

BM=2./ALOG(CR(2,L)/CR(1,L))

```

```

REP=DPDZ*(CR(1,L)*(1.+BM)+CR(2,L)*(1.-BM))*(FSX(L)/MU)/(NU*6912.)

```

```
IF(REP.GT.2100.) GO TO 51
```

```
IJ=L
```

```
GO TO 43
```

```
C
```

```
C LOCATING MAX. VELOCITY LINE FOR THE ELEMENT UNDER CONSIDERATION IF  
C FOUND IN TURBULENT REGION ( RE .GT. 2100 )
```

```
C
```

```
51 DO 49 K=1,2
```

```
SV(K,L)=SQRT(DPDZ*AC(K,L)/SE(K,L)/RHO/12.)
```

```
49 VMPT(K) =SV(K,L)*(3.8+2.78*ALOG(SX(K,L)*SV(K,L)/NU/12.))
```

```
AUX=2.*(VMPT(2)-VMPT(1))/(VMPT(1)+VMPT(2))
```

```
IF(ABS(AUX).LE.1.E-5) GO TO 43
```

```
IF(NT.GT.0) GO TO 52
```

```
C
```

```
C FIRST PREDICTION OF ETAT
```

```
C
```

```
FV(1)=VMPT(1)
```

```
FV(2)=VMPT(2)
```

```
ETAT=.999*ETAT
```

```
NT=1
```

```
GO TO 54
```

```
C
```

```
C SUBSEQUENT PREDICTIONS OF ETAT UPTO A MAX. OF 5
```

```
C
```

```
52 DO 53 K=1,2
```

```
CE(K)=(VMPT(K) -FV(K))/(ETAT-ETAL)
```

```
53 H(K)=VMPT(K) -CE(K)*ETAT
```

```
ETAT=(H(2)-H(1))/(CE(1)-CE(2))
```

```
NT=NT+1
```

```
IF(NT.GT.5) GO TO 44
```

```
GO TO 54
```

```
44 WRITE(6,45) L
```

```
45 FORMAT(/,10X,5H*****,*NUMBER OF TRIALS REQUIRED FOR LOCATING THE M  
1AX. VELOCITY LOCUS HAS GONE OVER 5 FOR THE ELEMENT*,I4,2X,5H*****)
```

```
43 CONTINUE
```

```
RETURN
```

```
END
```

```

SUBROUTINE VCTAO (I,IJ,JI,MU,NU,DPDZ,SV,FSX,VC,SE,CR,RHO,SUM,SOM,B
1,NTC)

```

C

```

C SUBROUTINE TO FIND THE CAPSULE VELOCITY FOR A GIVEN DP/DZ
C SHEAR STRESS DISTRIBUTION IS ALSO CALCULATED ON BOTH THE WALLS

```

C

```

    DIMENSION SE(2,I),SV(2,I),CR(2,I),B(2,I),FSX(I),TAO(2,120),TP(120)
    REAL NU,MU
    NTC=-1
    DO 65 K=1,2
    IF(K.EQ.2) GO TO 22
32  NTC=NTC+1
    IF(NTC.GT.10) GO TO 36

```

C

```

C JI REPRESENTS THE SECTION AFTER WHICH COUETTE FLOW BECOMES TURBULENT

```

C

```

    JI=0
    L=0
19  L=L+1
    REC=VC*(1./ALOG(CR(2,L)/CR(1,L))-CR(1,L)/(CR(2,L)-CR(1,L)))*(FSX(L
1)/NU)/6.
    IF(REC.GT.2400.) GO TO 24
    JI=L
    IF(L-I) 19,22,22
24  M=JI+1

```

C

```

C FINDING DISTANCE FROM THE WALLS WHERE U=VC/2 IN TURBULENT COUETTE FLOW

```

C

```

    DO 72 L=M,I
    D=SQRT(SE(2,L)/SE(1,L))
    DD=(VC/NU/24.)**(1.-D)
    B(1,L)=FSX(L)/2.
    N=0
25  BD=B(1,L)**D/(FSX(L)-B(1,L))
    IF(ABS(1.-BD/DD).LE.1.E-4) GO TO 68
    IF(N.GT.0) GO TO 73
    CE=B(1,L)
    FV=BD
    B(1,L)=0.95*B(1,L)
    N=1
    GO TO 25
73  H=(B(1,L)-CE)/(BD-FV)
    CE=B(1,L)
    FV=BD
    N=N+1
    IF(N.GT.10) GO TO 67
    B(1,L)=B(1,L)+H*(DD-BD)
    GO TO 25
67  WRITE(6,64) L
64  FORMAT(1H0,10X,5H*****,* NUMBER OF TRIALS FOR FINDING B HAS GONE O
1VER 10 FOR THE ELEMENT*,I5,7H *****,/)
68  B(2,L)=FSX(L)/2.
72  CONTINUE

```

```

22  SUM=0.0
    DO 20 L=1,I
C
C  SHEAR STRESS CALCULATION IN PRESSURE FLOW (LAMINAR OR TURBULENT)
C
    IF(NTC.GT.0 .AND. K.EQ.1) GO TO 26
    IF(L.GT.IJ) GO TO 21
    TP(L)=DPDZ*((CR(2,L)-CR(1,L))/ALOG(CR(2,L)/CR(1,L))-CR(K,L))/SQRT(
1CR(K,L))/24.
    GO TO 26
21  TP(L)=RHO*SV(K,L)*SV(K,L)
C
C  SHEAR STRESS CALCULATION IN COUETTE FLOW (LAMINAR OR TURBULENT)
C
26  IF(L.GT.JI) GO TO 16
    TC=24.*MU*VC/SQRT(CR(K,L))/ALOG(CR(2,L)/CR(1,L))
    GO TO 17
16  UT=.095*VC/ALOG10(VC*B(K,L)/NU/24.)
    TC=RHO*UT*UT
17  IF(K.EQ.1) TC=-TC
C
C  TESTING FOR NET (SHEAR + PRESSURE) FORCE ON THE CAPSULE TO BE ZERO
C
    TAO(K,L)=TP(L)+TC
20  SUM=SUM+TAO(K,L)*SE(K,L)/6.
    IF(K.EQ.2 .OR. ABS(SUM+SOM).LE.1.E-10) GO TO 65
    IF(NTC.GT.0) GO TO 35
C
C  PREDICTION OF VC ASSUMING A LINEAR RELATIONSHIP BETWEEN VC AND SUM
C
    FVC=VC
    AUY=SUM
    VC=1.1 *VC
    GO TO 32
35  CE =(SUM+SOM)*(VC-FVC)/(SUM-AUY)
    FVC=VC
    AUY=SUM
    VC=VC-CE
    GO TO 32
36  NTC=10
65  CONTINUE
    RETURN
    END

```

SUBROUTINE VELPCT (I,IJ,JI,CR,DPDZ,MU,NU,SX,FSX,SV,VC,AC,PI,R,VANN  
1,B)

C  
C SUBROUTINE TO FIND VANN , THE AVERAGE VELOCITY IN THE ANNULUS  
C

DIMENSION SX(2,I),SV(2,I),AC(2,I),CR(2,I),B(2,I),FSX(I),R(2),VAV(1  
120),VA(122),VPC(122)

REAL NU,MU  
SUM=0.0

C  
C ELEMENTAL AVERAGE VELOCITY IN LAMINAR PRESSURE FLOW  
C

DO 71 L=1,I  
IF(L.GT.IJ) GO TO 20  
VAP=2./ALOG(CR(2,L)/CR(1,L))  
VAP=DPDZ\*(CR(1,L)\*(1.+VAP)+CR(2,L)\*(1.-VAP))/MU/1152.  
GO TO 21

20 N=L+1

C  
C ELEMENTAL AVERAGE VELOCITY IN TURBULENT PRESSURE FLOW  
C

VPC(1)=0.0  
DO 80 J=2,N  
Y=FLOAT(J-1)\*FSX(L)/FLOAT(N)  
IF(Y.GT.SX(1,L)) GO TO 25  
K=1  
GO TO 26  
25 K=2  
Y=FSX(L)-Y  
26 YP=Y\*SV(K,L)/NU/12.  
IF(YP.LT.26.0) GO TO 78  
VPC(J)=SV(K,L)\*(3.8+2.78\*ALOG(YP))  
GO TO 80  
78 IF(YP.LT.5.0 ) GO TO 79  
VPC(J)=SV(K,L)\*(-3.05+5.\*ALOG(YP))  
GO TO 80  
79 VPC(J)=SV(K,L)\*YP  
80 CONTINUE  
Y=FSX(L)/FLOAT(N)/12.  
N=N+1  
VPC(N)=0.0  
CALL QSF (Y,VPC,VA,N)  
VAP=12.\*VA(N)/FSX(L)

C  
C ELEMENTAL AVERAGE VELOCITY IN LAMINAR COUETTE FLOW  
C

21 IF(L.GT.JI) GO TO 22  
VAC=VC\*(1./ALOG(CR(2,L)/CR(1,L))-CR(1,L)/(CR(2,L)-CR(1,L)))  
GO TO 23  
22 N=L+1

C  
 C ELEMENTAL AVERAGE VELOCITY IN TURBULENT COUETTE FLOW  
 C

```

VPC(1)=VC
B(2,L)=FSX(L)-B(1,L)
DO 75 J=2,N
Y=FLOAT(J-1)*FSX(L)/FLOAT(N)
IF(Y.GT.B(1,L)) GO TO 24
K=1
GO TO 27
24 K=2
Y=FSX(L)-Y
27 YD=Y/B(K,L)
REC=VC*B(K,L)/NU/24.
IF(YD.LT.0.1) GO TO 84
Y=1./(2.671-0.119*ALOG(REC))
VPC(J)=VC*(Y+(1.-Y)*SQRT(YD))/2.
GO TO 28

```

C  
 C FOR WALL REGION IN TURBULENT COUETTE FLOW  
 C

```

84 UT=.095*VC/ALOG10(REC)
YP=Y*UT/NU/12.
IF(YP.LT.15.0)GO TO 85
VPC(J)=5.6*UT*(1.+ALOG10(YP))
GO TO 28
85 VPC(J)=YP*UT
IF(YP.GT.10.) VPC(J)=0.8*VPC(J)
28 IF(K.EQ.1) VPC(J)=VC-VPC(J)
75 CONTINUE
Y=FSX(L)/FLOAT(N)/12.
N=N+1
VPC(N)=0.0
CALL QSF (Y,VPC,VA,N)
VAC=12.*VA(N)/FSX(L)
23 VAV(L)=VAP+VAC
71 SUM=SUM+VAV(L)*(AC(1,L)+AC(2,L))
VANN=2.*SUM/(PI*(R(2)*R(2)-R(1)*R(1)))
RETURN
END

```

C THE INPUT DATA

1.936 2.08768267E-051.07834849E-051.0  
.577350269190 1.00000  
.339981043585 .652145154863  
.861136311594 .347854845137  
.238619186083 .467913934573  
.661209386466 .360761573048  
.932469514203 .171324492379  
.183434642496 .362683783378  
.525532409916 .313706645878  
.796666477414 .222381034453  
.960289856498 .101228536290  
.148874338982 .295524224715  
.433395394129 .269266719310  
.679409568299 .219086362516  
.865063366689 .149451349151  
.973906528517 .066671344309  
.125333408511 .249147045813  
.367831498918 .233492536538  
.587317954287 .203167426723  
.769902674194 .160078328543  
.904117256394 .106939325995  
.981560634247 .047175336387  
.108054948707 .215263853463  
.319112368928 .205198463721  
.515248636358 .185538397478  
.687292904812 .157203167158  
.827201315070 .121518570688  
.928434883664 .080158087160  
.986283808697 .035119460332  
.095012509838 .189450610455  
.281603550779 .182603415045  
.458016777657 .169156519395  
.617876244403 .149595988817  
.755404408355 .124628971256  
.865631202388 .095158511682  
.944575023073 .062253523939  
.989400934992 .027152459412  
2.880 6.035 9.46413.17417.10221.22225.61530.42335.14740.449 .900 2.0  
5.73011.85018.39625.34032.62640.24648.23656.60065.33074.075 .930 2.0  
11.03722.49 34.62247.27860.48974.17 88.431103.24118.01133.86 .950 2.0  
17.1 34.4 53.0 71.94591.62 112.1 133.29155.0 177.2 200.48 .960 2.0  
30.58661.25 93.115126.32160.25194.93230.76266.92304.23342.56 .970 2.0  
68.36 136.72205.16275.4 349.0 423.0 498.1 575.6 654.0 732.54 .980 2.0  
121.14242.26363.39484.5 606.62737.63868.3 1000.61133.61267.5 .985 2.0  
272.2 543.32815.0 1086.61358.41630.01901.62189.82481.72772.4 .990 2.0  
1.320 2.800 4.460 6.320 8.33010.42012.75015.25017.78020.750 .900 3.0  
2.590 5.453 8.57611.92715.47819.36323.49827.67232.31036.900 .930 3.0  
4.90010.25016.00022.00028.30034.96542.00049.33057.03065.340 .950 3.0  
7.65015.73024.30033.26042.66052.56062.92073.60084.69095.880 .960 3.0  
13.6 27.73 42.52 57.86 73.74 90.26 107.49125.07143.52161.76 .970 3.0  
30.4 60.8 92.6 125.3 159.4 193.5 229.4 266.0 302.6 340.6 .980 3.0

53.84 107.65161.5 218.54276.83336.0 396.5 457.56519.35585.1 .985 3.0  
 120.8 241.47362.22483.0 603.68735.35865.4 997.3 1131.01263.7 .990 3.0  
 .350 .790 1.300 1.910 2.593 3.320 4.110 5.060 5.985 6.981 .900 6.0  
 .682 1.492 2.421 3.458 4.617 5.891 7.258 8.67210.34111.963 .930 6.0  
 1.290 2.740 4.400 6.200 8.15010.22212.52014.98017.49020.240 .950 6.0  
 1.963 4.170 6.596 9.22611.97514.96018.22821.73425.20829.090 .960 6.0  
 3.480 7.26011.29015.66020.22025.20030.40335.62541.52747.260 .970 6.0  
 7.60015.68024.30033.20042.65052.40062.62073.36084.57095.760 .980 6.0  
 13.46 27.34 42.07 57.28 73.08 89.33 106.6 124.04142.3 160.6 .985 6.0  
 30.2 60.36 91.93 124.72158.27192.76228.06264.05300.64338.44 .990 6.0  
 .099 .240 .417 .631 .873 1.141 1.481 1.819 2.185 2.575 .900 12.0  
 .187 .433 .737 1.088 1.498 1.970 2.466 3.000 3.575 4.310 .930 12.0  
 .343 .771 1.289 1.875 2.532 3.283 4.068 4.906 5.921 6.900 .950 12.0  
 .524 1.161 1.871 2.722 3.636 4.647 5.735 6.973 8.233 9.541 .960 12.0  
 .916 1.977 3.167 4.453 5.928 7.504 9.22011.07012.98015.172 .970 12.0  
 1.960 4.163 6.567 9.20012.02014.95018.22021.70025.19029.057 .980 12.0  
 3.465 7.17511.19315.51020.10024.95630.13535.40441.19446.900 .985 12.0  
 7.55015.65624.19033.10042.47552.34062.49573.05084.07095.395 .990 12.0  
 2.880 6.035 9.46413.17417.10221.22225.61530.42335.14740.449 .900 2.0  
 1.6456 2.08768267E-041.26864528E-048.0  
 5.73011.85018.39625.34032.62640.24648.23656.60065.33074.075 .930 2.0  
 11.03722.49 34.62247.27860.48974.17 88.431103.24118.01133.86 .950 2.0  
 17.1 34.4 53.0 71.94591.62 112.1 133.29155.0 177.2 200.48 .960 2.0  
 30.58661.25 93.115126.32160.25194.93230.76266.92304.23342.56 .970 2.0  
 68.36 136.72205.16275.4 349.0 423.0 498.1 575.6 654.0 732.54 .980 2.0  
 121.14242.26363.39484.5 606.62737.63868.3 1000.61133.61267.5 .985 2.0  
 272.2 543.32815.0 1086.61358.41630.01901.62189.82481.72772.4 .990 2.0  
 1.320 2.800 4.460 6.320 8.33010.42012.75015.25017.78020.750 .900 3.0  
 2.590 5.453 8.57611.92715.47819.36323.49827.67232.31036.900 .930 3.0  
 4.90010.25016.00022.00028.30034.96542.00049.33057.03065.340 .950 3.0  
 7.65015.73024.30033.26042.66052.56062.92073.60084.69095.880 .960 3.0  
 13.6 27.73 42.52 57.86 73.74 90.26 107.49125.07143.52161.76 .970 3.0  
 30.4 60.8 92.6 125.3 159.4 193.5 229.4 266.0 302.6 340.6 .980 3.0  
 53.84 107.65161.5 218.54276.83336.0 396.5 457.56519.35585.1 .985 3.0  
 120.8 241.47362.22483.0 603.68735.35865.4 997.3 1131.01263.7 .990 3.0  
 .350 .790 1.300 1.910 2.593 3.320 4.110 5.060 5.985 6.981 .900 6.0  
 .682 1.492 2.421 3.458 4.617 5.891 7.258 8.67210.34111.963 .930 6.0  
 1.290 2.740 4.400 6.200 8.15010.22212.52014.98017.49020.240 .950 6.0  
 1.963 4.170 6.596 9.22611.97514.96018.22821.73425.20829.090 .960 6.0  
 3.480 7.26011.29015.66020.22025.20030.40335.62541.52747.260 .970 6.0  
 7.60015.68024.30033.20042.65052.40062.62073.36084.57095.760 .980 6.0  
 13.46 27.34 42.07 57.28 73.08 89.33 106.6 124.04142.3 160.6 .985 6.0  
 30.2 60.36 91.93 124.72158.27192.76228.06264.05300.64338.44 .990 6.0  
 .099 .240 .417 .631 .873 1.141 1.481 1.819 2.185 2.575 .900 12.0  
 .187 .433 .737 1.088 1.498 1.970 2.466 3.000 3.575 4.310 .930 12.0  
 .343 .771 1.289 1.875 2.532 3.283 4.068 4.906 5.921 6.900 .950 12.0  
 .524 1.161 1.871 2.722 3.636 4.647 5.735 6.973 8.233 9.541 .960 12.0  
 .916 1.977 3.167 4.453 5.928 7.504 9.22011.07012.98015.172 .970 12.0  
 1.960 4.163 6.567 9.20012.02014.95018.22021.70025.19029.057 .980 12.0  
 3.465 7.17511.19315.51020.10024.95630.13535.40441.19446.900 .985 12.0  
 7.55015.65624.19033.10042.47552.34062.49573.05084.07095.395 .990 12.0

## REFERENCES

- (1) Piercy, N.A.V., Hooper, M.S. and Winny, H.F., "Viscous Flow through Pipes with Cores", *Philosophical Magazine*, Series 7, Volume 15, 1933, pages 647-675.
- (2) Heyda, J.F., "Heat Transfer in Turbulent Flow through Non-Concentric Annuli having Unequal Heat Release from the Walls", APEX-391, General Electric Report, June 1957.
- (3) Brighton, J.A. and Jones, J.B., "Fully Developed Turbulent Flow in Annuli", *Journal of Basic Engineering*, Transactions ASME, Series D, Volume 86, December 1964, pages 835-844.
- (4) Jonsson, V.K. and Sparrow, E.M., "Experiments on turbulent-flow phenomena in eccentric annular ducts", *Journal of Fluid Mechanics*, Volume 25, Part 1, 1966, pages 65-86.
- (5) Wilson, N.W., "A Theoretical Analysis of the Velocity Fields in Eccentric Annuli", M. Eng. Thesis, McMaster University, May 1966.
- (6) Hodgson, G.W. and Charles, M.E., "The Pipeline Flow of Capsules; Part 1: The Concept of Capsule Pipelining", *Canadian Journal of Chemical Engineering*, Volume 41, 1963, pages 43-45.
- (7) Charles, M.E., "The Pipeline Flow of Capsules; Part 2: Theoretical Analysis of the Concentric Flow of

- Cylindrical Forms", Canadian Journal of Chemical Engineering, Volume 41, No. 2, 1963, pages 46-51.
- (8) Ellis, H.S., "The Pipeline flow of Capsules; Part 3: An Experimental Investigation of the Transport by Water of Single Cylindrical and Spherical Capsules with Density equal to that of the Water", Canadian Journal of Chemical Engineering, Volume 42, No. 1, 1964, pages 1-8.
- (9) Ellis, H.S., "The Pipeline Flow of Capsules; Part 4: An Experimental Investigation of the Transport in Water of Single Cylindrical Capsules with Density greater than that of Water", Canadian Journal of Chemical Engineering, Volume 42, No. 2, 1964, pages 69-76.
- (10) Ellis, H.S., "The Pipeline Flow of Capsules; Part 5: An Experimental Investigation of the Transport by Water of Single Spherical Capsules with Density greater than that of the Water", Canadian Journal of Chemical Engineering, Volume 42, No. 4, 1964, pages 155-161.
- (11) Newton, R., Redberger, P.J. and Round, G.F., "The Pipeline Flow of Capsules; Part 6: Numerical Analysis of some Variables determining Free Flow", Canadian Journal of Chemical Engineering, Volume 42, No. 4, 1964, pages 168-173.
- (12) Ellis, H.S. and Bolt, L.H., "The Pipeline Flow of Capsules; Part 7: An Experimental Investigation of the Transport by two Oils of Single Cylindrical

and Spherical Capsules with Density equal to that of the Oil", Canadian Journal of Chemical Engineering, Volume 42, No. 5, 1964, pages 201-210.

- (13) Round, G.F. and Bolt, L.H., "The Pipeline Flow of Capsules; Part 8: An Experimental Investigation of the Transport in Oil of Single, Denser-than-Oil Spherical and Cylindrical Capsules", Canadian Journal of Chemical Engineering, Volume 43, No. 4, 1965, pages 197-205.
- (14) Jan Kruyer, Redberger, P.J. and Ellis, H.S., "The Pipeline Flow of Capsules; Part 9", Journal of Fluid Mechanics, Volume 30, Part 3, 1967, pages 513-531.
- (15) Kennedy, R.J., "Towards an Analysis of Plug Flow through Pipes", Canadian Journal of Chemical Engineering, Volume 44, No. 6, 1966, pages 354-356.
- (16) Ellis, H.S., "Effects of Scale-Up on the Performance of Cylindrical Capsules Flowing in Horizontal Pipelines", An ASME Publication, 67-PET-7.
- (17) Liddle, R.T., "A Photographic Study of Capsule Behaviour in a Pipeline", M.S. Thesis, Department of Civil Engineering, University of Alberta, May 1968.
- (18) Charles, M.E., Govier, G.W. and Hodgson, G.W., "The Horizontal Pipeline Flow of equal Density Oil-Water Mixtures", Canadian Journal of Chemical Engineering, Volume 39, 1961, pages 27-36.
- (19) Couette, M., Ann. Chem. Phys., Volume 6, 1890, pages 433-510.

- (20) Hinze, J.O., "Turbulence", McGraw-Hill Book Co., 1959, pages 517-8.
- (21) Knudsen, J.G. and Katz, D.L., "Fluid Dynamics and Heat Transfer", Chemical Engineering Series, McGraw-Hill Book Co., 1958, pages 158-164.
- (22) Robertson, J.M., "On Turbulent Plane-Couette Flow", Proceedings of 6th Midwestern Conference on Fluid Mechanics, University of Texas, 1959, pages 169-182.
- (23) von Karman, T., "The Fundamentals of the Statistical Theory of Turbulence", Journal of the Aeronautical Sciences. Volume 4, 1937, pages 134-138.
- (24) Pai, S.I., "On Turbulent Flow between Parallel Plates", Transactions ASME, Journal of Applied Mechanics, Volume 75, 1953, pages 109-114.
- (25) Munk, M.M., Catholic University of Am. Report, June 1955.
- (26) Yau Wu, M.S. Thesis, Theoretical and Applied Mechanics Department, Graduate College, University of Illinois, 1958.
- (27) Squire, W., "A Unified Theory of Turbulent Flow; Part II: Plane Couette Flow", Applied Science Research, Section A, Volume 9, 1960, pages 393-410.
- (28) A Private communication with Dr. J.M. Robertson, Prof. of Theoretical and Applied Mechanics, University of Illinois, U.S.A.
- (29) Ross, D., "A Physical Approach to Turbulent Boundary-Layer Problems", Transactions ASCE, Volume 121, 1956, pages 1219-1254.

- (30) Froberg, C.E., "Introduction to Numerical Analysis", Addison-Wesley Publishing Co., 1965, pages 181-187.
- (31) Lowan, A.N., Davids, N. and Levenson, A., "Table of the Zeros of the Legendre Polynomials of Order 1-16 and the Weight Coefficients for Gauss' Mechanical Quadrature Formula", Bulletin of American Mathematical Society, Volume 48, No. 10, October 1942, pages 739-743.